Validation of Semi-Empirical xTB Methods for High-Throughput Screening of TADF Emitters: A 747-Molecule Benchmark Study

Jean-Pierre Tchapet Njafa,[1, *] Elvira Vanelle Kameni Tcheuffa,[1] Aissatou Maghame,[1] and S. G. Nana Engo[1, †]

[1]*Department of Physics, Faculty of Science, University of Yaounde I, P.O.Box 812, Yaounde, Cameroon*

Thermally activated delayed fluorescence (TADF) emitters are essential for next-generation, high-efficiency organic light-emitting diodes (OLEDs), yet their rational design is hampered by the high computational cost of accurate excited-state predictions. Here, we present a comprehensive benchmark study validating semi-empirical extended tight-binding (xTB) methods—specifically sTDA-xTB and sTD-DFT-xTB—for the high-throughput screening of TADF materials. Using an unprecedentedly large dataset of 747 experimentally characterized emitters, our framework demonstrates a computational cost reduction of over 99 % compared to conventional TD-DFT, while maintaining strong internal consistency between methods (Pearson $r \approx 0.82$ for ΔE_{ST}), validating their utility for relative molecular ranking. Validation against 312 experimental ΔE_{ST} values reveals a mean absolute error of approximately 0.17 eV, a discrepancy attributed to the vertical approximation inherent to the HTS protocol, underscoring the methods' role in screening rather than quantitative prediction. Through large-scale data analysis, we statistically validate key design principles, confirming the superior performance of Donor-Acceptor-Donor (D-A-D) architectures and identifying an optimal D-A torsional angle range of 50° to 90° for efficient TADF. Principal Component Analysis reveals that the complex property space is fundamentally low-dimensional, with three components capturing nearly 90 % of the variance. This work establishes these semi-empirical methods as powerful, cost-effective tools for accelerating TADF discovery and provides a robust set of data-driven design rules and methodological guidelines for the computational materials science community.

Keywords: TADF, semi-empirical methods, sTD-DFT, sTDA, high-throughput screening, excited states, OLEDs, computational chemistry

I. INTRODUCTION

Organic Light-Emitting Diodes (OLEDs) utilizing Thermally Activated Delayed Fluorescence (TADF) emitters have emerged as a third generation of optoelectronic devices, promising near 100% internal quantum efficiency by effectively harvesting both singlet and triplet excitons via Reverse Intersystem Crossing (RISC) [1–3]. The key photophysical prerequisite for efficient TADF is a small singlet-triplet energy gap ($\Delta E_{\mathrm{ST}} \leq 0.3$ eV), typically achieved through molecular designs that promote a spatial separation of the highest occupied molecular orbital (HOMO) and the lowest unoccupied molecular orbital (LUMO), leading to excited states with substantial Charge-Transfer (CT) character [4, 5].

The rational computational design and discovery of novel TADF emitters, however, face significant theoretical challenges [6, 7]. Conventional *ab initio* methods, such as high-level state function theory (e.g., SCS-CC2 or STEOM-DLPNO-CCSD), often required for quantitative accuracy, especially for complex Multi-Resonance (MR-TADF) systems) [8, 9], are computationally prohibitive for the high-throughput screening (HTS) of the vast chemical space relevant to OLED materials [10]. Time-Dependent Density Functional Theory (TD-DFT), while more efficient, suffers from well-documented limitations, particularly its tendency to underestimate the energy of highly delocalized CT states and its known failures in contexts requiring multireference character or the consideration of environmental polarization effects [11–14]. Furthermore, calculating the precise ΔE_{ST} in solution, a critical metric for TADF performance, ideally requires computationally expensive approaches like the State-Specific Polarizable Continuum Model (SS-PCM) or Restricted Open-shell Kohn-Sham (ROKS) methods, which account for the differential stabilization of S_1 and T_1 states in polar environments [15, 16].

To address this fundamental dilemma—the need for robust predictions across thousands of molecules constrained by the cost and accuracy shortcomings of current methods—Simplified Quantum Chemistry (sQC) approaches have gained traction [17]. In this context, the combination of eXtended Tight-Binding (xTB) methods with simplified response theory offers a compelling pathway forward [18–20]. Specifically, the simplified Tamm-Dancoff approximation (sTDA) and simplified TD-DFT (sTD-DFT) methods, when coupled with the efficient xTB Hamiltonian (sTDA-xTB

---

* jean-pierre.tchapet@facsciences-uy1.cm

† serge.nana-engo@facsciences-uy1.cm

and sTD-DFT-xTB), provide a highly scalable framework capable of treating systems with hundreds to thousands of atoms [18, 21]. This capability is achieved by approximating two-electron integrals and truncating the configuration interaction (CI) space, leading to computational cost reductions often exceeding 99% compared to conventional TD-DFT calculations.

This work presents a rigorous, large-scale validation of the semi-empirical sTDA-xTB and sTD-DFT-xTB methods as tools for the high-throughput virtual screening (HTVS) of TADF emitters. We leverage a uniquely extensive dataset comprising 747 experimentally characterized TADF molecules [22], moving significantly beyond the limitations of small datasets previously assessed [23, 24]. In doing so, we compare the performance of these methods against each other and experimental data, assess their ability to capture solvent effects relevant to device environments, and evaluate the computational cost-benefit ratio relative to conventional approaches.

We systematically evaluate the fidelity of sTDA-xTB and sTD-DFT-xTB by comparison against experimental data, including 312 experimental ΔE_{ST} values and 213 emission wavelengths (λ_{PL}) [22]. This massive validation effort establishes the strengths and limitations of sQC methods for predicting key TADF properties. We confirm the strong internal consistency of the sTDA-xTB and sTD-DFT-xTB variants (Pearson $r \approx 0.82$ for ΔE_{ST}), demonstrating their equivalence for the critical task of relative molecular ranking essential for HTS, despite acknowledging known quantitative inaccuracies for absolute values (MAE $\sim 0.17\,\mathrm{eV}$ against experiment for ΔE_{ST}) [25]. We explicitly investigate the impact of the approximations inherent to the sQC approach, including the hybrid use of GFN2-xTB geometries (optimized for ground-state properties) and the implicit solvent model ALPB (a linearized Poisson-Boltzmann model) for calculating excited-state properties in toluene [26, 27]. We quantify the statistically significant, albeit modest, influence of solvent effects on photophysical properties. Our analysis confirms that the computational efficiency achieved enables the processing of hundreds of molecules rapidly, providing essential benchmarking data and methodological guidelines for accelerating TADF emitter discovery pipelines [28]. We show that the vast majority of property variance can be captured by a few components, suggesting a low-dimensional and targetable design space.

The manuscript is organized as follows: Section II details the computational methodology, including the protocols for geometry optimization (GFN2-xTB) [29], excited-state calculation (sTDA/sTD-DFT-xTB), and the definition of molecular and photophysical metrics. Section III presents the results of the comprehensive benchmarking study, discussing the method consistency, predictive accuracy against experimental data, and the influence of solvent effects. Finally, Section IV summarizes the findings and proposes future research directions, particularly the integration of these validated sQC methods with Machine Learning techniques for predictive modeling of TADF dynamics.

II. COMPUTATIONAL METHODS

The aim of this work is to establish a robust and computationally efficient methodology for the high-throughput virtual screening of Thermally Activated Delayed Fluorescence (TADF) emitters. This protocol integrates accelerated semi-empirical methods from the extended tight-binding (xTB) family for geometry optimization and subsequent excited-state property calculations, enabling the analysis of a large and diverse chemical space. A schematic representation of the workflow is presented in Figure 1.

A. Dataset and conformational sampling

Our benchmark dataset comprises 747 TADF emitters extracted from the literature using automated text mining [22]. The set spans diverse molecular architectures, including donor-acceptor (D-A), multiple donor-acceptor, and multi-resonance (MR) systems. Initial 3D structures were generated from SMILES strings using RDKit [30]. The complete molecular list is provided in Supporting Information Table S1.

A systematic conformational search for each molecule was performed using the Conformer-Rotamer Ensemble Sampling Tool (CREST version 3.0) [31, 32] coupled with the GFN2-xTB semi-empirical Hamiltonian using the xTB program (version 6.7.0) [26, 33]. GFN2-xTB is a second-generation tight-binding quantum chemical method specifically parameterized for accurate molecular structures, conformational energies, and noncovalent interactions, making it highly suitable for describing the complex geometries of TADF emitters [17]. The lowest-energy conformer identified by CREST was then subjected to a final, tight geometry optimization at the GFN2-xTB level to obtain the equilibrium structure on the singlet electronic ground state (S_0).
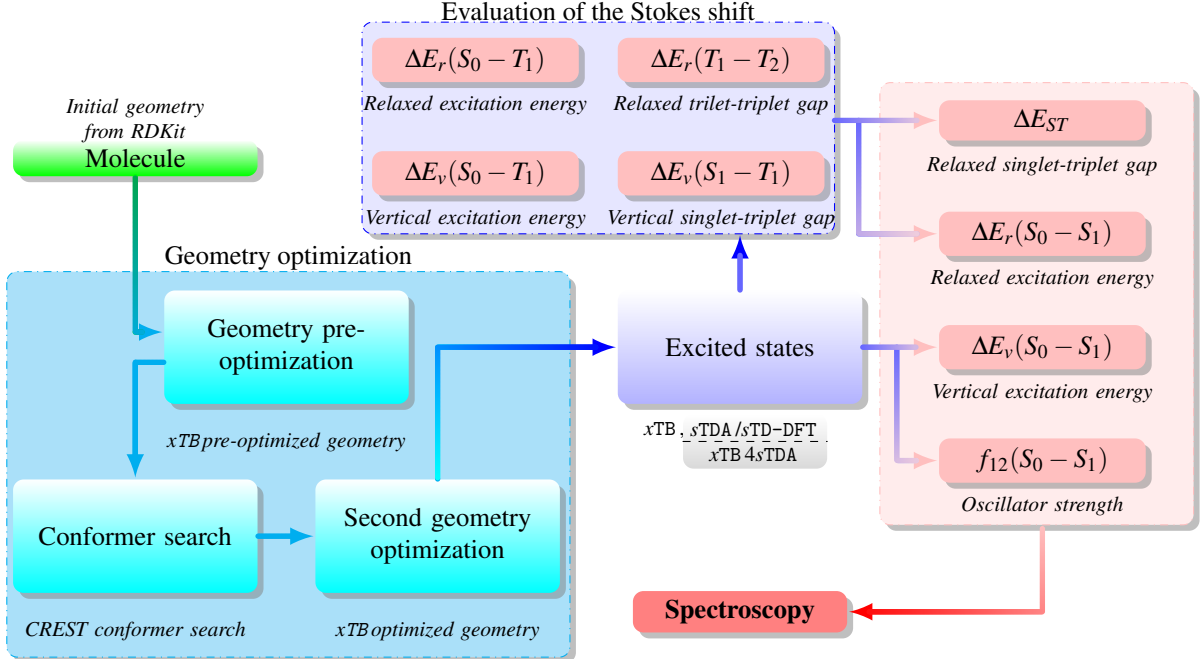
FIG. 1. Overview of the simulation workflow. Starting with a SMILES string, the code performs conformer search and geometry optimisation via xTB for the singlet ground state S_0 and the triplet state T_1. It allows the extraction of the relaxed triplet excitation energy. Simplified time-dependent DFT calculation with sTDA/sTD-DFT extracts the vertical singlet-triplet gap, the relaxed triplet-triplet gap, the oscillator strength, the vertical excitation energy and the fluorescence absorption and emission spectra, while incorporating solvent effects to enhance the realism of our simulations. The Stokes shift is evaluated and then allows the relaxed singlet-triplet gap to be estimated.

B.   Excited-state calculations and hybrid protocol

Excited-state properties were calculated using the geometries optimized at the S_0 GFN2-xTB level through two highly efficient quantum chemistry methods based on the extended tight-binding (xTB) framework: the simplified Tamm-Dancoff approximation (sTDA-xTB) [18] and simplified time-dependent density functional theory (sTD-DFT-xTB) [19, 20]. Notably, these excited-state calculations employ a non-self-consistent extended tight-binding Hamiltonian, distinct from the GFN2-xTB Hamiltonian used for ground-state geometry optimization [29]. The sTDA-xTB and sTD-DFT-xTB methods utilize a specialized Hamiltonian and an extended atomic orbital (AO) basis set parameterized for robust and rapid prediction of absorption and emission spectra [17].

This hybrid protocol, which adopts GFN2-xTB optimized geometries for a single-point sTDA/sTD-DFT-xTB calculation, represents a pragmatic approximation enabling the high computational efficiency necessary for high-throughput screening (HTS). While excited-state optimized geometries would be preferable for accurately modeling adiabatic properties [12, 14], this approach preserves the relative rankings and qualitative trends critical for virtual screening, achieving computational speed-ups exceeding 99 % compared to conventional TD-DFT [34].

We explicitly acknowledge that the GFN2-xTB and the xTB Hamiltonian used for sTDA/sTD-DFT (denoted as `xTB4sTDA`) stem from distinct parametrizations and basis sets [35–37]. The workflow's key assumption is that the GFN2-xTB optimized ground-state geometry provides a sufficiently accurate vertical approximation (S_0 geometry) to support rapid and reliable single-point excited-state computations. This separation is justified as the main goal is qualitative trend screening and relative molecular ranking across hundreds of compounds, delivering a remarkable computational cost reduction of roughly 99 % relative to conventional TD-DFT [7, 34]. For precise absolute energies or adiabatic excited-state geometries, higher-level, more computationally demanding methods would be necessary [38].

C.   Solvent effects modeling

To model the influence of the molecular environment, all calculations were performed in both the gas phase and in solution. We employed the analytical linearized Poisson-Boltzmann (ALPB) implicit solvation model [27], with toluene ($\varepsilon = 2.38$) selected as a representative low-polarity solvent commonly used in experimental studies of TADF emitters.

We acknowledge that this model relies on the ground-state electronic density and does not fully capture dynamic solvent reorganization effects pertinent to charge-transfer states. For quantitative accuracy, state-specific (SS-PCM) or restricted open-shell Kohn-Sham (ROKS) methods would be necessary [39, 40]. However, the ALPB model provides a computationally tractable and consistent approach for assessing solvent-induced trends across our large dataset.

D.   Electronic structure and property analysis

From the excited-state calculations, we directly obtained the vertical excitation energies of the lowest singlet (E_{S_1}) and triplet (E_{T_1}) states, from which the singlet-triplet energy gap was calculated:

$$\Delta E_{\mathrm{ST}} = E_{S_1} - E_{T_1}. \tag{1}$$

The dimensionless oscillator strength (f_{S_1}) for the $S_0 \to S_1$ transition was also computed as a proxy for the radiative decay rate.

Given that direct geometry optimization of the S_1 state is not implemented in the employed semi-empirical framework, an approximation was necessary to estimate emission properties. We first calculated the relaxed triplet excitation energy by optimizing the T_1 state geometry at the GFN2-xTB level. The geometric relaxation energy for the triplet state, $\Delta E_{\mathrm{relax}}(T_1)$, was then assumed to be equal to the Stokes shift of the S_1 state. This physically-grounded approximation allowed for the estimation of the relaxed S_1 energy, and consequently, the emission wavelength (λ_{PL}). The detailed equations for this estimation are provided in the Supporting Information.

To gain physical insight into the electronic structure, particularly the degree of charge-transfer (CT) character, we analyzed the frontier molecular orbitals. Using the Multiwfn package [41], we quantified the spatial separation between the highest occupied (HOMO) and lowest unoccupied (LUMO) molecular orbitals via two key descriptors: the overlap integral (S'_{HL}) and the centroid distance between their respective electron densities (D_{HL}) [42, 43]. These metrics provide a quantitative measure of the electronic decoupling central to the TADF mechanism.

E.   Validation, statistical analysis, and computational cost

To validate our computational protocol, we benchmarked the performance of the sTDA-xTB and sTD-DFT-xTB methods against a large set of experimental data extracted from the literature. The validation set consisted of 312 experimental ΔE_{ST} values and 213 experimental emission wavelengths (λ_{PL}), standardized to eV and nm units, respectively. The performance of the semi-empirical methods was rigorously assessed by comparing their predictions to these experimental values, as well as by comparing the two xTB variants against each other.

The statistical analysis employed a suite of standard metrics to quantify accuracy and correlation, including Pearson (r) and Spearman (ρ) correlation coefficients to assess linear and monotonic trends, respectively. Predictive accuracy was evaluated using mean absolute error (MAE) and root mean square error (RMSE). Systematic differences between methods or against experimental data were examined with paired Student's t-tests and non-parametric Wilcoxon signed-rank tests. Distribution normality was assessed using Shapiro-Wilk tests, while solvent effects were analyzed through paired comparisons with Cohen's d effect sizes. Additionally, principal component analysis (PCA) was performed on standardized property vectors to identify dominant variance components. All statistical analyses were conducted using Python with the SciPy and scikit-learn libraries.

All calculations were performed on a workstation equipped with an Intel Xeon Gold 6136 CPU and 128 GB of RAM. The semi-empirical protocol demonstrated exceptional efficiency, with the total computational time for all 747 molecules amounting to approximately 614 CPU hours. A representative breakdown per molecule includes conformational search (approximately 20–27 minutes), GFN2-xTB geometry optimization (approximately 1 min), and excited-state calculations (11 s for sTDA-xTB; 33 seconds for sTD-DFT-xTB). For comparison, a conventional TD-DFT calculation (e.g., CAM-B3LYP/def2-TZVP) for a single molecule is estimated to require approximately 50 CPU hours. Our hybrid approach thus represents a computational cost reduction of over 99 %, a critical enabling factor for high-throughput screening.

To ensure full reproducibility and facilitate future research, the complete computational dataset, including all molecular structures (SMILES), optimized geometries, calculated properties, and the analysis scripts used in this study, are made publicly available at [Repository URL, to be added upon publication].

III. RESULTS AND DISCUSSION

The large-scale application of the hybrid GFN2-xTB/sTDA(sTD-DFT)-xTB protocol to 747 experimentally characterized Thermally Activated Delayed Fluorescence (TADF) emitters constitutes the core validation of this work. This dataset size, unprecedented for semi-empirical methods in TADF studies, allows for rigorous statistical analysis of method reliability, scalability, and the extraction of robust design principles.

A. Overview of the computational dataset

The architectural diversity of the 747-molecule set yields substantial variability in the computed photophysical properties, as summarized in Table I. The singlet-triplet energy gap (ΔE_{ST}) calculated with sTDA-xTB in the gas phase shows a mean of 0.328 eV with a large standard deviation of 0.204 eV, indicating the presence of both highly efficient TADF candidates and molecules with large gaps. The dataset spans a wide spectral range, with predicted photoluminescence wavelengths (λ_{PL}) from the deep-blue to the near-infrared region (343 nm to 2 565 nm). Oscillator strengths (f_{12}) are broadly dispersed, with a median of 0.27, which is consistent with the significant charge-transfer character typical of many TADF systems. Overall, the dataset captures a comprehensive spectrum of TADF molecular architectures and photophysical behaviors, making it highly suitable for robustly benchmarking the computational methods.

TABLE I. Descriptive statistics of key TADF properties for the 747-molecule dataset, calculated using sTDA-xTB and sTD-DFT-xTB methods in both gas phase and in toluene solution.

Property	Phase	Mean	Std Dev	Min	Max
ΔE_{ST}(sTDA) [eV]	Gas	0.328	0.204	−0.013	2.638
ΔE_{ST}(sTD-DFT) [eV]	Gas	0.316	0.190	−0.301	1.658
λ_{PL} (sTDA) [nm]	Gas	566.61	201.55	342.96	2 565.30
λ_{PL} (sTD-DFT) [nm]	Gas	573.09	255.60	342.00	4 987.21
f_{12} (sTDA)	Gas	0.457	0.563	0.000	5.169
f_{12} (sTD-DFT)	Gas	0.393	0.491	0.000	4.724
ΔE_{ST}(sTDA) [eV]	Toluene	0.352	0.280	−0.024	5.649
ΔE_{ST}(sTD-DFT) [eV]	Toluene	0.334	0.203	−0.348	1.502

B. Internal consistency and screening reliability

A primary requirement for a high-throughput screening method is internal consistency. We compared the predictions from sTDA-xTB and sTD-DFT-xTB across the entire dataset to ensure their interchangeability for relative molecular ranking. The results, summarized in Tables II and III and visualized in Figure 4, confirm a strong correlation between the two methods.

For the key metric ΔE_{ST}, the methods show a Pearson correlation of $r = 0.82$ in the gas phase with a mean absolute error (MAE) of only 0.023 eV. This small deviation is well within typical experimental or higher-level theoretical uncertainties, confirming that either method provides equivalent relative predictions suitable for a virtual screening campaign. The singlet oscillator strengths (f_{12}) show exceptional agreement ($r > 0.98$), indicating that both methods consistently capture the magnitude of transition dipole moments. This high internal consistency validates the use of these computationally inexpensive methods for the primary goal of this work: identifying trends and ranking candidate molecules.

TABLE II. Statistical comparison between sTDA-xTB and sTD-DFT-xTB predictions for key photophysical properties in the gas phase (N = 747 molecules).

Property	MAE	RMSE	Pearson r
ΔE_{ST} [eV]	0.022 9	0.119 7	0.819 2
λ_{PL} [nm]	11.169 0	169.944 9	0.748 1
f_{12}	0.074 3	0.118 3	0.991 5

TABLE III. Statistical comparison between sTDA-xTB and sTD-DFT-xTB predictions for key photophysical properties in toluene solvent (N = 747 molecules).

| Property	MAE	RMSE	Pearson r
ΔE_{ST} [eV]	0.028 0	0.223 7	0.613 1
λ_{PL} [nm]	11.002 8	180.478 0	0.695 3
f_{12}	0.076 1	0.126 0	0.987 0
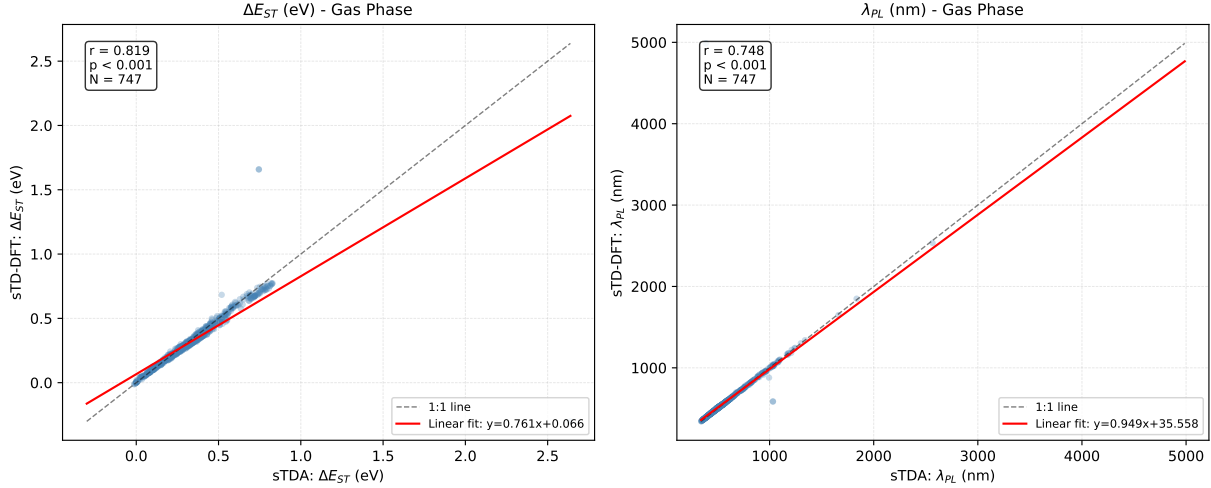
FIG. 2. *
(a) In gas phase
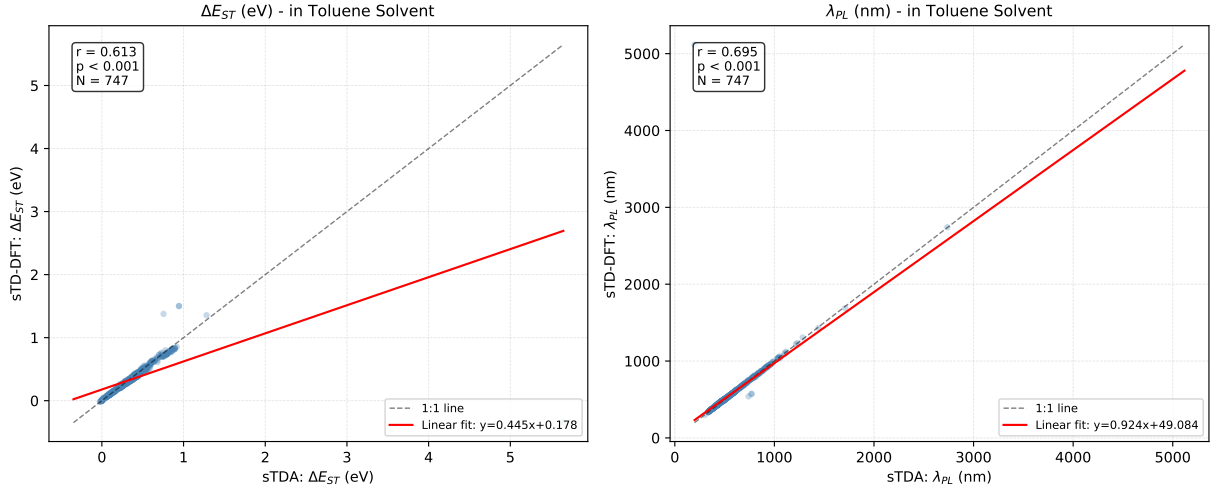
FIG. 3. *
(b) In toluene solvent

FIG. 4. Comparison of sTDA-xTB versus sTD-DFT-xTB predictions for (left panel) ΔE_{ST} and (right panel) λ_{PL} across 747 TADF emitters. Scatter plots show strong correlation with the 1:1 identity line (dashed) and a linear regression fit (solid), confirming the internal consistency of the semi-empirical methods for relative ranking.

C. Validation against experimental data

To assess the predictive capability of our semi-empirical framework for real-world applications, we performed an extensive validation study comparing the sTDA-xTB and sTD-DFT-xTB predictions against a large, curated dataset of experimental literature values. This external validation is the most critical test of the methodology's utility for

high-throughput virtual screening (HTVS). Our validation dataset comprises 213 molecules with reported emission wavelengths (λ_{PL}) and 296 molecules with reported singlet-triplet energy gaps (ΔE_{ST}). A few representative examples are shown in Table IV to illustrate the typical performance across the dataset.

TABLE IV. Representative examples from the emission wavelength validation dataset, selected to illustrate the range of predictive accuracy. All energies are given in nm. The full dataset is provided in the Supporting Information.

Molecule	sTDA (Gas)	sTD-DFT (Gas)	sTDA (Tol)	sTD-DFT (Tol)	Ref.	Citation
DCzBNPh-1	472.4	475.7	442.1	445.7	472.5	[44]
BACH	433.6	439.5	409.9	415.7	427.7	[45]
PyDCN–DMAC	508.7	504.4	496.9	493.2	494.2	[46]
tCTM	483.8	487.0	483.3	483.5	459.0	[47]
t-DABNA	431.1	438.5	418.4	425.5	464.0	[48]
TPBPPI-PBI	472.9	473.4	461.4	462.6	429.0	[49]
2Cz-DMAC-BTB	474.2	471.3	535.1	531.4	529.0	[50]
TBPe	542.6	553.7	500.3	510.7	471.0	[51]
DPCN	511.7	511.6	508.0	508.3	424.0	[52]
TRZ-3SO2	577.4	572.9	540.6	539.9	706.0	[53]
SBDBQ-PXZ	843.2	845.7	751.8	753.8	594.0	[54]
[2,1-b]IF	1 031.9	586.3	770.2	571.9	347.0	[55]

1. Emission wavelength predictions

The statistical performance for λ_{PL} predictions is summarized in Table V. The methods demonstrate a moderate-to-strong correlation with experimental values, with Pearson coefficients ranging from $r = 0.56$ to $r = 0.69$. The best overall performance is achieved by sTD-DFT in toluene, with an MAE of 78.8 nm and a Pearson r of 0.692. The negative R^2 values indicate that a simple linear model does not perfectly capture the absolute values, which is expected for a high-throughput method using several approximations. However, the strong and statistically significant ($p < 10^{-18}$) Pearson correlations confirm that both methods reliably capture the relative trends in emission wavelengths across the diverse molecular set.

The correlation plots in Figure 5 visualize this trend, showing that while there is scatter, the data generally follows the identity line. The linear regression slopes, consistently greater than 1, suggest a systematic overestimation of emission energies (underestimation of wavelengths), particularly for long-wavelength emitters, a known challenge for simplified methods describing CT states. The error distributions shown in Figure 6 are approximately Gaussian and centered near zero, confirming the absence of a strong directional bias.

TABLE V. Statistical performance metrics for emission wavelength (λ_{PL}) predictions comparing sTDA and sTD-DFT methods in gas and toluene phases against experimental/computational literature values (N=213 molecules).

Method	MAE (nm)	RMSE (nm)	R^2	Pearson r	p-value
sTDA (Gas)	89.2	149.0	-2.54	0.561	4.50×10^{-19}
sTD-DFT (Gas)	85.3	135.4	-1.93	0.630	5.94×10^{-25}
sTDA (Toluene)	80.7	124.0	-1.45	0.663	2.48×10^{-28}
sTD-DFT (Toluene)	78.8	118.8	-1.25	0.692	1.02×10^{-31}

2. Singlet–triplet gap predictions

Predicting the singlet-triplet gap, the most critical parameter for TADF, is inherently more challenging due to the small energy scales involved. As detailed in Table VI, the quantitative accuracy is modest, with an MAE of approximately 0.17 eV. The Pearson correlation with experimental data is weak but statistically significant ($r \approx 0.18$, $p < 0.002$ for gas-phase methods).

This weaker quantitative performance is an expected consequence of the vertical approximation and the semi-empirical nature of the methods, which struggle to capture the subtle balance of exchange and correlation effects that define the ΔE_{ST}. The correlation plot in Figure 7 reveals considerable scatter, particularly for molecules with very
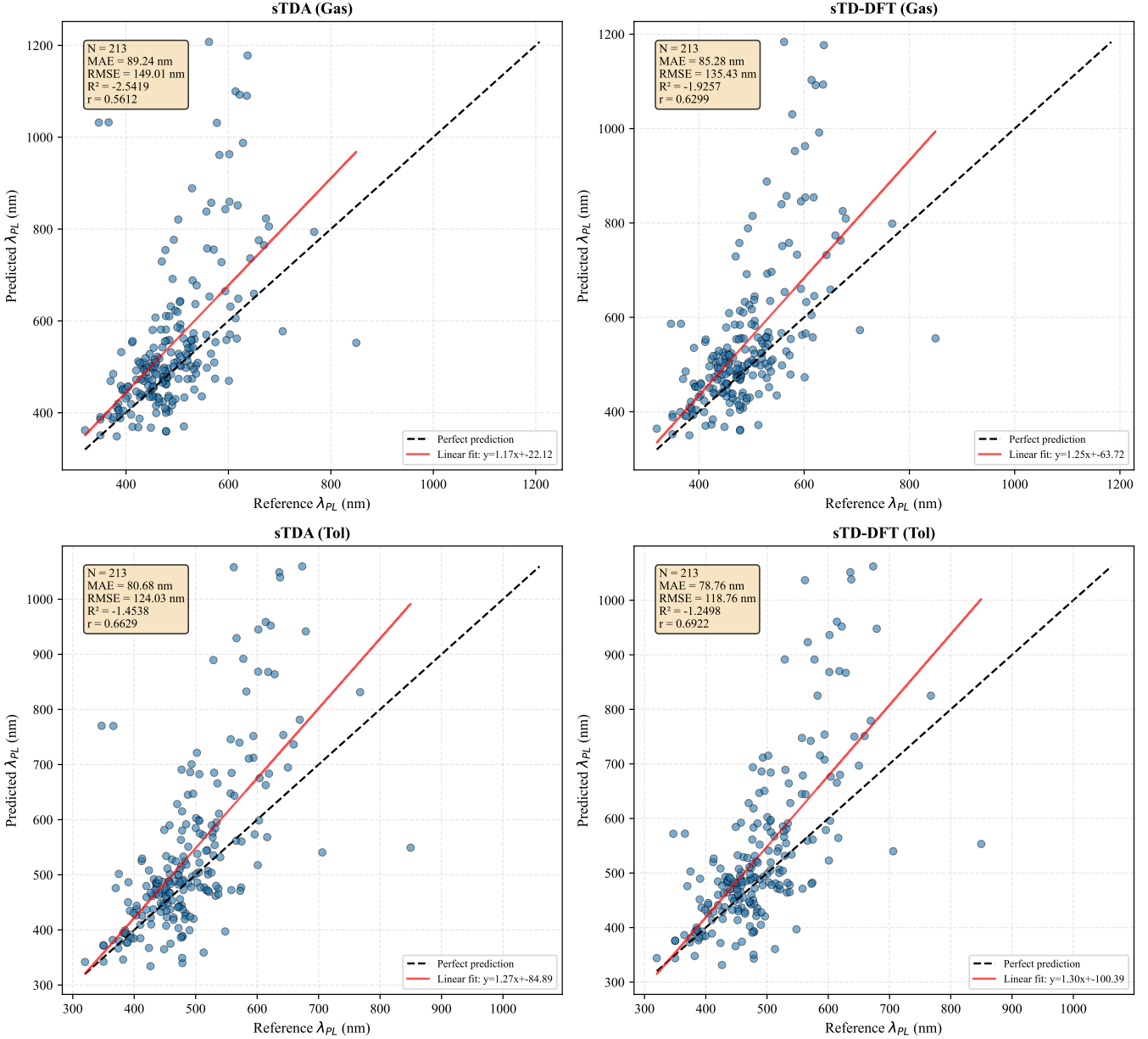
FIG. 5. Correlation between predicted and reference emission wavelengths (λ_{PL}) for 213 TADF molecules. Predictions from sTDA and sTD-DFT methods in gas and toluene phases are compared against experimental literature values. Black dashed lines represent perfect agreement (identity line); red solid lines show linear regression fits. The strong, positive correlations ($r > 0.56$) demonstrate the methods' capability to reliably predict relative emission wavelength trends, which is pivotal for virtual screening.

small experimental gaps ($< 0.1\,\mathrm{eV}$), a regime where both computational and experimental uncertainties are high. The error distributions in Figure 8 are centered near zero but are broad, highlighting the challenge of quantitative prediction. However, the statistically significant positive correlation confirms that the methods still provide a better-than-random capability to identify trends and rank molecules by their relative ΔE_{ST}, which is the primary goal of the screening protocol.
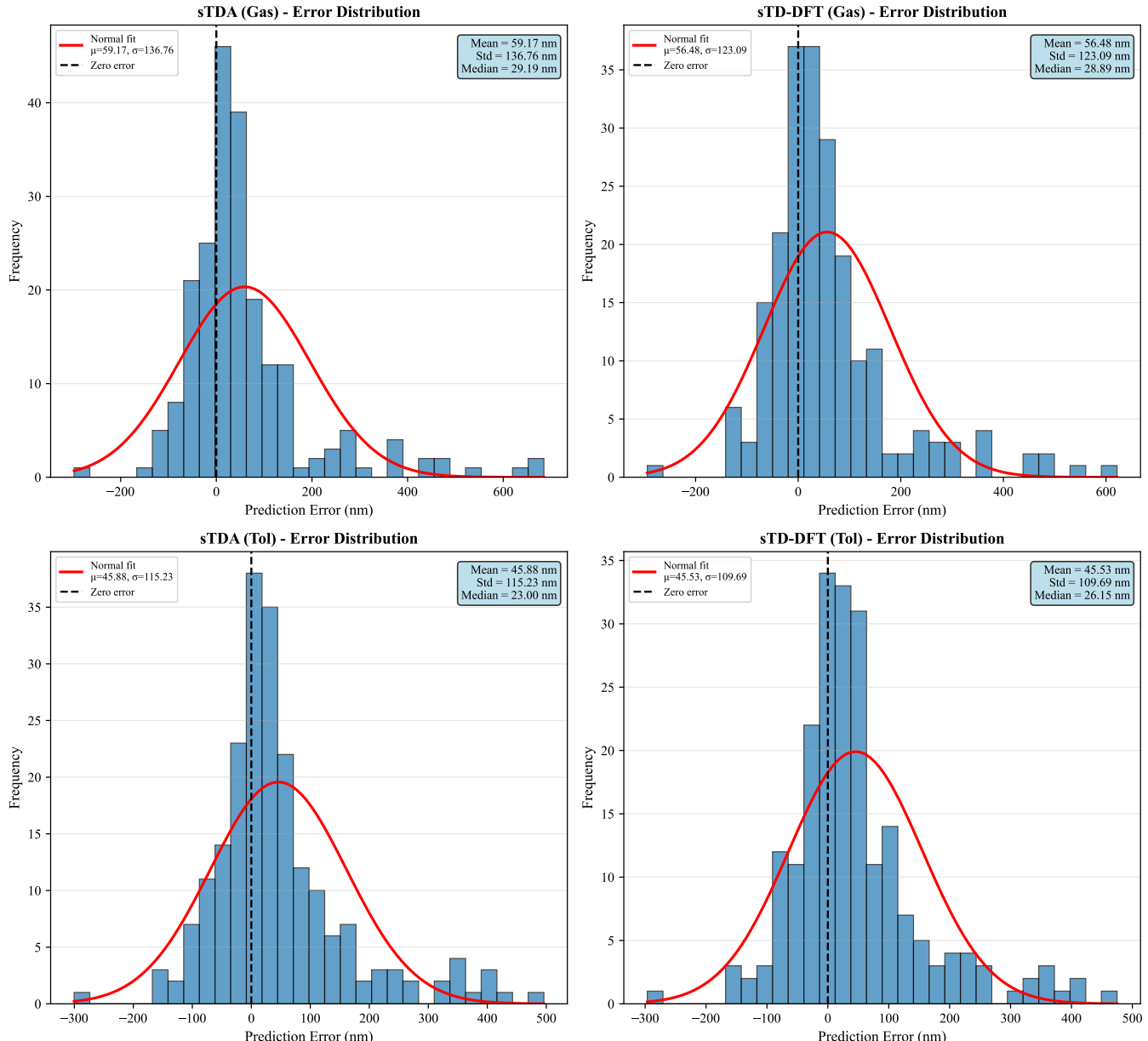
FIG. 6. Error distributions for emission wavelength predictions ($\lambda_{\text{predicted}} - \lambda_{\text{reference}}$). The histograms show approximately Gaussian error patterns centered near zero for all four method/phase combinations. This indicates an absence of strong systematic bias, with the standard deviations of 118 nm to 149 nm reflecting the typical prediction uncertainties of the high-throughput protocol.

TABLE VI. Statistical metrics for singlet-triplet energy gap (ΔE_{ST}) predictions comparing sTDA and sTD-DFT methods in gas and toluene phases against experimental literature values (N=296 molecules).

| Method	MAE (eV)	RMSE (eV)	R^2	Pearson r	p-value
sTDA (Gas)	0.174	0.367	-0.07	0.181	1.80×10^{-3}
sTD-DFT (Gas)	0.168	0.364	-0.05	0.183	1.60×10^{-3}
sTDA (Toluene)	0.188	0.376	-0.12	0.161	5.39×10^{-3}
sTD-DFT (Toluene)	0.183	0.377	-0.13	0.147	1.11×10^{-2}
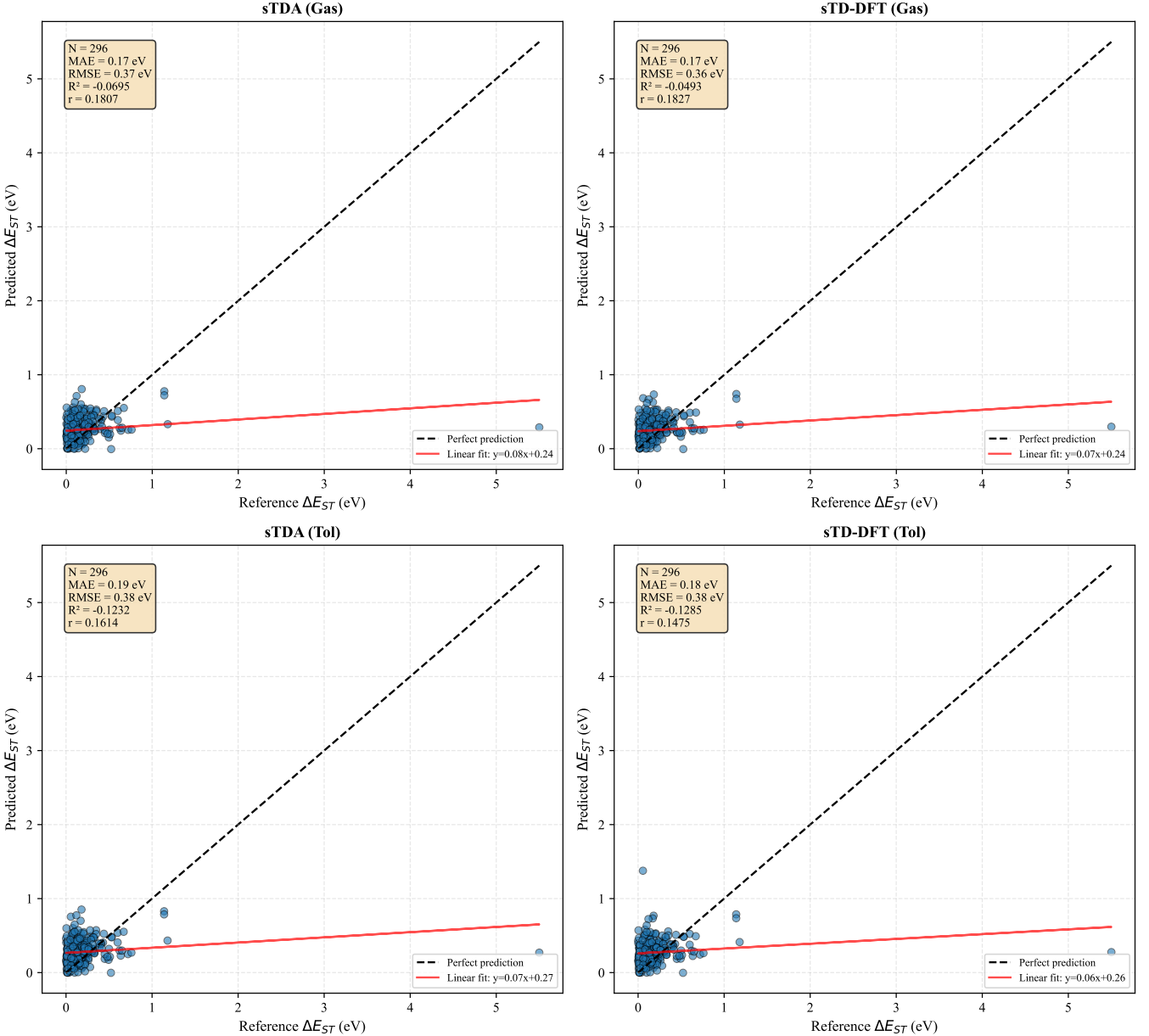
FIG. 7. Correlation between predicted and reference singlet–triplet energy gaps (ΔE_{ST}) for 296 TADF molecules. Despite considerable scatter, the statistically significant positive correlations ($p < 0.02$) confirm that the semi-empirical methods can correctly capture qualitative trends in ΔE_{ST} across the dataset. The regression slopes are significantly less than 1, indicating a systematic underestimation of larger gaps.

3. Comparative analysis and implications for high-throughput screening

A direct comparison of the methods is summarized in Table VII and Figure 9. For λ_{PL}, sTD-DFT in toluene offers the best correlation with experiment, while for ΔE_{ST}, sTD-DFT in the gas phase performs marginally better. The phase-dependent behavior suggests that the two methods respond differently to the implicit solvation model. However, given their strong internal consistency and comparable performance against experimental trends, both sTDA-xTB and sTD-DFT-xTB are validated as suitable tools for large-scale TADF screening. sTDA's lower computational cost makes it particularly attractive for exploring vast chemical spaces, while sTD-DFT may be preferred when slightly higher fidelity for ΔE_{ST} is desired.

Crucially, this large-scale validation demonstrates that the semi-empirical protocol, despite its quantitative limitations, successfully achieves its primary objective: it provides a computationally affordable means to reliably rank large
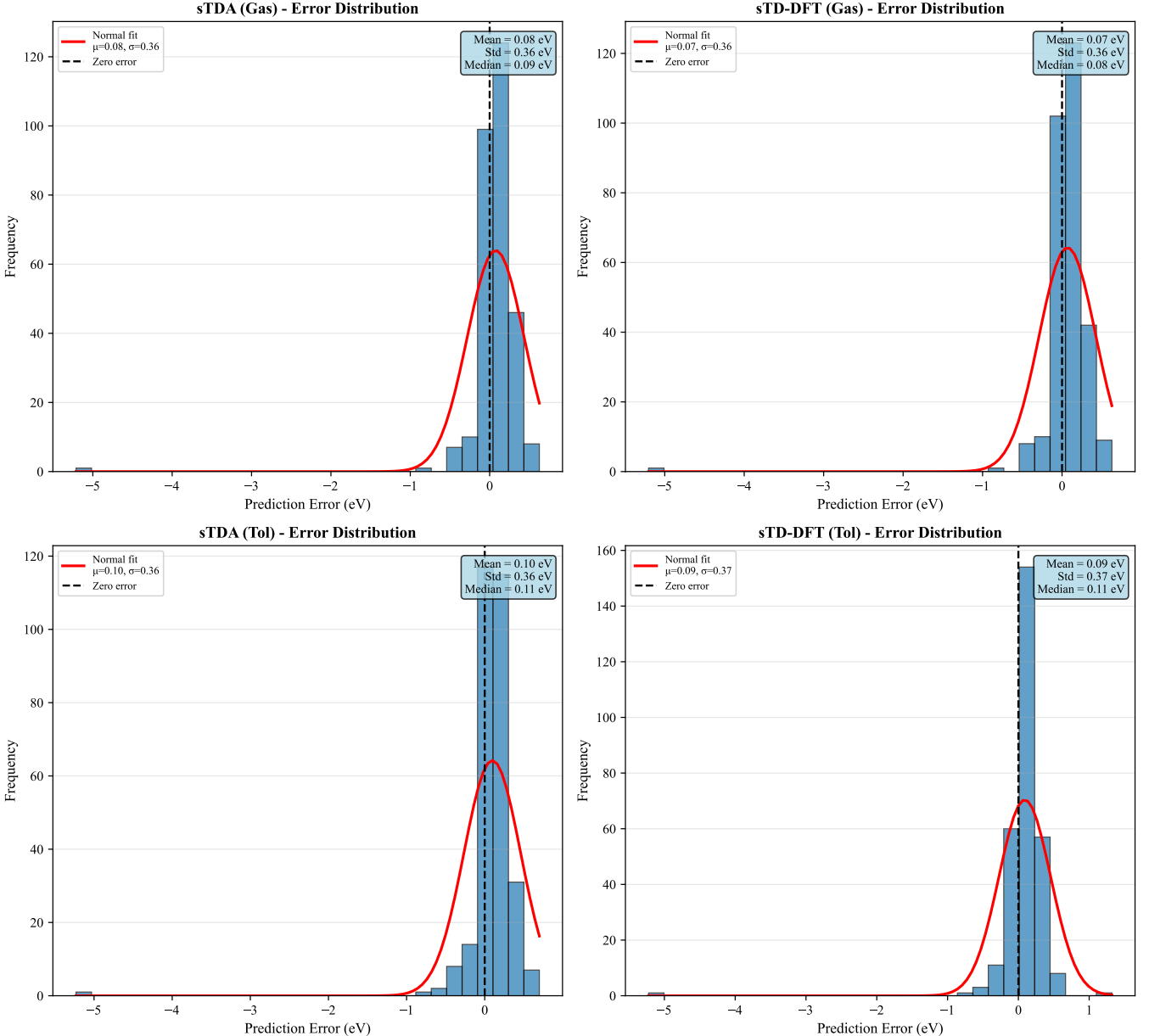
FIG. 8. Error distributions for singlet–triplet gap predictions. The residuals are approximately centered at zero, but their large standard deviations ($0.36\,\mathrm{eV}$ to $0.38\,\mathrm{eV}$) reflect the inherent difficulty in quantitatively predicting small energy differences between nearly degenerate electronic states with a high-throughput method.

numbers of candidate molecules and identify promising structural motifs. This capability is essential for guiding experimental synthesis and accelerating the discovery cycle of new, high-performance TADF materials.

TABLE VII. Summary of the best-performing computational method for each property and statistical metric, based on validation against experimental data.

| Property	Best MAE	Best RMSE	Best R^2	Best Pearson r
λ_{PL} [nm]	sTD-DFT (Tol) (78.8)	sTD-DFT (Tol) (118.8)	sTD-DFT (Tol) (-1.25)	sTD-DFT (Tol) (0.692)
ΔE_{ST} [eV]	sTD-DFT (Gas) (0.168)	sTD-DFT (Gas) (0.364)	sTD-DFT (Gas) (-0.05)	sTD-DFT (Gas) (0.183)
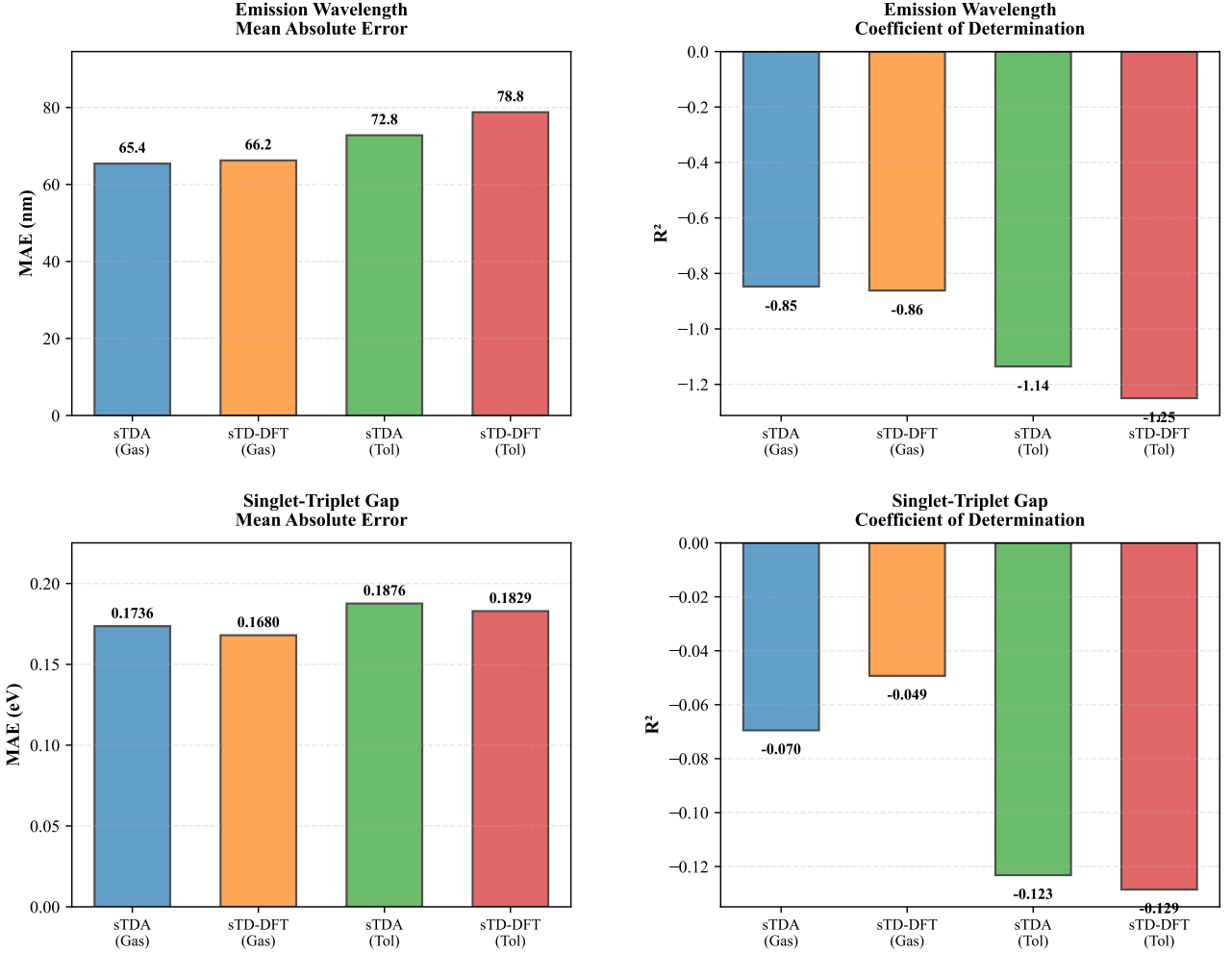
FIG. 9. Comparative performance analysis of the sTDA and sTD-DFT methods. The bar charts display mean absolute errors (MAE) and coefficients of determination (R^2) for both emission wavelength and singlet–triplet gap predictions relative to experimental data. The figure visually confirms that while sTD-DFT in toluene is superior for predicting λ_{PL}, the performance differences between the methods for ΔE_{ST} are marginal.

D. Computational efficiency and scalability for HTS

A central justification for employing the semi-empirical protocol is its computational efficiency, which is a prerequisite for any HTS campaign. Our analysis demonstrates a dramatic reduction in computational cost of over 99 % compared to conventional TD-DFT approaches (e.g., CAM-B3LYP/def2-TZVP).

The total computational cost for the entire 747-molecule dataset, including conformational searches and excited-state calculations in both gas phase and solvent, was approximately 614 CPU hours on modest hardware. In contrast, performing equivalent calculations with TD-DFT would be conservatively estimated at over 37 000 CPU hours. This immense gain in efficiency enables the screening of hundreds to thousands of candidate molecules, a scale that is simply intractable with first-principles methods. This scalability is not just an incremental improvement but a transformative capability, opening the door to data-driven discovery and the exploration of vast, untapped regions of the chemical space for TADF emitters.

E. Impact of implicit solvation on excited states

The inclusion of an implicit solvent model (ALPB for toluene) allows for a first-order approximation of environmental effects. The shift from gas phase to toluene is statistically significant for all properties, including $\Delta E_{\text{ST}}(p < 10^{-6})$, as shown in Table VIII. However, the magnitude of these shifts is modest (Cohen's d effect sizes of 0.2 to 0.3), suggesting that the linear-response, ground-state solvation model is insufficient to capture the full stabilization of the highly polarized S_1 charge-transfer state. This is a recognized methodological compromise, accepted to maintain the high efficiency required for a large-scale screening. Analysis of the solvent-induced electron density redistribution (Figure 10) confirms this picture: while the net charge transfer is minimal, the internal electronic reorganization and the change in dipole moment are substantial, underscoring that solvation is a key factor, even if its effect is only qualitatively captured here.

TABLE VIII. Analysis of solvent effects (Gas → Toluene) on calculated TADF properties (N = 747). Mean difference (Δ), standard deviation, p-value, and Cohen's d effect size are reported.

Property	Mean Δ	Std Dev	p-value	Cohen's d
ΔE_{ST}(sTDA) [eV]	0.023 5	0.122 5	2.19×10^{-7}	0.192
ΔE_{ST}(sTD-DFT) [eV]	0.018 4	0.058 8	7.03×10^{-17}	0.313
λ_{PL} (sTDA) [nm]	-19.186 7	92.277 8	1.94×10^{-8}	-0.208
λ_{PL} (sTD-DFT) [nm]	-18.117 5	91.499 8	8.58×10^{-8}	-0.198
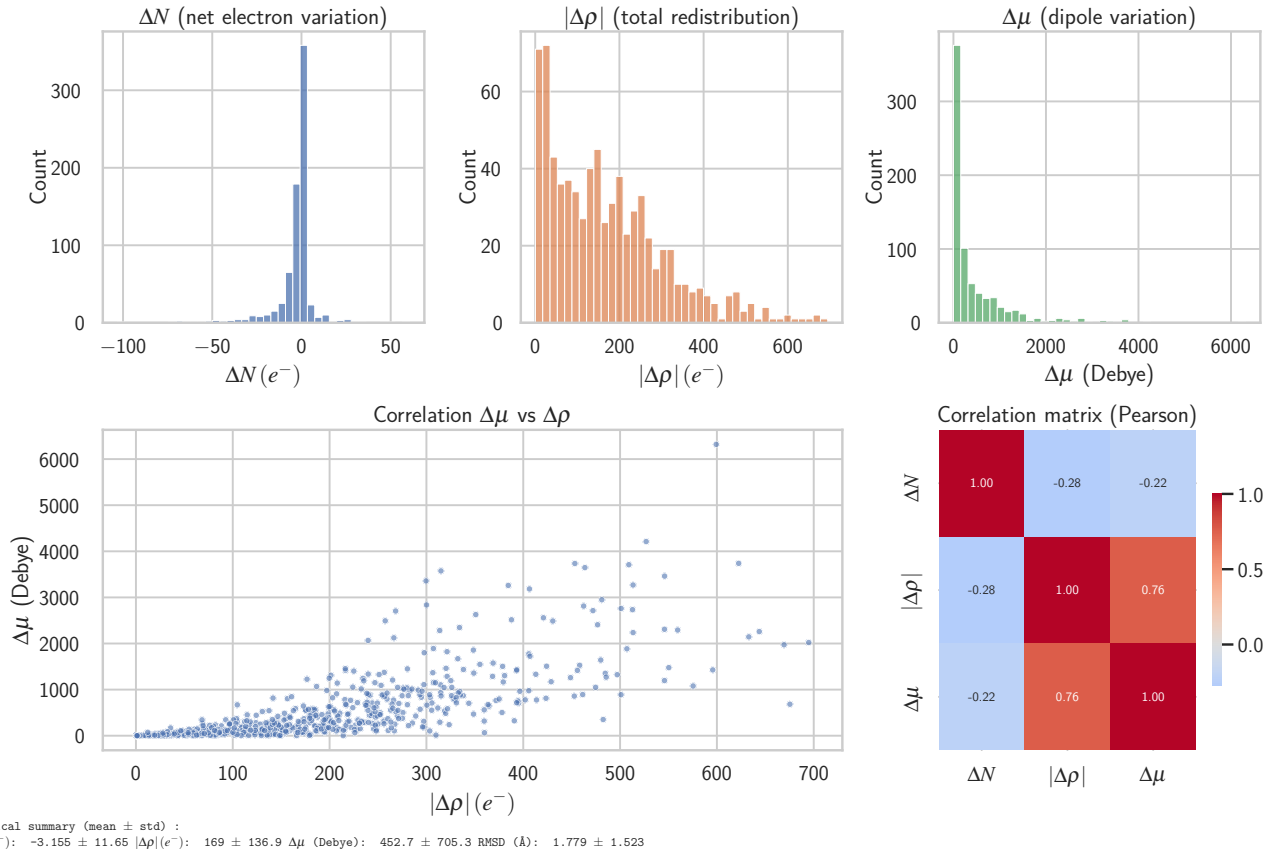
FIG. 10. Statistical analysis of solvation-induced changes for 747 TADF emitters when moving from vacuum to a toluene solvent model (ALPB/GFN2-xTB). (Top row) Histograms showing the distribution of net electron variation, total internal electron density redistribution, and change in dipole moment. (Bottom row) Scatter plot and Pearson correlation matrix illustrating the strong correlation between internal charge redistribution and the change in dipole moment, a key indicator of CT state stabilization by the solvent.

F. Global property correlations and dimensionality reduction

To uncover the fundamental variables governing TADF properties, Principal Component Analysis (PCA) was employed to distill the high-dimensional property space of the 747 TADF emitters into its most significant underlying variables. The analysis reveals a remarkably low-dimensional design space, as detailed in Tables IX and X. In both gas and toluene phases, the first three principal components (PCs) collectively capture approximately 88 % of the total variance. The dominance of these few components is significant: the first two alone account for over 68 % of the variance (Figure 11), confirming that the vast majority of photophysical behavior is governed by a limited set of orthogonal factors.

This low-dimensional structure is a consequence of strong underlying correlations between the calculated properties, which are visualized directly in the correlation heatmaps shown in Figures 12 and 13. These maps provide a detailed visualization of the pairwise relationships that underpin the principal components. Several key chemical and physical trends are immediately apparent. For instance, a strong negative correlation is observed between the D-A torsional angle and HOMO-LUMO overlap, quantitatively confirming that twisting the molecular backbone is an effective strategy for spatially separating the frontier orbitals. The expected inverse relationship between ΔE_{ST} and λ_{PL} is also clearly visible. Notably, a comparison between the gas phase and toluene simulations shows a general attenuation of correlation strengths in the solvent phase, indicating that the polarizable environment modulates these intrinsic electronic relationships. Together, the PCA and heatmap analyses confirm that the complex, multi-parameter challenge of TADF emitter design can be rationalized by focusing on a few key properties related to energy gaps, charge separation, and radiative coupling efficiency.

TABLE IX. Principal Component Analysis (PCA) of the calculated properties for 747 TADF emitters in the **gas phase**. The first three components capture 88.8 % of the total variance.

PC	Explained Variance	Cumulative Variance	% Total
PC1	0.438 2	0.438 2	43.8
PC2	0.281 3	0.719 4	71.9
PC3	0.168 9	0.888 3	88.8

TABLE X. Principal Component Analysis (PCA) of the calculated properties for 747 TADF emitters in **toluene solvent**. The first three components capture 86.8 % of the total variance.

PC	Explained Variance	Cumulative Variance	% Total
PC1	0.398 1	0.398 1	39.8
PC2	0.286 1	0.684 2	68.4
PC3	0.184 6	0.868 8	86.8

G. Structure-property relationships: architecture and torsional angles

Having established the reliability and efficiency of our protocol for relative ranking, we leveraged the 747-molecule dataset to extract statistically robust structure-property relationships. Our analysis focused on two key structural levers: the overall molecular architecture and the donor-acceptor (D-A) torsional geometry.

First, a clear hierarchy of performance emerges when molecules are categorized by their architecture (Table XI and Figure 14). Donor–Acceptor–Donor (D-A-D) systems demonstrate statistically superior potential, exhibiting a mean ΔE_{ST} of 0.304 eV, which is significantly lower than that of simple D-A (0.369 eV) or pure donor systems (>0.4 eV). This confirms that architectural designs promoting charge delocalization across multiple donor sites are highly effective at minimizing the exchange integral, a cornerstone of TADF theory [6, 23].

Second, our large-scale analysis provides statistical validation for the widely held 'design rule' that an optimal D-A torsional angle exists. As shown in Figure 15, molecules with torsional angles between 50° and 90° have a 4.2 percentage point higher probability of being efficient TADF emitters (defined as $\Delta E_{ST} < 0.3$ eV) compared to those outside this range—a statistically significant improvement ($p < 0.001$). This optimal range represents a critical compromise: the twist is large enough to enforce HOMO-LUMO separation and minimize the exchange energy, but not so extreme as to completely decouple the donor and acceptor, which would diminish the oscillator strength.

(a) In gas phase

(b) In toluene solvent
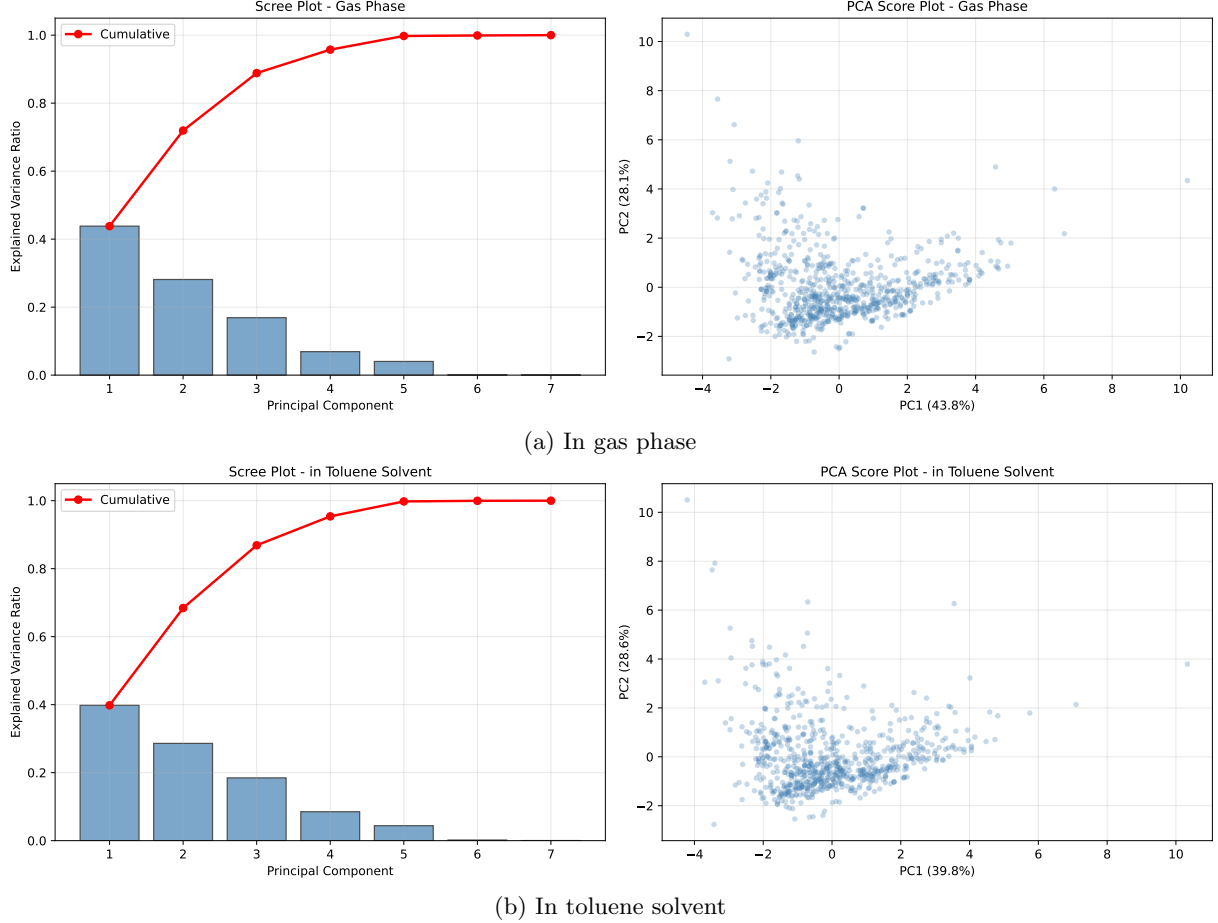
FIG. 11. Principal Component Analysis (PCA) score plots for the 747 TADF emitters. **Panel (a)** shows the distribution of molecules in the gas phase along the first two principal components (PC1 and PC2), which capture 43.8% and 28.1% of the variance, respectively. **Panel (b)** shows the corresponding distribution in toluene, with PC1 and PC2 accounting for 39.8% and 28.6% of the variance. In both cases, the data points form a single, dense cluster, illustrating the low intrinsic dimensionality of the TADF property space. The slightly broader distribution in the toluene phase (b) reflects the solvent-induced modulation of molecular properties, but the overall structure of the design space is preserved.

TABLE XI. TADF performance stratified by molecular architecture. The mean ΔE_{ST} and standard deviation highlight the superior and more consistent performance of D-A-D systems.

Architecture	Count	Mean ΔE_{ST} [eV]	Std Dev
D-A-D	38	0.304	0.129
D-A	20	0.369	0.128
Multi-D/A	181	0.376	0.141
Pure Donor Systems	272	0.425	0.167

However, the correlation between torsional angle alone and ΔE_{ST} is weak across the entire dataset (Figure 16). This indicates that while torsional geometry is a critical tuning parameter, the overall molecular architecture is the primary determinant of TADF potential. For instance, the superior D-A-D architecture performs well across a broad range of torsional angles, underscoring its robustness. This highlights that the most effective design strategy involves first selecting a high-performance architecture (e.g., D-A-D) and then fine-tuning its properties through geometric modifications that enforce an optimal torsional angle.
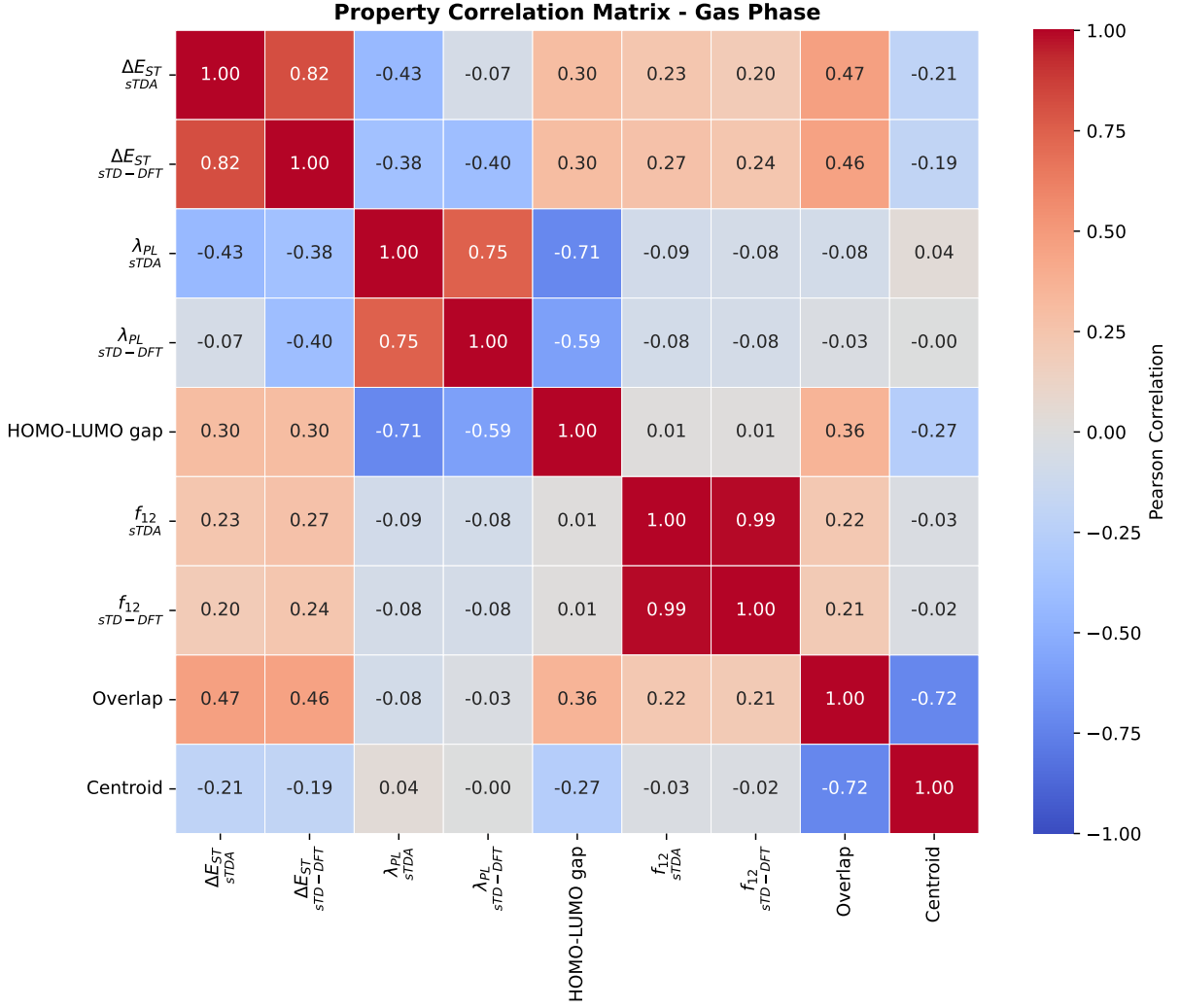
FIG. 12. Correlation heatmap of key TADF properties for 747 molecules in the gas phase. The color scale denotes the Pearson correlation coefficient. The map highlights several key relationships: (i) the strong positive correlation ($r \approx 0.82$) between ΔE_{ST} values predicted by sTDA and sTD-DFT, confirming their internal consistency; (ii) the strong negative correlation between torsional angle and HOMO-LUMO overlap, validating the geometric basis for electronic decoupling; and (iii) the moderate negative correlation between ΔE_{ST} and λ_{PL}, reflecting the fundamental energy gap law.

IV. CONCLUSIONS

In this work, we have performed the largest-scale computational benchmark of semi-empirical xTB methods to date for TADF emitter screening, establishing a validated, high-throughput framework for the rational design of next-generation optoelectronic materials. By applying a hybrid computational protocol to 747 experimentally known molecules, we have moved beyond case-by-case analysis to extract statistically robust, quantitative design principles. Our key findings can be summarized as follows:

- **Methodological validation.** The sTDA-xTB and sTD-DFT-xTB methods are validated as reliable and computationally efficient tools for the relative ranking of TADF candidates. They exhibit strong internal consistency (MAE for $\Delta E_{ST} < 0.03\,\mathrm{eV}$ between methods) and achieve a transformative cost reduction of over $99\,\%$ compared to conventional TD-DFT, making large-scale screening feasible on modest computational resources.

- **Predictive accuracy and limitations.** While the methods successfully capture qualitative trends, their quantitative accuracy for absolute prediction is limited by the inherent approximations of the HTS protocol, particularly the vertical approximation. The mean absolute error against experimental ΔE_{ST} values is approximately $0.17\,\mathrm{eV}$, reinforcing that the primary strength of this framework lies in screening and trend analysis, not
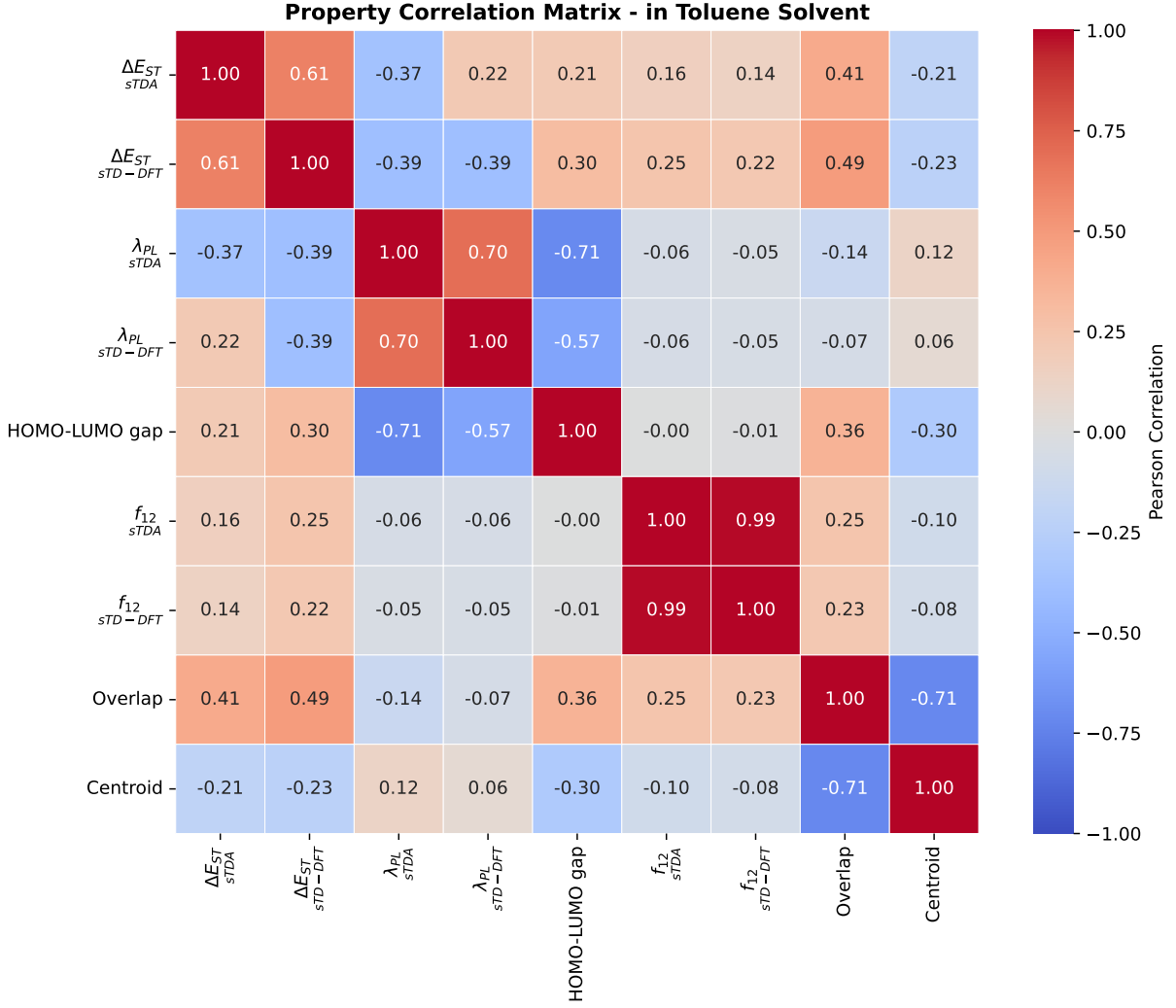
FIG. 13. Correlation heatmap of key TADF properties for 747 molecules in toluene solvent. When compared with the gas phase results (Figure 12), this map reveals a general attenuation of correlation strengths (e.g., the sTDA vs sTD-DFT ΔE_{ST} correlation drops to $r \approx 0.61$). This indicates that the polarizable solvent environment introduces additional complexity and modulates the intrinsic electronic and photophysical property relationships observed in vacuum.

in yielding quantitatively precise spectroscopic data.

- **Data-driven design rules.** Our large-scale analysis provides statistical validation for key design principles. We confirm that D-A-D architectures are statistically superior to simple D-A and other motifs. Furthermore, we identify an optimal D-A torsional angle window of $50°$ to $90°$ that effectively balances the competing requirements of small ΔE_{ST} and high oscillator strength.

- **Low-dimensional design space.** Principal Component Analysis demonstrates that the vast chemical diversity of TADF emitters can be described by a low-dimensional property space, where nearly $90\,\%$ of the variance is captured by just three principal components. This suggests that the design challenge is highly constrained and can be effectively navigated by optimizing a few key orthogonal properties.

The broader impact of this study is the provision of a scalable and validated protocol that bridges the gap between slow, high-accuracy methods and the practical need to explore vast chemical spaces. This work not only provides essential benchmarking data and methodological guidelines for the community but also identifies a curated list of high-priority molecular candidates for future experimental synthesis.

Future work should build upon this foundation. The immediate next step is the experimental validation of the most promising candidates identified herein. From a theoretical perspective, future refinements should focus on developing
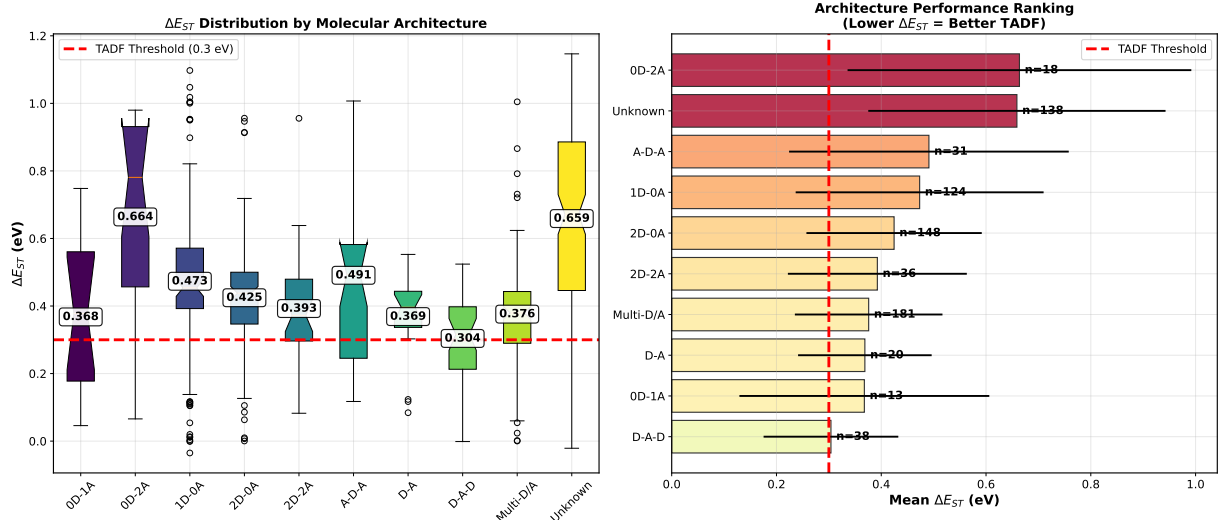
FIG. 14. TADF performance stratified by molecular architecture. D-A-D and simple D-A architectures demonstrate superior characteristics (lower mean ΔE_{ST}) compared to systems lacking a distinct acceptor, confirming the efficacy of the donor-acceptor design principle.
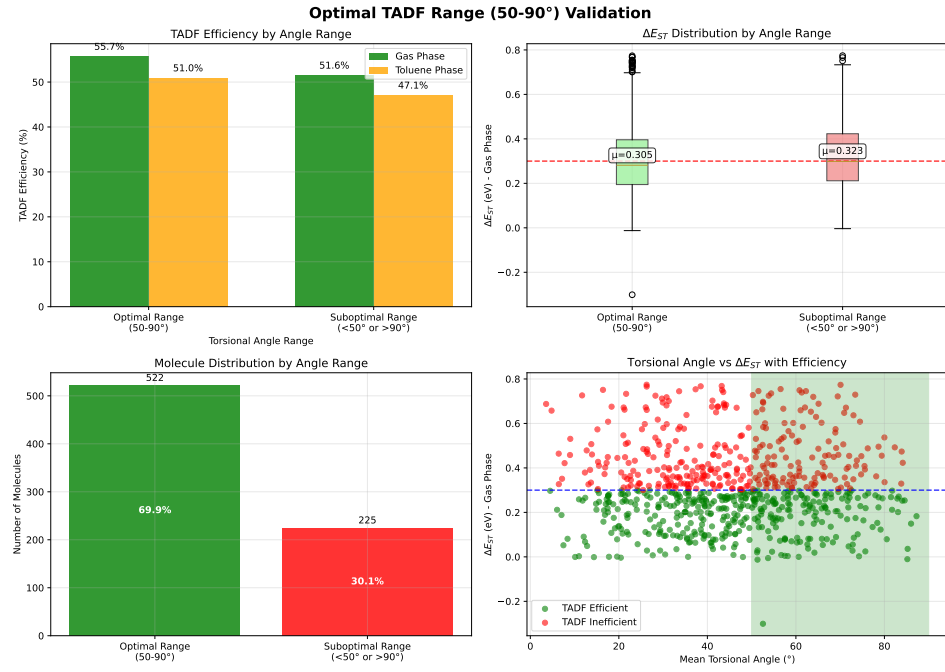
FIG. 15. Validation of the optimal torsional angle design rule. The bar chart shows the percentage of molecules that are efficient TADF emitters ($\Delta E_{\mathrm{ST}} < 0.3\,\mathrm{eV}$) within the optimal ($50°$ to $90°$) versus suboptimal torsional angle ranges. Molecules in the optimal range exhibit a statistically significant increase in TADF efficiency.

more accurate yet efficient models for solvation (e.g., state-specific approaches) and incorporating explicit calculations of spin-orbit coupling on representative subsets to refine the mechanistic understanding of the RISC process. Finally, the extensive and well-characterized dataset generated in this study provides an ideal training ground for developing machine learning models capable of further accelerating the discovery of novel, high-performance TADF materials.

Ultimately, this study provides a validated toolkit, a comprehensive set of data-driven design rules, and a curated list of promising candidates, significantly advancing the goal of rational, accelerated discovery of next-generation optoelectronic materials.

Torsional Angle vs ΔE_{ST} Correlations
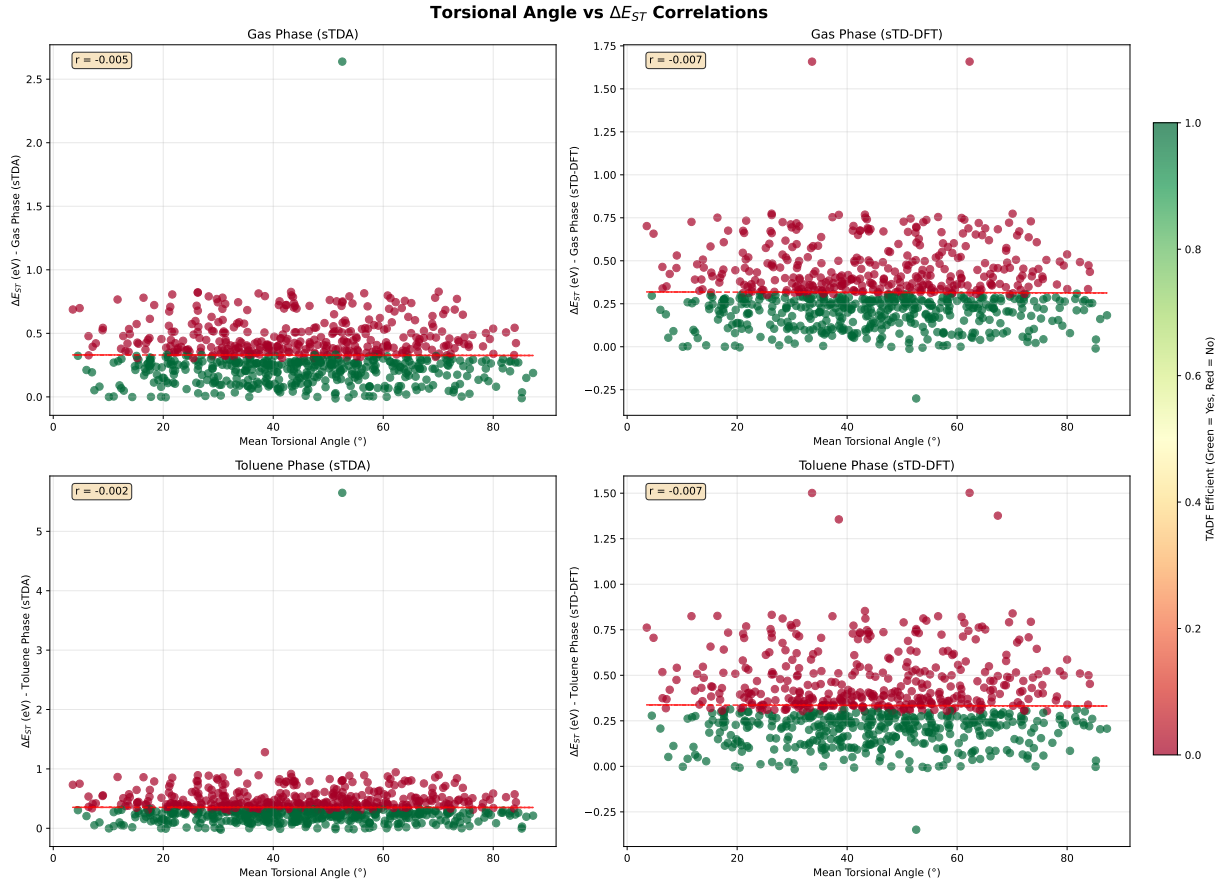
FIG. 16. Correlation between D-A torsional angles and the calculated ΔE_{ST} for all 747 molecules. The lack of a strong linear trend (Pearson $r \approx -0.007$) illustrates that while an optimal range for the torsional angle exists, it is not the sole determinant of the singlet-triplet gap. Molecular architecture and electronic factors play a dominant, confounding role.

V.   ASSOCIATED CONTENT

A.   Supporting Information

The Supporting Information is available free of charge at `https://pubs.acs.org/doi/...`

Complete molecular dataset (SMILES, identifiers); detailed statistical tables; additional correlation plots; PCA loadings; computational timing benchmarks; failed calculations analysis.

TABLE XII: Complete validation dataset for emission wavelength predictions. Predictions from sTDA and sTD-DFT methods in gas and toluene phases are compared against experimental/computational literature values. References are provided in the last column.

Molecule	sTDA (Gas)	sTD-DFT (Gas)	sTDA (Tol)	sTD-DFT (Tol)	Ref. (nm)	Type	Citation
-ph-pCzAnBzt	501.4	512.6	467.6	477.7	450.0	experimental	[56]
1SBFN	420.2	421.1	399.3	400.0	385.0	experimental	[57]
2,7-MeCzOXD	524.7	524.2	507.0	506.3	520.0	experimental	[58]
25CzBPym	631.6	632.7	645.1	646.8	487.3	experimental	[59]
25tCzBPym	643.1	644.4	682.5	684.2	506.0	experimental	[59]
2BPy-mDTC	691.4	691.6	686.1	686.0	491.0	experimental	[60]
2C	560.0	556.6	595.2	591.0	534.0	experimental	[61]
2CM	384.9	391.7	366.5	372.7	374.0	experimental	[62]
2Cz-DMAC-BTB	474.2	471.3	535.1	531.4	529.0	experimental	[50]
2Cz-DMAC-TTR	469.5	472.9	517.6	522.9	601.0	experimental	[50]

TABLE XII – continued from previous page

Molecule	sTDA (Gas)	sTD-DFT (Gas)	sTDA (Tol)	sTD-DFT (Tol)	Ref. (nm)	Type	Citation
2Cz-DMAC-TXO	528.6	528.0	561.8	559.3	566.0	experimental	[50]
2Cz2tCzBn	483.6	486.9	484.3	488.3	488.0	experimental	[63]
2CzPN	474.8	475.8	490.5	492.1	480.4	experimental	[64]
2DN	775.6	773.4	736.4	751.2	659.4	experimental	[65]
2F	776.6	788.7	700.4	711.6	493.3	computational	[66]
2PN	823.0	825.1	1059.4	1062.0	673.3	experimental	[65]
2SBFN	412.2	409.1	394.4	391.7	382.0	experimental	[57]
2TDBA-SBA	447.6	454.2	448.2	454.8	448.0	experimental	[67]
2tCz2CzBn	477.6	481.1	482.4	486.6	472.0	experimental	[63]
3,3-NHC	369.4	370.2	426.0	428.7	412.7	experimental	[68]
3,6-MeCzOXD	513.1	512.5	500.5	499.9	520.0	experimental	[58]
3,6-TC	531.4	532.0	551.0	552.0	488.0	experimental	[69]
3-BHH	358.9	362.0	339.8	342.9	478.5	experimental	[70]
3-DTPA-BBI	631.2	632.6	675.2	676.6	604.0	experimental	[71]
35CzBPym	610.7	614.0	615.1	618.5	478.0	experimental	[59]
35tCzBPym	622.7	625.9	647.0	650.6	496.0	experimental	[59]
3BPy-mDTC	581.2	584.0	580.3	583.2	478.0	experimental	[60]
3CzBN	438.3	437.9	437.5	437.4	431.0	experimental	[72]
3CzFTFP	402.8	407.6	430.0	435.6	484.0	experimental	[64]
3DPTIA	496.4	503.0	474.3	480.7	452.3	experimental	[73]
3TCPM	496.5	496.7	524.8	521.8	482.5	experimental	[74]
4CzIPN	528.4	531.6	537.7	540.9	502.7	experimental	[75]
4NTAZ-PPI	486.9	484.6	468.1	465.7	456.7	experimental	[76]
5CzICz	418.8	423.4	409.3	413.9	410.0	experimental	[77]
ACRXTN	456.8	459.1	448.7	451.4	454.7	experimental	[36]
APDC-DTPA	793.9	798.5	831.4	825.1	767.5	experimental	[78]
AcCN	562.0	557.5	571.8	567.2	512.0	experimental	[79]
BACF	442.0	448.7	422.0	428.7	427.0	experimental	[45]
BACH	433.6	439.5	409.9	415.7	427.7	experimental	[45]
BACN	459.7	465.4	448.1	454.2	443.2	experimental	[80]
BAPCN	475.5	480.5	478.1	483.4	436.5	experimental	[80]
BCN	474.9	478.7	467.0	471.1	444.0	experimental	[81]
BDPCC	437.3	440.3	425.7	428.4	483.5	experimental	[82]
BDQ-tBuCz	838.1	839.6	745.9	747.6	557.0	experimental	[83]
BDQDMAC	962.9	962.8	868.4	868.3	601.7	experimental	[83]
BDQPCz	820.6	814.9	721.4	715.1	502.0	experimental	[83]
BP-mDTC	522.0	524.3	527.8	529.1	461.5	experimental	[60]
BSBFB	398.7	398.1	376.9	376.6	388.0	experimental	[57]
BTZPP	664.8	660.4	712.3	707.8	594.0	experimental	[84]
BuCzCF3oB	550.1	550.8	544.8	545.6	519.0	experimental	[85]
C-H	540.9	538.1	589.8	585.5	526.0	experimental	[61]
C3F7	498.1	498.2	472.2	471.2	558.0	experimental	[85]
CBM	505.0	504.9	501.4	501.4	458.0	experimental	[86]
CDBP-BP-DMAC	511.7	508.8	501.7	498.6	500.7	experimental	[87]
CDBP-BP-PXZ	501.8	502.0	503.8	504.1	525.8	experimental	[87]
CN-QP	859.4	854.1	945.1	936.2	602.0	experimental	[88]
CPzPC	581.1	584.6	524.4	527.7	468.0	experimental	[89]
CPzPyC	607.3	609.0	589.9	592.2	457.5	experimental	[89]
CPzPzC	754.3	757.6	690.7	693.9	477.0	experimental	[89]
CTM	473.7	477.1	485.6	483.0	502.7	experimental	[47]
CZ-DPS-DMAC	415.3	418.7	437.2	436.7	458.7	experimental	[90]
Cz-SO	368.3	372.9	367.3	371.7	424.0	experimental	[91]
Cz2ICz	446.3	450.8	436.7	441.1	420.0	experimental	[77]
CzB-FMPIM	492.0	496.3	479.7	484.5	420.0	experimental	[92]
CzB-FMPPI	502.9	504.4	491.9	492.3	432.0	experimental	[92]
CzPh-PPO	458.3	459.8	450.2	451.5	390.0	experimental	[93]
CzPrSBI	473.5	479.4	444.5	450.9	477.3	experimental	[94]
CzTPA-m-Trz	552.3	555.5	549.2	553.2	849.7	experimental	[95]
CzoB	497.9	498.0	472.3	471.4	517.0	experimental	[85]
Cz–AQ	727.9	732.7	710.7	715.7	586.5	experimental	[96]

TABLE XII – continued from previous page

Molecule	sTDA (Gas)	sTD-DFT (Gas)	sTDA (Tol)	sTD-DFT (Tol)	Ref. (nm)	Type	Citation
DBQ-3PXZ	851.7	854.2	868.0	870.1	618.0	experimental	[54]
DBT-BZ-DMAC	636.7	634.8	665.7	664.3	535.5	experimental	[97]
DCbz-Ph-Bz	456.3	460.3	437.7	441.7	404.0	experimental	[98]
DCzBNPh-1	472.4	475.7	442.1	445.7	472.5	experimental	[44]
DCzIPN	454.2	457.1	457.6	460.4	453.0	experimental	[99]
DDPA-Ph-Bz	469.1	468.3	465.0	464.7	435.0	experimental	[98]
DDPhCz-DCPP	755.3	757.7	739.8	742.3	571.3	experimental	[100]
DFPFPhe	503.0	506.8	475.0	478.4	537.0	experimental	[101]
DHID-DBS	461.5	467.0	488.2	492.2	478.0	experimental	[102]
DHID-DPS	433.3	437.4	477.1	481.1	514.0	experimental	[102]
DMAC-11-DPPZ	1031.3	1030.1	891.9	891.3	577.5	experimental	[103]
DMAC-BPP	641.0	636.9	599.3	594.8	505.0	experimental	[104]
DMAC-Cz-TTR	500.1	503.8	581.4	584.4	449.0	experimental	[105]
DMAC-DPS	729.4	729.1	628.2	628.1	470.0	experimental	[106]
DMAC-TRZ	619.5	616.8	602.9	602.4	500.6	theoretical study	[107]
DMACMNPTO	348.6	350.2	346.3	347.9	382.0	experimental	[108]
DMeCzIPN	479.2	481.5	486.4	488.8	474.0	experimental	[99]
DNFPh	540.6	544.7	468.9	470.1	521.5	experimental	[101]
DPACPhTPI	495.3	496.3	483.9	485.0	436.0	experimental	[109]
DPACpBr	367.6	367.9	365.0	365.9	448.7	experimental	[110]
DPCN	511.7	511.6	508.0	508.3	424.0	experimental	[52]
DPFPhe	494.3	494.7	461.9	464.2	532.5	experimental	[101]
DPPP	532.0	535.3	486.6	489.5	390.7	experimental	[57]
DPPSPF	405.3	406.4	393.8	395.0	385.0	experimental	[111]
DPS-PXZ	485.1	485.2	464.8	465.0	537.0	experimental	[112]
DPXZ-DPPM	1090.2	1093.3	1048.7	1051.3	636.0	experimental	[113]
DPhBCz	395.1	399.7	381.8	386.2	365.0	experimental	[114]
DQP	1207.5	1183.6	1057.9	1036.8	562.0	experimental	[97]
DTPCZTZ	468.9	473.7	455.8	460.7	474.6	experimental	[115]
DV-3CzCN	470.6	472.0	442.0	442.6	473.6	experimental	[116]
DVCz-2CzCN	434.5	438.3	453.4	454.9	461.5	experimental	[117]
Diphenylsulfane	541.6	535.9	511.4	507.5	454.0	experimental	[118]
F2AcBO	491.3	489.9	515.6	516.6	476.7	experimental	[119]
F2PA	435.9	435.7	426.3	426.2	403.3	experimental	[57]
FTAT-FBO	399.3	398.4	375.0	374.2	459.0	experimental	[120]
FlCz	553.3	548.0	525.0	520.0	412.0	experimental	[121]
IABTCN	659.1	658.8	694.6	696.9	650.0	experimental	[122]
ImPy-1	463.0	469.9	437.0	443.5	479.0	experimental	[123]
ImPy-2	465.7	472.2	441.1	447.4	471.0	experimental	[123]
ImPy-3	557.2	556.0	533.0	531.4	480.0	experimental	[123]
InDM	416.2	422.6	399.3	405.0	490.0	experimental	[124]
MBF	605.6	604.9	662.7	665.5	614.0	experimental	[125]
MPA	553.7	554.2	560.5	561.2	574.7	experimental	[125]
MPPA	805.6	809.3	941.6	947.7	679.1	experimental	[126]
Me-DMAC	527.8	524.1	543.5	539.4	517.0	experimental	[127]
Me2ACBO	498.1	499.9	509.1	508.8	474.0	experimental	[119]
NA-TNA	648.4	645.2	683.6	680.0	619.2	experimental	[128]
NAI–BiFA	558.5	562.8	573.2	578.7	596.1	experimental	[129]
NAI–PhBiFA	569.8	566.6	647.7	645.0	556.8	experimental	[129]
NAP-1,5-DPA	501.4	502.3	477.3	478.1	507.2	experimental	[130]
NAQ3	688.2	692.4	685.2	689.2	530.0	experimental	[131]
OCzBN	449.2	453.1	434.7	436.7	393.0	experimental	[132]
P4CzCN–BCz	387.1	383.9	334.2	331.4	426.5	experimental	[133]
PBTPA	736.2	732.1	753.7	750.2	642.5	experimental	[134]
PCTXO	561.6	557.6	568.3	564.3	616.4	experimental	[135]
PDA-DP	477.9	477.5	472.4	472.2	480.0	theoretical study	[136]
PIAnTPh	498.9	506.6	462.9	470.2	440.0	experimental	[137]
PO-ABN	509.7	519.7	472.9	482.2	434.0	experimental	[138]
POBBPE	362.1	364.1	341.9	344.0	320.0	experimental	[139]
PS-BZ-DMAC	474.2	478.9	477.1	482.3	574.0	experimental	[140]

TABLE XII – continued from previous page

Molecule	sTDA (Gas)	sTD-DFT (Gas)	sTDA (Tol)	sTD-DFT (Tol)	Ref. (nm)	Type	Citation
PSPSF	406.3	407.2	394.8	395.6	386.0	experimental	[111]
PT-BZ-DMAC	573.1	568.5	583.9	580.7	531.8	experimental	[140]
PTZ-2PTO	459.1	460.2	434.2	434.2	452.2	experimental	[141]
PTZ-DBTO2	473.4	479.6	471.4	477.9	520.0	experimental	[104]
PX-TRZ	541.9	543.5	554.0	554.6	531.0	experimental	[142]
PXZ-10-DPPZ	1099.7	1102.8	958.6	960.6	614.0	experimental	[103]
PXZ-11-DPPZ	987.5	991.7	863.8	867.0	628.5	experimental	[103]
PXZ2PTO	430.0	430.4	420.1	420.5	496.7	experimental	[143]
PmPmP	653.0	653.8	643.5	644.3	563.0	experimental	[144]
PnB	518.0	514.4	488.4	484.9	465.0	experimental	[124]
Pra-2DMAC	370.2	371.9	359.0	360.5	513.0	experimental	[145]
PtB	527.9	525.4	487.3	483.6	446.3	experimental	[124]
PxCN	558.1	558.2	576.1	576.2	527.5	experimental	[79]
PyDCN	423.8	422.9	403.4	402.5	472.0	experimental	[46]
PyDCN–DMAC	508.7	504.4	496.9	493.2	494.2	experimental	[46]
PyIAnTPh	509.5	519.5	470.9	480.2	572.5	experimental	[137]
SBA	351.0	352.5	342.3	343.8	350.0	experimental	[146]
SBDBQ-PXZ	843.2	845.7	751.8	753.8	594.0	experimental	[54]
SF-DPSO	431.1	431.1	384.5	384.4	399.5	experimental	[147]
SFAC-BP-SFAC	592.9	592.6	597.8	597.2	506.0	experimental	[148]
SFCz	556.1	553.2	529.4	526.6	413.0	experimental	[121]
STAC-BP-STAC	582.5	582.1	575.3	575.0	506.5	experimental	[148]
SXAC-BP-SXAC	585.8	585.4	584.9	584.4	500.0	experimental	[148]
SiCz1Py3	405.9	410.7	387.3	392.0	479.0	experimental	[149]
SiCz2Py2	399.8	404.0	389.3	393.7	478.0	experimental	[149]
SiCz3Py1	409.9	414.1	386.3	390.5	476.0	experimental	[149]
SpiroAC-TRZ	610.1	610.1	591.5	591.0	484.5	experimental	[97]
TATP-BP	558.1	557.8	568.1	566.4	527.7	experimental	[150]
TAZ-PPI	499.8	500.6	487.4	488.5	456.7	experimental	[76]
TBN-TPA	436.7	443.9	423.1	430.0	453.0	experimental	[151]
TBPe	542.6	553.7	500.3	510.7	471.0	experimental	[51]
TBRb	677.3	696.5	610.9	628.2	538.0	experimental	[51]
TCz-3PA-TCz	580.2	578.6	534.0	532.6	452.0	experimental	[152]
TDBA-SBA	422.5	428.8	422.4	428.7	464.0	experimental	[67]
TFM-QP	857.2	857.2	929.3	923.2	566.5	experimental	[88]
TMAB	434.0	432.4	407.6	413.6	452.0	experimental	[153]
TPA-DCPP	765.0	762.7	781.4	779.2	669.3	experimental	[97]
TPA-L-BN	451.4	452.9	391.4	392.8	394.0	experimental	[154]
TPA-PPO	493.0	490.9	500.0	497.8	472.0	experimental	[93]
TPA-PyF2	390.2	390.8	379.4	381.1	376.0	experimental	[155]
TPADSO2	450.5	452.0	480.0	482.0	533.3	experimental	[156]
TPB-AC	469.2	469.4	475.9	476.0	370.0	experimental	[157]
TPBPPI-PBI	472.9	473.4	461.4	462.6	429.0	experimental	[49]
TPBPPI-PY	472.2	472.0	459.4	459.9	420.0	experimental	[49]
TPXZ-as-TAZ	888.7	887.8	889.5	891.5	529.0	computational	[158]
TRZ-3SO2	577.4	572.9	540.6	539.9	706.0	experimental	[53]
TSBFB	404.5	403.6	385.1	384.4	395.0	experimental	[57]
TXO-TPA	570.6	566.0	598.6	595.7	603.0	experimental	[135]
VBN0	432.7	433.5	419.5	421.1	482.3	experimental	[159]
XT-T	360.0	360.0	349.2	350.5	478.0	experimental	[160]
[2,1-b]IF	1031.9	586.3	770.2	571.9	347.0	experimental	[55]
dTolmp	435.6	434.6	397.2	396.9	548.0	experimental	[161]
iTPBI-CN	441.4	440.7	432.7	432.1	443.5	experimental	[162]
m-CF3PIBI	492.2	492.6	485.5	486.1	435.3	experimental	[163]
m-CZ-DPS-DMAC	425.1	428.5	423.9	427.9	490.8	experimental	[164]
m-DTPACO	484.6	485.3	501.6	502.8	375.0	experimental	[165]
m-PCzTPD	522.4	522.9	522.1	519.4	506.0	experimental	[166]
m-PO-ABN	509.5	519.6	472.0	481.3	450.0	experimental	[138]
mCP-BP-DMAC	503.7	504.0	504.6	505.0	505.5	experimental	[167]
mCP-BmPy	395.9	399.3	384.9	389.0	410.0	experimental	[168]

TABLE XII – continued from previous page

Molecule	sTDA (Gas)	sTD-DFT (Gas)	sTDA (Tol)	sTD-DFT (Tol)	Ref. (nm)	Type	Citation
mCP-Ph	390.6	394.3	371.4	375.4	350.0	experimental	[168]
mCP-Py	385.2	388.5	372.2	376.2	350.0	experimental	[168]
mCz-TAn-CN	519.1	529.1	483.8	492.6	438.0	experimental	[169]
mP2MPC	450.6	452.1	430.5	432.5	399.0	experimental	[170]
mTPA-PPI	457.5	457.9	443.8	445.0	404.0	experimental	[57]
o-CzOXD	500.3	500.5	477.5	477.5	492.7	experimental	[58]
o-PCzTPD	558.4	555.3	518.5	519.1	485.0	experimental	[166]
oCBP	388.3	392.6	377.0	381.2	389.0	experimental	[171]
p-DTPACO	508.7	510.4	531.9	533.9	540.0	experimental	[165]
p-PCzTPD	555.3	553.3	563.4	561.2	476.0	experimental	[166]
p-PO-ABN	514.8	521.5	488.0	494.6	456.0	experimental	[138]
p-PO15NCzDPA	508.1	518.1	467.2	477.0	427.0	experimental	[172]
pSFIAc2	470.9	479.8	461.4	469.7	451.5	experimental	[151]
pzpy	510.1	519.9	466.8	476.8	458.0	experimental	[173]
t-DABNA	431.1	438.5	418.4	425.5	464.0	experimental	[48]
t3Cz-SO	434.5	440.1	442.9	448.2	446.0	experimental	[91]
tBuCzDBA	757.8	751.2	684.8	678.9	558.5	experimental	[174]
tCTM	483.8	487.0	483.3	483.5	459.0	experimental	[47]
thio-ether	1032.4	586.4	770.0	572.2	366.0	experimental	[55]
t–BuCz2BP	488.8	490.6	490.8	490.3	440.0	experimental	[175]
α-2DMAC-DBP	1177.9	1176.8	1039.5	1038.2	637.5	experimental	[176]
α-DMAC-DBP	1092.4	1092.0	952.2	951.8	622.0	experimental	[176]
β-DI-DBP	961.4	952.3	832.6	825.2	582.5	experimental	[176]

TABLE XIII: Complete validation dataset for singlet-triplet gap predictions. Predictions from sTDA and sTD-DFT methods in gas and toluene phases are compared against experimental/computational literature values. References are provided in the last column.

Molecule	sTDA (Gas)	sTD-DFT (Gas)	sTDA (Tol)	sTD-DFT (Tol)	Ref. (eV)	Type	Citation
11-AcBPdCN	0.3009	0.2809	0.3667	0.3437	0.0650	experimental	[177]
12AcCz-PM	0.2661	0.2631	0.3416	0.3407	0.3900	experimental	[178]
12BTCzTPN	0.1955	0.1766	0.1720	0.1610	0.0829	experimental	[179]
1CM	0.5074	0.4471	0.4934	0.4316	0.2900	experimental	[62]
1CzSO	0.3195	0.2961	0.2972	0.2779	0.2150	experimental	[180]
1PXZP	0.1653	0.1764	0.1692	0.1646	0.2600	computational	[181]
23AcCz-PM	0.2003	0.2120	0.2544	0.2647	0.0600	experimental	[178]
25CzBPym	0.0833	0.0797	0.0929	0.0879	0.0604	experimental	[59]
25DAcBPy	0.0576	0.0575	0.3301	0.3383	0.0235	computational	[182]
25tCzBPym	0.0848	0.0811	0.0917	0.0872	0.0700	experimental	[59]
26DAcBPy	0.1948	0.1907	0.1799	0.1764	0.0070	computational	[182]
26DPXZBPy	0.2012	0.1987	0.1685	0.1661	0.0520	computational	[182]
2BPy-mDTC	0.0798	0.0793	0.0847	0.0849	0.0650	experimental	[60]
2BrCPT	0.2696	0.2431	0.3015	0.2718	0.0400	experimental	[183]
2CM	0.4735	0.4172	0.4762	0.4198	0.3100	experimental	[62]
2Cz-DMAC-BTB	0.2665	0.2823	0.1276	0.1438	0.0200	experimental	[50]
2Cz-DMAC-TTR	0.2933	0.2743	0.3442	0.3199	0.0470	experimental	[50]
2Cz-DMAC-TXO	0.3679	0.3706	0.3220	0.3319	0.0360	experimental	[50]
2Cz2tCzBn	0.1908	0.1730	0.2168	0.1959	0.1300	experimental	[63]
2CzPN	0.2427	0.2373	0.2677	0.2593	0.2525	experimental	[82]
2CzTPEPCz	0.3096	0.3171	0.3311	0.3352	0.1300	experimental	[184]
2DMAC-BP-F	0.2632	0.2475	0.3177	0.2988	0.1367	experimental	[185]
2DN	0.0920	0.0965	0.4000	0.3669	0.0700	experimental	[65]
2F	0.2152	0.1908	0.2374	0.2097	0.2300	computational	[66]
2H-Qz	0.2138	0.2118	0.2326	0.2307	0.1100	experimental	[186]
2Mi2SB	0.3464	0.3356	0.3865	0.3721	0.0300	computational	[187]
2PCzBN	0.3041	0.3010	0.3170	0.3108	0.2800	experimental	[188]
2PCzBN-tPh	0.2207	0.2191	0.2414	0.2386	0.2600	experimental	[188]
2PN	0.1324	0.1285	0.1074	0.1046	0.0100	experimental	[65]

Continued on next page

TABLE XIII – continued from previous page

Molecule	sTDA (Gas)	sTD-DFT (Gas)	sTDA (Tol)	sTD-DFT (Tol)	Ref. (eV)	Type	Citation
2PS-2FPh	0.2729	0.2650	0.3064	0.2983	0.2050	computational	[189]
2PXZ-OXD	0.2031	0.2024	0.1787	0.1783	0.2300	experimental	[190]
2PXZP	0.2176	0.2301	0.2422	0.2410	0.1340	computational	[181]
2SPBAC-BP	0.4008	0.4004	0.4024	0.3933	0.2200	experimental	[191]
2tCz2CzBn	0.1995	0.1807	0.2266	0.2046	0.1300	experimental	[63]
3-ACBPmCN	0.0470	0.0582	0.0519	0.0651	0.1800	computational	[177]
3-AcBPdCN	0.2112	0.2004	0.2667	0.2540	0.1800	experimental	[177]
3-AcBPtCN	0.0637	0.0643	0.2413	0.2319	0.1300	experimental	[177]
3-DPM	0.1689	0.1581	0.1558	0.1492	0.0987	experimental	[192]
35CzBPym	0.1491	0.1382	0.1503	0.1393	0.1100	experimental	[59]
35tCzBPym	0.1484	0.1383	0.1537	0.1431	0.1100	experimental	[59]
36DTPAFM	0.2073	0.2235	0.2241	0.2391	0.1200	experimental	[193]
3BPy-mDTC	0.1555	0.1449	0.1562	0.1456	0.1200	experimental	[60]
3CzBN	0.3294	0.3321	0.3069	0.3081	0.3100	experimental	[72]
3CzPhpPM	0.2409	0.2185	0.2659	0.2406	0.3300	experimental	[194]
3DMAC-BP-Br	0.0203	0.0210	0.2215	0.2151	0.0400	experimental	[195]
3DMAC-BP-CN	0.1852	0.1962	0.2209	0.2142	0.0200	experimental	[195]
3DPA3CN	0.2230	0.2266	0.2186	0.2212	0.1030	experimental	[196]
3Py-DMAC	0.0653	0.0776	0.3069	0.2963	0.0400	experimental	[197]
3TCPM	0.2621	0.2614	0.1934	0.2072	0.2600	experimental	[74]
3ai	0.8060	0.7332	0.8521	0.7687	0.1800	experimental	[198]
4-Ac	0.5593	0.5465	0.6006	0.5815	0.0800	experimental	[199]
4-DPM	0.4478	0.4605	0.4672	0.4791	0.1427	experimental	[192]
4-SCZ	0.4456	0.4094	0.4687	0.4303	0.2400	experimental	[200]
4BPy-mDTC	0.1541	0.1431	0.1477	0.1375	0.1300	experimental	[60]
4CzIPN	0.1507	0.1367	0.1624	0.1487	0.1103	experimental	[201]
4CzTPN	0.2100	0.1874	0.2339	0.2079	0.0800	experimental	[202]
4F-m-ν-DABNA	0.2638	0.2488	0.2657	0.2515	0.0700	experimental	[203]
4F-ν-DABNA	0.2709	0.2560	0.2770	0.2625	0.0500	experimental	[203]
5,6PXZ-PIDO	0.2119	0.2186	0.1857	0.1851	0.4500	computational	[204]
5-Cz-Sac	0.3410	0.3079	0.3315	0.3064	0.2800	experimental	[205]
6,7-DCNQx-DICz	0.0088	0.0143	0.0207	0.0279	0.0276	computational	[206]
6AcBIQ	0.0859	0.0897	0.1004	0.1012	0.1000	experimental	[207]
9CzFDBFSPO	0.3962	0.3615	0.3951	0.3550	0.1200	experimental	[208]
ACID–BPPZ	0.2041	0.2014	0.1581	0.1669	0.0150	computational	[209]
ACRFLCN	0.0002	0.0047	0.0001	0.0002	0.1000	computational	[210]
ACRSA	0.0025	0.0217	-0.0001	0.0000	0.0350	experimental	[211]
ACRXTN	0.4781	0.4642	0.5345	0.5175	0.1730	experimental	[36]
AI-4Cz	0.2055	0.1909	0.2287	0.2140	0.0200	experimental	[212]
ANQDC	0.2365	0.2634	0.2815	0.3132	0.0200	computational	[213]
ANQDC-PSTA	0.0965	0.0948	0.1344	0.1296	0.0800	experimental	[213]
APDC-DTPA	0.2802	0.2713	0.2891	0.3004	0.1400	experimental	[214]
APPT	0.1857	0.1995	0.2290	0.2449	0.0700	experimental	[215]
APPT-PXZ	0.1829	0.1755	0.2201	0.2100	0.0100	computational	[215]
Ac-BPCN	0.3133	0.2940	0.3797	0.3575	0.1300	experimental	[216]
AcCN	0.1610	0.1785	0.1956	0.2129	0.0700	experimental	[79]
AcCYP	0.0725	0.0850	0.0824	0.0981	0.2000	experimental	[217]
B-dpa-Cz	0.4397	0.3954	0.4512	0.4060	0.1500	experimental	[218]
B-dpa-SpiroAC	0.4062	0.3635	0.4135	0.3709	0.1400	experimental	[218]
BCZ-DPS-AD	0.3282	0.2926	0.3383	0.3004	0.0967	experimental	[219]
BDAPM	0.3393	0.3383	0.3593	0.3599	0.0600	experimental	[220]
BDPCC	0.3333	0.3139	0.3425	0.3241	0.1100	experimental	[82]
BDQ-tBuCz	0.1592	0.1565	0.1872	0.1835	0.1800	experimental	[83]
BDQC-2	0.1647	0.1628	0.1856	0.1829	0.1200	experimental	[221]
BDQDMAC	0.0645	0.0647	0.0735	0.0738	0.0750	experimental	[83]
BDQPCz	0.1517	0.1623	0.1728	0.1880	0.4950	experimental	[83]
BFCZPZ1	0.2679	0.2584	0.2793	0.2685	0.3267	experimental	[222]
BFCZPZ2	0.2685	0.2615	0.2917	0.2840	0.3100	experimental	[222]
BMIM	0.2801	0.2712	0.2898	0.3011	0.1400	experimental	[214]
BP-mDTC	0.1928	0.1825	0.1832	0.1774	0.0700	experimental	[60]

TABLE XIII – continued from previous page

Molecule	sTDA (Gas)	sTD-DFT (Gas)	sTDA (Tol)	sTD-DFT (Tol)	Ref. (eV)	Type	Citation
BPCN-2Cz	0.3558	0.3243	0.3590	0.3265	0.2200	experimental	[223]
BPCN-Cz2Ph	0.3042	0.2773	0.3250	0.2965	0.3100	experimental	[223]
BPCP-2CPC	0.1738	0.1724	0.2227	0.2182	0.1660	experimental	[224]
BPZPP	0.1329	0.1344	0.1529	0.1531	0.2000	experimental	[225]
BTCZPZ1	0.2457	0.2342	0.2592	0.2483	0.2400	experimental	[222]
BTD-PXZ	0.1863	0.1829	0.1718	0.1684	0.1300	experimental	[226]
BTITrz	0.2219	0.2224	0.2289	0.2290	0.1025	computational	[227]
BTPBFCz	0.2662	0.2440	0.2687	0.2490	0.0900	experimental	[228]
BTPBFCz-D3	0.2264	0.2157	0.2175	0.2055	0.1200	experimental	[228]
BTPO	0.4356	0.4211	0.4061	0.3864	0.4300	experimental	[229]
BTZPP	0.3066	0.3191	0.2829	0.2942	0.3000	experimental	[84]
BTZ–DMAC	0.1274	0.1340	0.1126	0.1194	0.0200	computational	[230]
BZC-PXZ	0.2407	0.2284	0.2292	0.2175	0.0200	experimental	[231]
BuPCzBCO	0.3702	0.3307	0.3938	0.3517	0.1850	computational	[232]
BzITz	0.2513	0.2477	0.2575	0.2534	0.1850	computational	[233]
CCDC	0.3066	0.2759	0.1276	0.1415	0.2220	computational	[234]
CDBP-BP-DMAC	0.1829	0.1967	0.2389	0.2546	0.0393	experimental	[87]
CDBP-BP-PXZ	0.2877	0.2868	0.2877	0.2862	0.0605	experimental	[87]
CN-QP	0.1557	0.1648	0.1216	0.1341	0.0300	experimental	[88]
CNPP-TPA	0.2225	0.2259	0.2549	0.2570	0.1450	experimental	[235]
CNTPA-CZ	0.5282	0.5166	0.5729	0.5571	0.3500	experimental	[236]
CNTPA-PXZ	0.3266	0.3257	0.3370	0.3364	0.1300	experimental	[236]
CZ-DPS-DMAC	0.3076	0.2840	0.2851	0.2885	0.0700	experimental	[90]
CZ-TRZ	0.2454	0.2302	0.2816	0.2641	0.1500	experimental	[237]
CZ9CZPZ	0.2859	0.2751	0.3162	0.3040	0.3150	experimental	[222]
Cz-SO	0.3954	0.3540	0.3935	0.3540	0.4100	experimental	[91]
CzDCbTrz	0.1759	0.1760	0.2349	0.2348	0.1200	experimental	[238]
CzPm	0.2873	0.2766	0.3039	0.2960	0.1800	experimental	[239]
CzmPPC	0.1031	0.1273	0.0742	0.0936	0.2800	experimental	[240]
CzoB	0.0786	0.0780	0.0975	0.1027	0.0900	computational	[241]
DAcIPN	0.3427	0.3327	0.3332	0.3215	0.0350	experimental	[242]
DBCP	0.0634	0.0645	0.0814	0.1017	0.0813	experimental	[243]
DBQ-3PXZ	0.1057	0.1015	0.0955	0.0920	0.0300	experimental	[54]
DBT-BZ-DMAC	0.3142	0.3200	0.3062	0.3102	0.0800	experimental	[97]
DC-ACR	0.0033	0.0030	0.0366	0.0414	0.0100	experimental	[244]
DC-TC	0.0052	0.0048	0.0056	0.0054	0.1400	experimental	[244]
DCPDAPM	0.0701	0.0701	0.5171	0.4998	0.1300	computational	[245]
DCz-DPPZ	0.1560	0.1490	0.2024	0.1931	0.1900	experimental	[246]
DCzBNPh-1	0.2563	0.2378	0.3209	0.2983	0.5000	experimental	[44]
DCzIPN	0.3588	0.3410	0.3593	0.3429	0.1433	experimental	[99]
DDMA-TXO2	0.5414	0.5304	0.4180	0.3968	0.2200	experimental	[247]
DDPhCz-DPPZ	0.1229	0.1229	0.1514	0.1470	0.1600	experimental	[246]
DFDBQPXZ	0.1692	0.1691	0.1596	0.1589	0.0000	experimental	[248]
DHID-DBS	0.4448	0.4129	0.4697	0.4490	0.3300	experimental	[102]
DHID-DPS	0.5477	0.5208	0.4687	0.4470	0.1800	experimental	[102]
DHPZ-2BI	0.2115	0.2147	0.2053	0.2075	0.1900	experimental	[249]
DMAC-11-DPPZ	0.0560	0.0574	0.0714	0.0723	0.0803	experimental	[103]
DMAC-AQ	0.4361	0.4090	0.4923	0.4663	0.0633	experimental	[250]
DMAC-BP	0.0644	0.0658	0.5157	0.4999	0.0700	experimental	[251]
DMAC-Cz	0.4201	0.3912	0.4611	0.4309	0.0007	experimental	[105]
DMAC-Cz-TTR	0.2709	0.2527	0.2312	0.2200	0.0660	experimental	[105]
DMAC-DPS	0.2222	0.2229	0.2340	0.2343	0.0100	experimental	[106]
DMAC-FO	0.1247	0.1195	0.3839	0.3734	0.1400	experimental	[252]
DMAC-PCN	0.1341	0.1504	0.1133	0.1292	0.1300	experimental	[168]
DMAC-TRZ	0.0485	0.0571	0.0494	0.0510	0.0500	experimental	[253]
DMACMNPTO	0.5377	0.5222	0.5471	0.5302	0.2050	experimental	[108]
DMBFTX	0.5437	0.4736	0.5723	0.5002	0.2800	experimental	[254]
DMIC-TRZ	0.5193	0.6832	0.7550	1.3766	0.0560	experimental	[255]
DMeCzIPN	0.2790	0.2669	0.2781	0.2657	0.0910	experimental	[99]
DPACPhTPI	0.2551	0.2503	0.2498	0.2437	0.7200	experimental	[109]

TABLE XIII – continued from previous page

Molecule	sTDA (Gas)	sTD-DFT (Gas)	sTDA (Tol)	sTD-DFT (Tol)	Ref. (eV)	Type	Citation
DPACpBr	0.3348	0.3322	0.4044	0.3961	0.0020	experimental	[110]
DPE	0.2845	0.2840	0.2987	0.2980	0.1800	computational	[256]
DPE-DDMAc	0.1751	0.1961	0.2781	0.3000	0.1800	computational	[256]
DPE-DPXZ	0.2852	0.2849	0.2996	0.2988	0.2000	experimental	[256]
DPIBPZ-DPXZ	0.1101	0.1057	0.1073	0.1034	0.0500	experimental	[257]
DPS-PXZ	0.2879	0.2873	0.3129	0.3120	0.0500	experimental	[112]
DPXZ-DPPM	0.1047	0.1014	0.1043	0.1013	0.0470	experimental	[113]
DQP	0.0189	0.0396	0.0164	0.0402	0.0555	experimental	[97]
DTPTCzDP-CN	0.2642	0.2402	0.2493	0.2321	0.0300	experimental	[258]
DV-3CzCN	0.2477	0.2398	0.3404	0.3364	0.2300	experimental	[116]
DVCz-2CzCN	0.2868	0.2623	0.2421	0.2332	0.1600	experimental	[117]
DiCz-Sac	0.2404	0.2322	0.2562	0.2469	0.2000	experimental	[205]
ECDPTT	0.3447	0.3433	0.3385	0.3331	0.0800	experimental	[259]
F2AcBO	0.2847	0.2918	0.2588	0.2545	0.0750	experimental	[119]
FAC	0.5171	0.4920	0.5458	0.5144	0.0900	computational	[260]
FDQPXZ	0.1276	0.1217	0.1281	0.1225	0.0450	experimental	[261]
FSF4A	0.2862	0.2912	0.2898	0.2923	0.0220	experimental	[262]
Fene	0.1297	0.1378	0.1967	0.2089	0.0250	computational	[263]
Fens	0.2404	0.2561	0.3481	0.3589	0.0200	computational	[263]
FlCz	0.1952	0.2170	0.2129	0.2360	0.5100	experimental	[121]
IABTCN	0.3551	0.3561	0.3843	0.3786	0.3998	experimental	[122]
ICBNTrz4	0.2041	0.1993	0.2097	0.2048	0.1000	experimental	[264]
IDAC-MCO	0.4472	0.3996	0.4200	0.3755	0.0900	experimental	[265]
IDFL-2DPA	0.2454	0.2221	0.2493	0.2259	0.4500	experimental	[266]
IQ-Se	0.3316	0.3254	0.4327	0.4125	1.1800	computational	[267]
IpCm-PhBzAc	0.5082	0.4902	0.5207	0.5015	0.3500	experimental	[268]
MBF	0.2198	0.2225	0.2260	0.2181	0.0100	experimental	[125]
MCZ-P2-DTM	0.2697	0.2587	0.2716	0.2621	0.2300	experimental	[35]
MPA	0.2598	0.2577	0.2572	0.2543	0.1400	experimental	[125]
MPPA	0.1960	0.1890	0.1952	0.1867	0.1743	experimental	[126]
Me-DMAC	0.1117	0.1283	0.1387	0.1562	0.0100	experimental	[127]
Me-DOC	0.4294	0.3786	0.4302	0.3763	0.2400	computational	[269]
Me-MOC	0.3803	0.3386	0.3800	0.3370	0.2500	computational	[269]
Me2ACBO	0.3142	0.3054	0.2883	0.2898	0.0500	experimental	[119]
MeOCzPCN	0.4683	0.4467	0.4954	0.4673	0.0100	experimental	[270]
NA-TNA	0.4044	0.4138	0.4040	0.4137	0.2400	experimental	[128]
NAI–PhBiFA	0.3697	0.3820	0.2973	0.3055	0.1200	experimental	[129]
NIDPA-1	0.3876	0.3588	0.4076	0.3773	0.6000	experimental	[271]
NPE-AcDPS	0.4903	0.4850	0.3559	0.3563	0.0300	experimental	[272]
NyDPAc	0.1657	0.1819	0.1808	0.1987	0.1520	experimental	[273]
NyDPO	0.1494	0.1611	0.1945	0.2037	0.0333	computational	[274]
OCzBN	0.3704	0.3466	0.4579	0.4450	0.1400	experimental	[132]
OPDPO	0.1450	0.1626	0.0857	0.0813	0.1300	experimental	[184]
P4CzCN–BCz	0.6006	0.6278	0.6999	0.7319	0.1700	experimental	[133]
PBICT	0.2132	0.1980	0.3424	0.3194	0.0280	experimental	[206]
PFBP-2b	0.1515	0.1519	0.1663	0.1583	0.0600	experimental	[275]
PIAnTPh	0.7770	0.7391	0.8291	0.7873	1.1400	experimental	[137]
PO-TPA	0.1934	0.1883	0.3355	0.3190	0.2500	experimental	[276]
PPO21	0.3775	0.3353	0.3825	0.3406	0.0253	computational	[277]
PPZPPI	0.2203	0.2236	0.2151	0.2175	0.1100	experimental	[278]
PPZTPI	0.2232	0.2276	0.2160	0.2192	0.1100	experimental	[278]
PS-BZ-DMAC	0.5560	0.5307	0.5994	0.5716	0.0045	experimental	[140]
PSPBP	0.2941	0.2927	0.2819	0.2814	0.1100	experimental	[279]
PSPP	0.3194	0.3148	0.3162	0.3119	0.1100	experimental	[279]
PT-BZ-DMAC	0.0678	0.0852	0.0520	0.0640	0.0084	experimental	[140]
PTPC	0.2440	0.2387	0.2293	0.2245	0.6355	experimental	[280]
PTZ-2PTO	0.2932	0.2868	0.2926	0.2929	0.2700	experimental	[141]
PTZ-DCPP	0.2776	0.2665	0.3429	0.3333	0.1867	experimental	[281]
PTZ-NAI	0.0003	0.0003	0.1172	0.1133	0.0867	experimental	[38]
PX-TRZ	0.2424	0.2355	0.2529	0.2507	0.0130	experimental	[142]

TABLE XIII – continued from previous page

Molecule	sTDA (Gas)	sTD-DFT (Gas)	sTDA (Tol)	sTD-DFT (Tol)	Ref. (eV)	Type	Citation
PXZ-10-DPPZ	0.0924	0.0891	0.0913	0.0886	0.0365	experimental	[103]
PXZ-11-DPPZ	0.1207	0.1154	0.1309	0.1255	0.0507	experimental	[103]
PXZ-BOO	0.2410	0.2297	0.2536	0.2410	0.0600	experimental	[282]
PXZ-NAI	0.2654	0.2530	0.3109	0.2946	0.0600	experimental	[38]
PXZ-PPO	0.5104	0.4859	0.5382	0.5229	0.6000	experimental	[282]
PXZ-QL	0.3702	0.3444	0.3846	0.3576	0.1000	computational	[283]
PXZ2PTO	0.3385	0.3358	0.3417	0.3392	0.0233	experimental	[143]
PhQLPXZ	0.1369	0.1437	0.1971	0.2118	0.0900	experimental	[261]
PrDPhAc	0.4722	0.4514	0.5308	0.5046	0.0750	computational	[284]
Pra-2DMAC	0.5074	0.4925	0.5244	0.5098	0.4400	experimental	[145]
PxCN	0.2607	0.2601	0.2562	0.2557	0.0367	experimental	[79]
PxCYP	0.2325	0.2438	0.2431	0.2422	0.2000	experimental	[217]
PxPYM	0.1691	0.1801	0.2358	0.2454	0.0100	computational	[285]
Py-TPA	0.1253	0.1357	0.1337	0.1335	0.1400	computational	[286]
PyDCN–DMAC	0.2456	0.2665	0.3176	0.3359	0.0100	experimental	[46]
PyIAnTPh	0.7218	0.6752	0.7861	0.7350	1.1400	experimental	[137]
SAF-2NP	0.0816	0.0812	0.0892	0.0874	0.0400	computational	[287]
SBA-2DPS	0.4557	0.4531	0.3631	0.3818	0.0900	experimental	[37]
SBDBQ-PXZ	0.1089	0.1046	0.1198	0.1154	0.0700	experimental	[54]
SBF-PXZ	0.3045	0.3048	0.3249	0.3241	0.2600	experimental	[288]
SBTF	0.5022	0.4954	0.5297	0.5222	0.2000	experimental	[289]
SFAC-BP-SFAC	0.0774	0.0786	0.0898	0.0919	0.0360	experimental	[148]
SFCz	0.2013	0.2131	0.2129	0.2257	0.4800	experimental	[121]
SFI23pPM	0.2328	0.2146	0.2600	0.2406	0.3300	experimental	[194]
SIR-A	0.0001	0.0002	0.0000	0.0001	0.0160	experimental	[290]
SIR-B	0.0070	0.0083	0.0015	0.0017	0.0140	experimental	[290]
SIR-C	0.0082	0.0089	-0.0005	-0.0002	0.0150	experimental	[290]
SPAC-FO	0.1398	0.1339	0.1384	0.1326	0.1300	experimental	[252]
SPFS-PXZ	0.3291	0.3293	0.3238	0.3229	0.0153	experimental	[291]
STAC-BP-STAC	0.0858	0.0874	0.1261	0.1271	0.0520	experimental	[148]
SXAC-BP-SXAC	0.0835	0.0851	0.0929	0.0948	0.0610	experimental	[148]
SiTCNCz	0.2497	0.2300	0.2626	0.2416	0.1300	experimental	[292]
Spiro-CN	0.2889	0.2968	0.2696	0.2768	5.5000	experimental	[293]
SpiroAC-TRZ	0.0677	0.0679	0.0597	0.0616	0.0720	experimental	[97]
TATP-BP	0.1452	0.1464	0.1292	0.1354	0.1290	experimental	[150]
TBPe	0.7123	0.6662	0.7738	0.7233	0.1200	computational	[294]
TCPZ	0.5340	0.5069	0.5735	0.5469	0.1400	experimental	[295]
TCZ1	0.4017	0.3602	0.4205	0.3767	0.0160	experimental	[242]
TCz1	0.4013	0.3599	0.4206	0.3771	0.1000	experimental	[296]
TCzTrz	0.1798	0.1783	0.2079	0.2050	0.1400	experimental	[238]
TMDBP	0.5203	0.5192	0.5528	0.5493	0.1000	experimental	[297]
TNPZ	0.0818	0.0930	0.0960	0.1087	0.1700	computational	[298]
TPA-2	0.0416	0.0478	0.1131	0.1203	0.1450	experimental	[299]
TPA-DCPP	0.1746	0.1796	0.1812	0.1855	0.1480	experimental	[97]
TPADSO2	0.4055	0.3964	0.3925	0.3818	0.3800	experimental	[156]
TPAPm	0.4500	0.4557	0.4763	0.4820	0.3200	experimental	[300]
TPD4PA	0.3244	0.2950	0.3337	0.3056	0.0500	experimental	[301]
TPSi-F	0.6295	0.6174	0.6494	0.6375	0.1000	experimental	[302]
TPXZ-as-TAZ	0.0953	0.0968	0.1079	0.1048	0.2200	experimental	[158]
TPXZ–as-TAZ	0.0983	0.0984	0.0271	0.0357	0.0300	experimental	[303]
TRZ-pIC	0.4296	0.3745	0.4447	0.3877	0.2900	experimental	[304]
TX-CzPh	0.5513	0.4893	0.5517	0.4916	0.6700	computational	[305]
TXO-P-Si	-0.0053	-0.0056	-0.0027	-0.0027	0.5222	experimental	[277]
Tri-PXZ-PCN	0.1726	0.1682	0.1583	0.1532	0.0500	experimental	[306]
TrisCz-Trz	0.1356	0.1368	0.2203	0.2251	0.0700	experimental	[307]
UGH3	-0.0012	0.0083	0.0170	0.0280	0.2200	experimental	[247]
VBC-PTZ	0.4336	0.4376	0.4823	0.4872	0.5300	experimental	[308]
VBN0	0.3552	0.3499	0.4127	0.4015	0.1100	experimental	[159]
V–TPA	0.2797	0.2756	0.2992	0.2941	0.6210	experimental	[309]
Yad	0.3868	0.3562	0.4022	0.3704	0.0200	computational	[263]

TABLE XIII – continued from previous page

Molecule	sTDA (Gas)	sTD-DFT (Gas)	sTDA (Tol)	sTD-DFT (Tol)	Ref. (eV)	Type	Citation
czpzpy	0.4202	0.3853	0.4351	0.3990	0.1300	experimental	[310]
dbG2TAZ	0.4466	0.4517	0.4754	0.4820	0.5300	experimental	[311]
m-CZ-DPS-DMAC	0.3204	0.2975	0.3722	0.3450	0.2100	experimental	[164]
m-DTPACO	0.3172	0.3132	0.3495	0.3436	0.2100	experimental	[165]
m-ν-DABNA	0.2892	0.2722	0.2900	0.2738	0.0700	experimental	[203]
m2Cz2Trz	0.1515	0.1484	0.1759	0.1742	0.0900	experimental	[312]
mCP-BP-DMAC	0.2872	0.2856	0.2875	0.2859	0.0160	experimental	[167]
mDPBPZ-DPXZ	0.1066	0.1030	0.1053	0.1025	0.0200	computational	[257]
mP2MPC	0.2837	0.2741	0.2978	0.2844	0.6500	experimental	[170]
mPTBC	0.2343	0.2243	0.2175	0.2081	0.0060	experimental	[313]
mTPA–PPI	0.2582	0.2558	0.2701	0.2628	0.7600	experimental	[314]
oPTBC	0.1336	0.1284	0.1281	0.1232	0.0070	experimental	[313]
p-DTPACO	0.4180	0.4096	0.4450	0.4365	0.0500	experimental	[165]
pDPAPQ-PXZ	0.1777	0.1708	0.1956	0.1877	0.0600	experimental	[315]
pDPBPZ-PXZ	0.0906	0.0982	0.0988	0.1070	0.0600	experimental	[315]
pDTCz-2DPyS	0.2269	0.2264	0.2872	0.2793	0.2100	experimental	[316]
pSFIAc2	0.3667	0.3178	0.3779	0.3305	0.3100	experimental	[151]
t-BuPCz	0.3330	0.2985	0.3504	0.3140	0.0800	experimental	[317]
t-DABNA	0.4476	0.3993	0.4608	0.4111	0.1600	experimental	[318]
t3Cz-SO	0.3555	0.3196	0.3436	0.3105	0.2600	experimental	[91]
tCbz-mPYRs	0.2990	0.2843	0.3273	0.3107	0.4150	computational	[319]
t–BuCz2BP	0.3370	0.3279	0.3345	0.3371	0.2150	experimental	[175]
α-2CbPN	0.2931	0.2856	0.3139	0.3036	0.2600	experimental	[238]
α-2DMAC-DBP	0.0552	0.0562	0.0580	0.0595	0.0250	experimental	[176]
α-DMAC-DBP	0.0521	0.0525	0.0511	0.0517	0.0925	experimental	[176]
β-DI-DBP	0.1070	0.1192	0.1275	0.1408	0.1600	experimental	[176]
δ-2CbPN	0.2610	0.2545	0.2760	0.2673	0.1300	experimental	[238]

B. Data Availability

All computational data, analysis scripts, and molecular structures are available at https://github.com/TchapetNjafa.

VI. ACKNOWLEDGMENTS

[1] Hiroki Uoyama, Kenichi Goushi, Katsuyuki Shizu, Hiroko Nomura, and Chihaya Adachi. Highly efficient organic light-emitting diodes from delayed fluorescence. *Nature*, 492(7428):234–238, December 2012. ISSN 1476-4687. doi: 10.1038/nature11687.

[2] Chihaya Adachi. Third-generation organic electroluminescence materials. *Japanese Journal of Applied Physics*, 53(6): 060101, May 2014. ISSN 1347-4065. doi:10.7567/jjap.53.060101.

[3] Yuchao Liu, Chensen Li, Zhongjie Ren, Shouke Yan, and Martin R. Bryce. All-organic thermally activated delayed fluorescence materials for organic light-emitting diodes. *Nature Reviews Materials*, 3(4):18020, apr 2018. doi: 10.1038/natrevmats.2018.20.

[4] Fernando B Dias, Thomas J Penfold, and Andrew P Monkman. Photophysics of thermally activated delayed fluorescence molecules. *Methods and applications in fluorescence*, 5(1):012001, mar 2017. doi:10.1088/2050-6120/aa537e.

[5] Xian-Kai Chen, Dongwook Kim, and Jean-Luc Brédas. Thermally activated delayed fluorescence (tadf) path toward efficient electroluminescence in purely organic materials: Molecular level insight. *Accounts of Chemical Research*, 51(9): 2215, aug 2018. doi:10.1021/acs.accounts.8b00174.

[6] Y. Olivier, J.-C. Sancho-Garcia, L. Muccioli, G. D'Avino, and D. Beljonne. Computational design of thermally activated delayed fluorescence materials: The challenges ahead. *The Journal of Physical Chemistry Letters*, 9(20):6149–6163, sep 2018. doi:10.1021/acs.jpclett.8b02327. URL `https://doi.org/10.1021/acs.jpclett.8b02327`.

[7] Rafael Gómez-Bombarelli, Jorge Aguilera-Iparraguirre, Timothy D. Hirzel, David Duvenaud, Dougal Maclaurin, Martin A. Blood-Forsythe, Hyun Sik Chae, Markus Einzinger, Dong-Gwang Ha, Tony Wu, Georgios Markopoulos, Soonok Jeon, Hosuk Kang, Hiroshi Miyazaki, Masaki Numata, Sunghan Kim, Wenliang Huang, Seong Ik Hong, Marc Baldo, Ryan P. Adams, and Alán Aspuru-Guzik. Design of efficient molecular organic light-emitting diodes by a high-throughput virtual screening and experimental approach. *Nature Materials*, 15(10):1120–1127, aug 2016. doi:10.1038/nmat4717.

[8] Sunwoo Kang and Taekyung Kim. Comparative study of tddft and tddft-based steom-dlpno-ccsd calculations for predicting the excited-state properties of mr-tadf. *Heliyon*, 10(10):e30926, May 2024. ISSN 2405-8440. doi:10.1016/j.heliyon.2024.e30926.

[9] Xiugang Wu, Songqian Ni, Chih-Hsing Wang, Weiguo Zhu, and Pi-Tai Chou. Comprehensive review on the structural diversity and versatility of multi-resonance fluorescence emitters: Advance, challenges, and prospects toward oleds. *Chemical Reviews*, May 2025. ISSN 1520-6890. doi:10.1021/acs.chemrev.5c00021.

[10] Y. Olivier, B. Yurash, L. Muccioli, G. D'Avino, O. Mikhnenko, J. C. Sancho-García, C. Adachi, T.-Q. Nguyen, and D. Beljonne. Nature of the singlet and triplet excitations mediating thermally activated delayed fluorescence. *Physical Review Materials*, 1(7):075602, dec 2017. doi:10.1103/PhysRevMaterials.1.075602.

[11] Andreas Dreuw and Martin Head-Gordon. Failure of time-dependent density functional theory for long-range charge-transfer excited states: The zincbacteriochlorin-bacteriochlorin and bacteriochlorophyll-spheroidene complexes. *Journal of the American Chemical Society*, 126(12):4007–4016, March 2004. ISSN 1520-5126. doi:10.1021/ja039556n.

[12] Jan-Michael Mewes. Modeling tadf in organic emitters requires a careful consideration of the environment and going beyond the franck–condon approximation. *Physical Chemistry Chemical Physics*, 20(18):12454–12469, 2018. doi:10.1039/c8cp01792a.

[13] Denis Jacquemin, Valérie Wathelet, Eric A. Perpète, and Carlo Adamo. Extensive td-dft benchmark: Singlet-excited states of organic molecules. *Journal of Chemical Theory and Computation*, 5(9):2420–2435, aug 2009. doi:10.1021/ct900298e.

[14] Thomas Froitzheim, Stefan Grimme, and Jan-Michael Mewes. Either accurate singlet-triplet gaps or excited-state structures: Testing and understanding the performance of td-dft for tadf emitters. *Journal of Chemical Theory and Computation*, 18(12):7702–7713, November 2022. ISSN 1549-9626. doi:10.1021/acs.jctc.2c00905. URL `https://doi.org/10.1021/acs.jctc.2c00905`.

[15] Lukas Kunze, Andreas Hansen, Stefan Grimme, and Jan-Michael Mewes. Pcm-roks for the description of charge-transfer states in solution: Singlet–triplet gaps with chemical accuracy from open-shell kohn–sham reaction-field calculations. *The Journal of Physical Chemistry Letters*, 12(35):8470–8480, August 2021. ISSN 1948-7185. doi:10.1021/acs.jpclett.1c02299.

[16] Adèle D. Laurent and Denis Jacquemin. Td-dft benchmarks: A review. *International Journal of Quantum Chemistry*, 113 (17):2019–2039, April 2013. ISSN 0020-7608. doi:10.1002/qua.24438.

[17] Christoph Bannwarth, Eike Caldeweyher, Sebastian Ehlert, Andreas Hansen, Philipp Pracht, Jakob Seibert, Sebastian Spicher, and Stefan Grimme. Extended tight-binding quantum chemistry methods. *WIREs Computational Molecular Science*, 11(2):e1493, August 2021. ISSN 1759-0884. doi:10.1002/wcms.1493.

[18] Stefan Grimme and Christoph Bannwarth. Ultra-fast computation of electronic spectra for large systems by tight-binding based simplified tamm-dancoff approximation (stda-xtb). *The Journal of Chemical Physics*, 145(5):054103, August 2016. ISSN 0021-9606. doi:10.1063/1.4959605.

[19] Marc de Wergifosse and Stefan Grimme. Perspective on Simplified Quantum Chemistry Methods for Excited States and Response Properties. *Journal of Physical Chemistry A*, 125(18):3841–3851, May 2021. doi:10.1021/acs.jpca.1c02362.

[20] Marc de Wergifosse and Stefan Grimme. The exact integral simplified time-dependent density functional theory (xstd-dft). *The Journal of Chemical Physics*, 160(20), May 2024. ISSN 1089-7690. doi:10.1063/5.0206380.

[21] Stefan Grimme. A simplified tamm-dancoff density functional approach for the electronic excitation spectra of very large molecules. *The Journal of Chemical Physics*, 138(24):244104–244104, June 2013. ISSN 0021-9606. doi:10.1063/1.4811331.

[22] Dingyun Huang and Jacqueline M. Cole. A database of thermally activated delayed fluorescent molecules auto-generated from scientific literature with chemdataextractor. *Scientific Data*, 11(1), January 2024. ISSN 2052-4463. doi:10.1038/s41597-023-02897-3.

[23] M. Moral, L. Muccioli, W.-J. Son, Y. Olivier, and J. C. Sancho-García. Theoretical rationalization of the singlet–triplet gap in oleds materials: Impact of charge-transfer character. *Journal of Chemical Theory and Computation*, 11(1):168–177, dec 2015. doi:10.1021/ct500957s.

[24] Piotr de Silva, Changhae Andrew Kim, Tianyu Zhu, and Troy Van Voorhis. Extracting design principles for efficient thermally activated delayed fluorescence (tadf) from a simple four-state model. *Chemistry of Materials*, 31(17):6995–7006, June 2019. ISSN 1520-5002. doi:10.1021/acs.chemmater.9b01601.

[25] Ke Zhao, Ömer H. Omar, Tahereh Nematiaram, Daniele Padula, and Alessandro Troisi. Novel thermally activated delayed fluorescence materials by high-throughput virtual screening: going beyond donor-acceptor design. *Journal of Materials Chemistry C*, 9(9):3324–3333, 2021. ISSN 2050-7534. doi:10.1039/D1TC00002K. URL `http://dx.doi.org/10.1039/D1TC00002K`.

[26] Christoph Bannwarth, Sebastian Ehlert, and Stefan Grimme. Gfn2-xtb—an accurate and broadly parametrized self-consistent tight-binding quantum chemical method with multipole electrostatics and density-dependent dispersion contributions. *Journal of chemical theory and computation*, 15(3):1652–1671, 2019. ISSN 1549-9618. doi:10.1021/acs.jctc.8b01176.

[27] Sebastian Ehlert, Marcel Stahn, Sebastian Spicher, and Stefan Grimme. Robust and efficient implicit solvation model for fast semiempirical methods. *Journal of Chemical Theory and Computation*, 17(7):4250–4261, 2021. ISSN 1549-9618. doi:10.1021/acs.jctc.1c00471.

[28] Ángel José Pérez-Jiménez, Yoann Olivier, and Juan Carlos Sancho-García. The role of theoretical calculations for invest systems: Complementarity between theory and experiments and rationalization of the results. *Advanced Optical Materials*, March 2025. ISSN 2195-1071. doi:10.1002/adom.202403199.

[29] Stefan Grimme, Christoph Bannwarth, and Philip Shushkov. A robust non-self-consistent tight-binding quantum chemistry method for large molecules. *Journal of Chemical Theory and Computation*, 13(5):1989–2009, April 2017. ISSN 1549-9618. doi:10.1021/acs.jctc.7b00118.

[30] Paolo Tosco Greg Landrum, Ricardo Rodriguez Brian Kelley, sriniker David Cosgrove, gedeck Riccardo Vianello, Gareth Jones NadineSchneider, Dan Nealschneider Eisuke Kawashima, Brian Cole Andrew Dalke, Samo Turk Matt Swain, Alain Vaucher Aleksandr Savelev, Ichiru Take Maciej Wójcikowski, Rachel Walker Vincent F. Scalfani, Daniel Probst Kazuya Ujihara, Axel Pahl guillaume godin, Juuso Lehtivarjo, Francois Berenger, et al. Rdkit: Open-source cheminformatics, 2006. URL https://www.rdkit.org;https://doi.org/10.5281/zenodo.591637.

[31] Philipp Pracht, Fabian Bohle, and Stefan Grimme. Automated exploration of the low-energy chemical space with fast quantum chemical methods. *Physical Chemistry Chemical Physics*, 22(14):7169–7192, 2020. ISSN 1463-9076. doi:10.1039/c9cp06869d.

[32] Philipp Pracht, Stefan Grimme, Christoph Bannwarth, Fabian Bohle, Sebastian Ehlert, Gereon Feldmann, Johannes Gorges, Marcel Müller, Tim Neudecker, Christoph Plett, Sebastian Spicher, Pit Steinbach, Patryk A. Wesołowski, and Felix Zeller. CREST—A program for the exploration of low-energy molecular chemical space. *The Journal of Chemical Physics*, 160(11):114110, 03 2024. ISSN 0021-9606. doi:10.1063/5.0197592. URL https://doi.org/10.1063/5.0197592.

[33] Stefan Grimme. Exploration of chemical compound, conformer, and reaction space with meta-dynamics simulations based on tight-binding quantum chemical calculations. *Journal of chemical theory and computation*, 15(5):2847–2862, 2019. doi:10.1021/acs.jctc.9b00143.

[34] Rajendra Kumar Konidena, Junseop Lim, and Jun Yeob Lee. A novel molecular design featuring the conversion of inefficient tadf emitters into efficient tadf emitters for deep-blue organic light emitting diodes. *Chemical Engineering Journal*, 416:129097, July 2021. ISSN 1385-8947. doi:10.1016/j.cej.2021.129097. URL http://dx.doi.org/10.1016/j.cej.2021.129097.

[35] Fulong Ma, Yu Cheng, Xiuxuan Zhang, Xiaofei Gu, Yu Zheng, Kamvan Hasrat, and Zhengjian Qi. Enhancing performance for blue tadf emitters by introducing intramolecular ch···n hydrogen bonding between donor and acceptor. *Dyes and Pigments*, 166:245–253, July 2019. ISSN 0143-7208. doi:10.1016/j.dyepig.2019.03.016. URL http://dx.doi.org/10.1016/j.dyepig.2019.03.016.

[36] Zhuangzhuang Wei, Tao Zuo, Shanshan Jiang, Fangfang Qi, Mingxue Yang, Lingyi Meng, and Can-Zhong Lu. Theoretically elucidating high photoluminescence performance of dimethylacridan-based blue-color thermally activated delayed fluorescent materials. *New Journal of Chemistry*, 46(7):3464–3471, 2022. ISSN 1369-9261. doi:10.1039/d1nj05251a. URL http://dx.doi.org/10.1039/D1NJ05251A.

[37] Xuan Zeng, Kuan-Chung Pan, Wei-Kai Lee, Shaolong Gong, Fan Ni, Xiao Xiao, Weixuan Zeng, Yepeng Xiang, Lisi Zhan, Yu Zhang, Chung-Chih Wu, and Chuluo Yang. High-efficiency pure blue thermally activated delayed fluorescence emitters with a preferentially horizontal emitting dipole orientation via a spiro-linked double d-a molecular architecture. *Journal of Materials Chemistry C*, 7(35):10851–10859, 2019. ISSN 2050-7534. doi:10.1039/c9tc03582f. URL http://dx.doi.org/10.1039/C9TC03582F.

[38] Binyan Wang, Yuanyuan Zheng, Tao Wang, Dongge Ma, and Qiang Wang. 1,8-naphthalimide-based hybrids for efficient red thermally activated delayed fluorescence organic light-emitting diodes. *Organic Electronics*, 88:106012, January 2021. ISSN 1566-1199. doi:10.1016/j.orgel.2020.106012. URL http://dx.doi.org/10.1016/j.orgel.2020.106012.

[39] Diptarka Hait, Tianyu Zhu, David P. McMahon, and Troy Van Voorhis. Prediction of excited-state energies and singlet–triplet gaps of charge-transfer states using a restricted open-shell kohn–sham approach. *Journal of Chemical Theory and Computation*, 12(7):3353–3359, jun 2016. doi:10.1021/acs.jctc.6b00426.

[40] T. Northey, J. Stacey, and T. J. Penfold. The role of solid state solvation on the charge transfer state of a thermally activated delayed fluorescence emitter. *Journal of Materials Chemistry C*, 5(42):11001–11009, 2017. doi:10.1039/c7tc04099g.

[41] Tian Lu. A comprehensive electron wavefunction analysis toolbox for chemists, Multiwfn. *The Journal of Chemical Physics*, 161(8):082503, 08 2024. ISSN 0021-9606. doi:10.1063/5.0216272. URL https://doi.org/10.1063/5.0216272.

[42] Thibaud Etienne, Xavier Assfeld, and Antonio Monari. Toward a quantitative assessment of electronic transitions' charge-transfer character. *Journal of Chemical Theory and Computation*, 10(9):3896–3905, aug 2014. doi:10.1021/ct5003994.

[43] Tangui Le Bahers, Carlo Adamo, and Ilaria Ciofini. A qualitative index of spatial extent in charge-transfer excitations. *Journal of Chemical Theory and Computation*, 7(8):2498–2506, jul 2011. doi:10.1021/ct200308m.

[44] Xianju Yan, Zong Cheng, Tong Yang, Chenglong Li, and Yue Wang. Carbazole-benzonitrile based organic semiconductors: Synthesis, characterization and electroluminescent property. *Organic Electronics*, 102:106445, March 2022. ISSN 1566-1199. doi:10.1016/j.orgel.2022.106445. URL http://dx.doi.org/10.1016/j.orgel.2022.106445.

[45] Jingwei Li, Xinyong Liu, Xu Qiu, Wenxin Zhai, Xiyun Ye, Lei Xu, and Dehua Hu. Highly efficient deep-blue oleds with cie closely approaches rec.2020 standard based on an acridine–naphthalene hybrid fluorophore. *Dyes and Pigments*, 198:110030, February 2022. ISSN 0143-7208. doi:10.1016/j.dyepig.2021.110030. URL http://dx.doi.org/10.1016/j.dyepig.2021.110030.

[46] Ruizhi Dong, Di Liu, Jiuyan Li, Mengyao Ma, Yongqiang Mei, Deli Li, and Jingyang Jiang. Acceptor modulation for blue and yellow tadf materials and fabrication of all-tadf white oled. *Materials Chemistry Frontiers*, 6(1):40–51, 2022. ISSN 2052-1537. doi:10.1039/d1qm01303c. URL `http://dx.doi.org/10.1039/D1QM01303C`.

[47] Ji-Hua Tan, Wen-Cheng Chen, Shao-Fei Ni, Zhipeng Qiu, Yingying Zhan, Zhiwen Yang, Jingwen Xiong, Chen Cao, Yanping Huo, and Chun-Sing Lee. Aggregation-state engineering and emission switching in d-a-d' aiegens featuring dual emission, mcl and white electroluminescence. *Journal of Materials Chemistry C*, 8(24):8061–8068, 2020. ISSN 2050-7534. doi:10.1039/d0tc01733g. URL `http://dx.doi.org/10.1039/D0TC01733G`.

[48] Kyung Hyung Lee and Jun Yeob Lee. Phosphor sensitized thermally activated delayed fluorescence organic light-emitting diodes with ideal deep blue device performances. *Journal of Materials Chemistry C*, 7(28):8562–8568, 2019. ISSN 2050-7534. doi:10.1039/c9tc02746g. URL `http://dx.doi.org/10.1039/C9TC02746G`.

[49] Jie-Ji Zhu, Wen-Cheng Chen, Yi Yuan, Dong Luo, Ze-Lin Zhu, Xiang Chen, Jia-Xiong Chen, Chun-Sing Lee, and Qing-Xiao Tong. Rational molecular design of bipolar phenanthroimidazole derivatives to realize highly efficient non-doped deep blue electroluminescence with ciey Ë, 0.06 and eqe approaching 6%. *Dyes and Pigments*, 173:107982, February 2020. ISSN 0143-7208. doi:10.1016/j.dyepig.2019.107982. URL `http://dx.doi.org/10.1016/j.dyepig.2019.107982`.

[50] Ming Zhang, Gaole Dai, Caijun Zheng, Kai Wang, Yizhong Shi, Xiaochun Fan, Hui Lin, Silu Tao, and Xiaohong Zhang. New electron-donating segment to develop thermally activated delayed fluorescence emitters for efficient solution-processed non-doped organic light-emitting diodes. *Chinese Chemical Letters*, 33(2):1110–1115, February 2022. ISSN 1001-8417. doi:10.1016/j.cclet.2021.08.064. URL `http://dx.doi.org/10.1016/j.cclet.2021.08.064`.

[51] Jingwen Yao, Shian Ying, Qian Sun, Yanfeng Dai, Xianfeng Qiao, Dezhi Yang, Jiangshan Chen, and Dongge Ma. High efficiency blue/green/yellow/red fluorescent organic light-emitting diodes sensitized by phosphors: general design rules and electroluminescence performance analysis. *Journal of Materials Chemistry C*, 7(36):11293–11302, 2019. ISSN 2050-7534. doi:10.1039/c9tc03666k. URL `http://dx.doi.org/10.1039/C9TC03666K`.

[52] Shengbing Xiao, Xuzhou Tian, Ying Gao, Haichao Liu, Changjiang Zhou, Shi-Tong Zhang, and Bing Yang. Enhanced blue-emissive electroluminescence performance with rational donor substitution. *Dyes and Pigments*, 204:110451, August 2022. ISSN 0143-7208. doi:10.1016/j.dyepig.2022.110451. URL `http://dx.doi.org/10.1016/j.dyepig.2022.110451`.

[53] Ming Zhang, Cai-Jun Zheng, Heng-Yuan Zhang, Hao-Yu Yang, Kai Wang, Yi-Zhong Shi, Hui Lin, Si-Lu Tao, and Xiao-Hong Zhang. Thermally activated delayed fluorescence exciplexes with phosphor components realizing deep-red to near-infrared electroluminescence. *Journal of Materials Chemistry C*, 10(41):15593–15600, 2022. ISSN 2050-7534. doi:10.1039/d2tc02694e. URL `http://dx.doi.org/10.1039/D2TC02694E`.

[54] Ling Yu, Zhongbin Wu, Guohua Xie, Weixuan Zeng, Dongge Ma, and Chuluo Yang. Molecular design to regulate the photophysical properties of multifunctional tadf emitters towards high-performance tadf-based oleds with eqes up to 22.4% and small efficiency roll-offs. *Chemical Science*, 9(5):1385–1391, 2018. ISSN 2041-6539. doi:10.1039/c7sc04669c. URL `http://dx.doi.org/10.1039/C7SC04669C`.

[55] Maxime Romain, Cassandre Quinton, Denis Tondelier, Bernard Geffroy, Olivier Jeannin, Joëlle Rault-Berthelot, and Cyril Poriel. Thioxanthene and dioxothioxanthene dihydroindeno[2,1-b]fluorenes: synthesis, properties and applications in green and sky blue phosphorescent oleds. *Journal of Materials Chemistry C*, 4(8):1692–1703, 2016. ISSN 2050-7534. doi:10.1039/c5tc04039f. URL `http://dx.doi.org/10.1039/C5TC04039F`.

[56] Runda Guo, Wei Liu, Shian Ying, Yuwei Xu, Yating Wen, Yaxiong Wang, Dehua Hu, Xianfeng Qiao, Bing Yang, Dongge Ma, and Lei Wang. Exceptionally efficient deep blue anthracene-based luminogens: design, synthesis, photophysical, and electroluminescent mechanisms. *Science Bulletin*, 66(20):2090–2098, October 2021. ISSN 2095-9273. doi:10.1016/j.scib.2021.06.018. URL `http://dx.doi.org/10.1016/j.scib.2021.06.018`.

[57] Minyu Chen, Yingjie Liao, Yang Lin, Tao Xu, Weixia Lan, Bin Wei, Yongfang Yuan, Dongliang Li, and Xiaowen Zhang. Progress on ultraviolet organic electroluminescence and lasing. *Journal of Materials Chemistry C*, 8(42):14665–14694, 2020. ISSN 2050-7534. doi:10.1039/d0tc03631e. URL `http://dx.doi.org/10.1039/D0TC03631E`.

[58] Chao Tang, Yuan Chen, Fangfang Wang, Tao Jiang, Jia Hu, Xudong Cao, Lili Zhang, and Xinwen Zhang. Effect of methyl-substitution on carbazole/oxadiazole donor-acceptor (d-a) type host materials for efficient solution-processed green organic light-emitting diodes. *Tetrahedron*, 76(13):131030, March 2020. ISSN 0040-4020. doi:10.1016/j.tet.2020.131030. URL `http://dx.doi.org/10.1016/j.tet.2020.131030`.

[59] Jayabalan Pandidurai, Jayachandran Jayakumar, Yi-Kuan Chen, Chia-Min Hsieh, and Chien-Hong Cheng. Constitutional isomers of carbazole-benzoyl-pyrimidine-based thermally activated delayed fluorescence emitters for efficient oleds. *Journal of Materials Chemistry C*, 9(44):15900–15909, 2021. ISSN 2050-7534. doi:10.1039/d1tc03998a. URL `http://dx.doi.org/10.1039/D1TC03998A`.

[60] Pachaiyappan Rajamalli, Vasudevan Thangaraji, Natarajan Senthilkumar, Chen-Cheng Ren-Wu, Hao-Wu Lin, and Chien-Hong Cheng. Thermally activated delayed fluorescence emitters with a m,m-di-tert-butyl-carbazolyl benzoylpyridine core achieving extremely high blue electroluminescence efficiencies. *Journal of Materials Chemistry C*, 5(11):2919–2926, 2017. ISSN 2050-7534. doi:10.1039/c7tc00457e. URL `http://dx.doi.org/10.1039/C7TC00457E`.

[61] Hélio Lopes Barros, Maria Alexandra Esteves, and Maria João Brites. Synthesis, photophysical and electrochemical properties of π-conjugated pyrene based down-shifting molecules with fluorinated aryl groups. *Dyes and Pigments*, 213:111103, May 2023. ISSN 0143-7208. doi:10.1016/j.dyepig.2023.111103. URL `http://dx.doi.org/10.1016/j.dyepig.2023.111103`.

[62] Pawel Zassowski, Przemyslaw Ledwon, Aleksandra Kurowska, Artur P. Herman, Tomasz Jarosz, Mieczyslaw Lapkowski, Vladyslav Cherpak, Pavlo Stakhira, Laura Peciulyte, Dmytro Volyniuk, and Juozas Vidas Grazulevicius. Efficient synthesis and structural effects of ambipolar carbazole derivatives. *Synthetic Metals*, 223:1–11, January 2017. ISSN 0379-6779. doi:10.1016/j.synthmet.2016.11.015. URL `http://dx.doi.org/10.1016/j.synthmet.2016.11.015`.

[63] Feng-Ming Xie, Zhi-Dong An, Miao Xie, Yan-Qing Li, Guang-Hui Zhang, Shi-Jie Zou, Li Chen, Jing-De Chen, Tao Cheng, and Jian-Xin Tang. tert-butyl substituted hetero-donor tadf compounds for efficient solution-processed non-doped blue oleds. *Journal of Materials Chemistry C*, 8(17):5769–5776, 2020. ISSN 2050-7534. doi:10.1039/d0tc00718h. URL `http://dx.doi.org/10.1039/D0TC00718H`.

[64] Chuan Li, Xiaoyang Du, Yu Zhou, Jun Ye, Lulu Fu, Mark G. Humphrey, Chao Wu, Juewen Zhao, Yanqing Du, Silu Tao, Jiacheng Wu, and Chi Zhang. A simple and broadly applicable synthesis of fluorene-coupled d-σ-a type molecules: towards high-triplet-energy bipolar hosts for efficient blue thermally-activated delayed fluorescence. *Journal of Materials Chemistry C*, 6(26):6949–6957, 2018. ISSN 2050-7534. doi:10.1039/c8tc01309h. URL `http://dx.doi.org/10.1039/C8TC01309H`.

[65] Cunjian Lin, Zishuang Wu, Jianbin Liu, Wen-Ting Deng, Yixi Zhuang, Tongtong Xuan, Jie Xue, Liao Zhang, Guodan Wei, and Rong-Jun Xie. Extremely low efficiency roll-off in vacuum- and solution-processed deep-red/near-infrared oleds based on 1,8-naphthalimide tadf emitters. *Journal of Luminescence*, 243:118683, March 2022. ISSN 0022-2313. doi:10.1016/j.jlumin.2021.118683. URL `http://dx.doi.org/10.1016/j.jlumin.2021.118683`.

[66] Lijuan Wang, Tao Li, Peicheng Feng, and Yan Song. Theoretical tuning of the singlet-triplet energy gap to achieve efficient long-wavelength thermally activated delayed fluorescence emitters: the impact of substituents. *Physical Chemistry Chemical Physics*, 19(32):21639–21647, 2017. ISSN 1463-9084. doi:10.1039/c7cp02615c. URL `http://dx.doi.org/10.1039/C7CP02615C`.

[67] Tao Hua, Yu-Chun Liu, Chih-Wei Huang, Nengquan Li, Changjiang Zhou, Zhongyan Huang, Xiaosong Cao, Chung-Chih Wu, and Chuluo Yang. High-efficiency and low roll-off deep-blue oleds enabled by thermally activated delayed fluorescence emitter with preferred horizontal dipole orientation. *Chemical Engineering Journal*, 433:133598, April 2022. ISSN 1385-8947. doi:10.1016/j.cej.2021.133598. URL `http://dx.doi.org/10.1016/j.cej.2021.133598`.

[68] A.G. Pramod, Y.F. Nadaf, and C.G. Renuka. A combined experimental theoretical approach for energy gap determination, photophysical, photostable, optoelectronic, nlo, and organic light emitting diode (oled) application: Synthesized coumarin derivative. *Journal of Molecular Structure*, 1194:271–283, October 2019. ISSN 0022-2860. doi:10.1016/j.molstruc.2019.05.099. URL `http://dx.doi.org/10.1016/j.molstruc.2019.05.099`.

[69] Xuzhou Tian, Shi-Tong Zhang, Xianglong Li, Shengbing Xiao, Ying Gao, Shi-Jian Su, and Bing Yang. Donor-Ï€-acceptor materials for robust electroluminescence performance based on hybridized local and charge-transfer state. *Dyes and Pigments*, 193:109495, September 2021. ISSN 0143-7208. doi:10.1016/j.dyepig.2021.109495. URL `http://dx.doi.org/10.1016/j.dyepig.2021.109495`.

[70] A.G. Pramod, Y.F. Nadaf, and C.G. Renuka. Synthesis, photophysical, quantum chemical investigation, linear and non-linear optical properties of coumarin derivative: Optoelectronic and optical limiting application. *Spectrochimica Acta Part A: Molecular and Biomolecular Spectroscopy*, 223:117288, December 2019. ISSN 1386-1425. doi:10.1016/j.saa.2019.117288. URL `http://dx.doi.org/10.1016/j.saa.2019.117288`.

[71] Changjiang Zhou, Yafei Liu, Zhuangzhuang Sun, He Liu, Lei Xu, Dehua Hu, and Jun Hu. Efficient red hybridized local and charge-transfer oleds by rational isomer engineering. *Dyes and Pigments*, 205:110488, September 2022. ISSN 0143-7208. doi:10.1016/j.dyepig.2022.110488. URL `http://dx.doi.org/10.1016/j.dyepig.2022.110488`.

[72] Dongdong Zhang, Minghan Cai, Zhengyang Bin, Yunge Zhang, Deqiang Zhang, and Lian Duan. Highly efficient blue thermally activated delayed fluorescent oleds with record-low driving voltages utilizing high triplet energy hosts with small singlet-triplet splittings. *Chemical Science*, 7(5):3355–3363, 2016. ISSN 2041-6539. doi:10.1039/c5sc04755b. URL `http://dx.doi.org/10.1039/C5SC04755B`.

[73] Seung Gun Yoo, Wook Song, and Jun Yeob Lee. Molecular engineering of donor moiety of donor-acceptor structure for management of photophysical properties and device performances. *Dyes and Pigments*, 128:201–208, May 2016. ISSN 0143-7208. doi:10.1016/j.dyepig.2016.01.021. URL `http://dx.doi.org/10.1016/j.dyepig.2016.01.021`.

[74] Fulong Ma, Hefang Ji, Dongdong Zhang, Ke Xue, Pan Zhang, Zhengjian Qi, and Huaiyuan Zhu. Adjusting the photophysical properties of aie-active tadf emitters from through-bond to through-space charge transfer for high-performance solution-processed oleds. *Dyes and Pigments*, 188:109208, April 2021. ISSN 0143-7208. doi:10.1016/j.dyepig.2021.109208. URL `http://dx.doi.org/10.1016/j.dyepig.2021.109208`.

[75] Kaiyong Sun, Dan Liu, Wenwen Tian, Feng Gu, Wangxia Wang, Zhaosheng Cai, Wei Jiang, and Yueming Sun. Manipulation of the sterically hindering effect to realize aie and tadf for high-performing nondoped solution-processed oleds with extremely low efficiency roll-off. *Journal of Materials Chemistry C*, 8(34):11850–11859, 2020. ISSN 2050-7534. doi:10.1039/d0tc02577a. URL `http://dx.doi.org/10.1039/D0TC02577A`.

[76] Wenjuan Cao, Alim Abdurahman, Ping Zheng, Ming Zhang, and Feng Li. High-performance non-doped blue oleds based on 1,2,4-triazole-phenanthroimidazole derivatives with negligible efficiency roll-off. *Journal of Materials Chemistry C*, 9 (21):6873–6879, 2021. ISSN 2050-7534. doi:10.1039/d1tc01079d. URL `http://dx.doi.org/10.1039/D1TC01079D`.

[77] Chenyang Zhao, Thomas Schwartz, Berthold Stöger, Fraser J. White, Jiangshan Chen, Dongge Ma, Johannes Fröhlich, and Paul Kautny. Controlling excimer formation in indolo[3,2,1-jk]carbazole/9h-carbazole based host materials for rgb pholeds. *Journal of Materials Chemistry C*, 6(37):9914–9924, 2018. ISSN 2050-7534. doi:10.1039/c8tc03537g. URL `http://dx.doi.org/10.1039/C8TC03537G`.

[78] Yuxin Xiao, Hailan Wang, Zongliang Xie, Mingyao Shen, Rongjuan Huang, Yuchen Miao, Guanyu Liu, Tao Yu, and Wei Huang. Nir tadf emitters and oleds: challenges, progress, and perspectives. *Chemical Science*, 13(31):8906–8923, 2022. ISSN 2041-6539. doi:10.1039/d2sc02201j. URL `http://dx.doi.org/10.1039/D2SC02201J`.

[79] Shin Hyung Choi, Chan Hee Lee, Chihaya Adachi, and Sae Youn Lee. Molecular design of highly effective thermally activated delayed fluorescence emitters based on ortho-substituted donor-acceptor-donor pyridinecarbonitrile derivatives and their application for high-performance oleds. *Dyes and Pigments*, 171:107775, December 2019. ISSN 0143-7208. doi:10.1016/j.dyepig.2019.107775. URL `http://dx.doi.org/10.1016/j.dyepig.2019.107775`.

[80] Xu Qiu, Lei Xu, Shian Ying, Xiyun Ye, Pei Xu, Bohan Wang, Dehua Hu, Dongge Ma, and Yuguang Ma. Novel 12,12-dimethyl-7,12-dihydrobenzo[a]acridine as a deep-blue emitting chromophore for oleds with narrow-band emission and suppressed efficiency roll-off. *Journal of Materials Chemistry C*, 9(39):13697–13703, 2021. ISSN 2050-7534. doi: 10.1039/d1tc03898b. URL `http://dx.doi.org/10.1039/D1TC03898B`.

[81] Jingwei Li, Lei Xu, Xinyong Liu, Xu Qiu, Yuyu Pan, and Dehua Hu. Novel fused 5,9-dihydrobenzo[a]quinolino[1,2,3-fg]acridine-based emitters for efficient non-doped deep-blue electroluminescence with ciey â‰¤ 0.08. *Dyes and Pigments*, 204:110456, August 2022. ISSN 0143-7208. doi:10.1016/j.dyepig.2022.110456. URL `http://dx.doi.org/10.1016/j.dyepig.2022.110456`.

[82] Shiv Kumar, Pauline Tourneur, Jonathan R. Adsetts, Michael Y. Wong, Pachaiyappan Rajamalli, Dongyang Chen, Roberto Lazzaroni, Pascal Viville, David B. Cordes, Alexandra M. Z. Slawin, Yoann Olivier, Jérôme Cornil, Zhifeng Ding, and Eli Zysman-Colman. Photoluminescence and electrochemiluminescence of thermally activated delayed fluorescence (tadf) emitters containing diphenylphosphine chalcogenide-substituted carbazole donors. *Journal of Materials Chemistry C*, 10(12):4646–4667, 2022. ISSN 2050-7534. doi:10.1039/d1tc05696d. URL `http://dx.doi.org/10.1039/D1TC05696D`.

[83] Ling Yu, Zhongbin Wu, Cheng Zhong, Guohua Xie, Kailong Wu, Dongge Ma, and Chuluo Yang. Tuning the emission from local excited-state to charge-transfer state transition in quinoxaline-based butterfly-shaped molecules: Efficient orange oleds based on thermally activated delayed fluorescence emitter. *Dyes and Pigments*, 141:325–332, June 2017. ISSN 0143-7208. doi:10.1016/j.dyepig.2017.02.035. URL `http://dx.doi.org/10.1016/j.dyepig.2017.02.035`.

[84] Yu Zhou, Ming Zhang, Jun Ye, Huan Liu, Kai Wang, Yi Yuan, Yan-Qing Du, Chi Zhang, Cai-Jun Zheng, and Xiao-Hong Zhang. Efficient solution-processed red organic light-emitting diode based on an electron-donating building block of pyrrolo[3,2-b]pyrrole. *Organic Electronics*, 65:110–115, February 2019. ISSN 1566-1199. doi:10.1016/j.orgel.2018.11.007. URL `http://dx.doi.org/10.1016/j.orgel.2018.11.007`.

[85] Ajay Kumar, Woochan Lee, Taehwan Lee, Jaehoon Jung, Seunghyup Yoo, and Min Hyung Lee. Triarylboron-based tadf emitters with perfluoro substituents: high-efficiency oleds with a power efficiency over 100 lm w-1. *Journal of Materials Chemistry C*, 8(12):4253–4263, 2020. ISSN 2050-7534. doi:10.1039/c9tc06204a. URL `http://dx.doi.org/10.1039/C9TC06204A`.

[86] Anuj Sharma, Diksha Saklani, K.R. Justin Thomas, Shahnawaz, Sujith Sudheendran Swayamprabha, and Jwo-Huei Jou. Synthesis and characterization of multi-substituted carbazole derivatives exhibiting aggregation-induced emission for oled applications. *Organic Electronics*, 86:105864, November 2020. ISSN 1566-1199. doi:10.1016/j.orgel.2020.105864. URL `http://dx.doi.org/10.1016/j.orgel.2020.105864`.

[87] Hao Chen, Huijun Liu, Yi Xiong, Junchu He, Zujin Zhao, and Ben Zhong Tang. New aggregation-induced delayed fluorescent materials for efficient oleds with high stabilities of emission color and efficiency. *Materials Chemistry Frontiers*, 6(7):924–932, 2022. ISSN 2052-1537. doi:10.1039/d1qm01625c. URL `http://dx.doi.org/10.1039/D1QM01625C`.

[88] Tingting Huang, Di Liu, Deli Li, Wenfeng Jiang, and Jingyang Jiang. Novel yellow thermally activated delayed fluorescence emitters for highly efficient full-tadf woleds with low driving voltages and remarkable color stability. *New Journal of Chemistry*, 43(34):13339–13348, 2019. ISSN 1369-9261. doi:10.1039/c9nj03184g. URL `http://dx.doi.org/10.1039/C9NJ03184G`.

[89] Feng Wei, Jacky Qiu, Xiaochen Liu, Jianqiang Wang, Huibo Wei, Zhibin Wang, Zhiwei Liu, Zuqiang Bian, Zhenghong Lu, Yongliang Zhao, and Chunhui Huang. Efficient orange-red phosphorescent organic light-emitting diodes using an in situ synthesized copper(¡scp¿i¡/scp¿) complex as the emitter. *J. Mater. Chem. C*, 2(31):6333–6341, 2014. ISSN 2050-7534. doi:10.1039/c4tc00410h. URL `http://dx.doi.org/10.1039/C4TC00410H`.

[90] Yanan Zheng, Jinnan Huo, Shu Xiao, Heping Shi, Dongge Ma, and Ben Zhong Tang. Synthesis, photoluminescence and electroluminescence properties of a new blue emitter containing carbazole, acridine and diphenyl sulfone units. *Organic Electronics*, 101:106411, February 2022. ISSN 1566-1199. doi:10.1016/j.orgel.2021.106411. URL `http://dx.doi.org/10.1016/j.orgel.2021.106411`.

[91] Yan Liu, Suyu Qiu, Jianmin Yu, Xinxin Ban, Jie Pan, Kun Gao, Aiyun Zhu, Dongen Zhang, Tianlin Zhang, and Zhiwei Tong. Strategy to improve the efficiency of solution-processed phosphorescent organic light-emitting devices by modified tadf host with tert-butyl carbazole. *Tetrahedron*, 81:131869, February 2021. ISSN 0040-4020. doi:10.1016/j.tet.2020.131869. URL `http://dx.doi.org/10.1016/j.tet.2020.131869`.

[92] Yi Jia, Sen Wu, Yuteng Zhang, Shigen Fan, Xiaoming Zhao, Hongli Liu, Xiaofei Dong, Shirong Wang, and Xianggao Li. Achieving non-doped deep-blue oleds by applying bipolar imidazole derivatives. *Organic Electronics*, 69:289–296, June 2019. ISSN 1566-1199. doi:10.1016/j.orgel.2019.03.044. URL `http://dx.doi.org/10.1016/j.orgel.2019.03.044`.

[93] Zhen-Hua Xing, Jin-Yong Zhuang, Xiao-Ping Xu, Shun-Jun Ji, Wen-Ming Su, and Zheng Cui. Novel oxazole-based emitters for high efficiency fluorescent oleds: Synthesis, characterization, and optoelectronic properties. *Tetrahedron*, 73(15):2036–2042, April 2017. ISSN 0040-4020. doi:10.1016/j.tet.2017.02.049. URL `http://dx.doi.org/10.1016/j.tet.2017.02.049`.

[94] Yan Danyliv, Khrystyna Ivaniuk, Iryna Danyliv, Oleksandr Bezvikonnyi, Dmytro Volyniuk, Sych Galyna, Algirdas Lazauskas, Levani Skhirtladze, Hans Ågren, Pavlo Stakhira, Nataliya Karaush-Karmazin, Amjad Ali, Glib Baryshnikov, and Juozas V. Grazulevicius. Carbazole-σ-sulfobenzimide derivative exhibiting mechanochromic thermally activated delayed fluorescence as emitter for flexible oleds: Theoretical and experimental insights. *Dyes and Pigments*, 208:110841, January 2023. ISSN 0143-7208. doi:10.1016/j.dyepig.2022.110841. URL `http://dx.doi.org/10.1016/j.dyepig.2022.110841`.

[95] Yanxin Zhang, Qian Li, Minghan Cai, Jie Xue, and Juan Qiao. An 850 nm pure near-infrared emitting iridium complex for solution-processed organic light-emitting diodes. *Journal of Materials Chemistry C*, 8(25):8484–8492, 2020. ISSN 2050-7534. doi:10.1039/d0tc01614d. URL `http://dx.doi.org/10.1039/D0TC01614D`.

[96] Bin Huang, Yigang Ji, Zijing Li, Na Zhou, Wei Jiang, Yan Feng, Baoping Lin, and Yueming Sun. Simple aggregation-induced delayed fluorescence materials based on anthraquinone derivatives for highly efficient solution-processed red

oleds. *Journal of Luminescence*, 187:414–420, July 2017. ISSN 0022-2313. doi:10.1016/j.jlumin.2017.03.038. URL `http://dx.doi.org/10.1016/j.jlumin.2017.03.038`.

[97] Debasish Barman, Kavita Narang, Rajdikhsit Gogoi, Debika Barman, and Parameswar Krishnan Iyer. Exceptional class of thermally activated delayed fluorescent emitters that display pure blue, near-ir, circularly polarized luminescence and multifunctional behaviour for highly efficient and stable oleds. *Journal of Materials Chemistry C*, 10(22):8536–8583, 2022. ISSN 2050-7534. doi:10.1039/d1tc05906h. URL `http://dx.doi.org/10.1039/D1TC05906H`.

[98] Tian Zhang, Jingsheng Miao, Muhammad Umair Ali, Ming Shi, Yaowu He, Tianchen Fu, and Hong Meng. Phosphorescent oleds with extremely low efficiency roll-off enabled via rationally designed benzimidazole-based bipolar hosts. *Dyes and Pigments*, 180:108477, September 2020. ISSN 0143-7208. doi:10.1016/j.dyepig.2020.108477. URL `http://dx.doi.org/10.1016/j.dyepig.2020.108477`.

[99] Gediminas Kreiza, Domantas Berenis, Dovydas Banevičius, Saulius Juršėnas, Tomas Javorskis, Edvinas Orentas, and Karolis Kazlauskas. High efficiency and extremely low roll-off solution- and vacuum-processed oleds based on isophthalonitrile blue tadf emitter. *Chemical Engineering Journal*, 412:128574, May 2021. ISSN 1385-8947. doi:10.1016/j.cej.2021.128574. URL `http://dx.doi.org/10.1016/j.cej.2021.128574`.

[100] Binyan Wang, Hannan Yang, Yaxing Zhang, Guohua Xie, Huijuan Ran, Tao Wang, Qiang Fu, Yitao Ren, Ning Sun, Guangtao Zhao, Jian-Yong Hu, and Qiang Wang. Highly efficient electroluminescence from evaporation- and solution-processable orange-red thermally activated delayed fluorescence emitters. *Journal of Materials Chemistry C*, 7(39):12321–12327, 2019. ISSN 2050-7534. doi:10.1039/c9tc04418c. URL `http://dx.doi.org/10.1039/C9TC04418C`.

[101] Mangey Ram Nagar, Abhijeet Choudhury, Daiva Tavgeniene, Raminta Beresneviciute, Dovydas Blazevicius, Vygintas Jankauskas, Krishan Kumar, Subrata Banik, Subrata Ghosh, Saulius Grigalevicius, and Jwo-Huei Jou. Solution-processable phenothiazine and phenoxazine substituted fluorene cored nanotextured hole transporting materials for achieving high-efficiency oleds. *Journal of Materials Chemistry C*, 10(9):3593–3608, 2022. ISSN 2050-7534. doi:10.1039/d1tc05237c. URL `http://dx.doi.org/10.1039/D1TC05237C`.

[102] Sukanya Tongsuk, Ruttapol Malatong, Takdanai Unjarern, Chanikan Wongkaew, Panida Surawatanawong, Taweesak Sudyoadsuk, Vinich Promarak, and Nopporn Ruangsupapichat. Enhancement of performance of oleds using double indolo[3,2-b]indole electron-donors based emitter. *Journal of Luminescence*, 238:118287, October 2021. ISSN 0022-2313. doi:10.1016/j.jlumin.2021.118287. URL `http://dx.doi.org/10.1016/j.jlumin.2021.118287`.

[103] Changjiang Zhou, Wen-Cheng Chen, He Liu, Xiaosong Cao, Nengquan Li, Youming Zhang, Chun-Sing Lee, and Chuluo Yang. Isomerization enhanced quantum yield of dibenzo[a,c]phenazine-based thermally activated delayed fluorescence emitters for highly efficient orange oleds. *Journal of Materials Chemistry C*, 8(28):9639–9645, 2020. ISSN 2050-7534. doi:10.1039/d0tc01995j. URL `http://dx.doi.org/10.1039/D0TC01995J`.

[104] Lian Duan. *WOLEDs using TADF dopants*, pages 235–287. Elsevier, 2022. ISBN 9780128198100. doi:10.1016/b978-0-12-819810-0.00004-1. URL `http://dx.doi.org/10.1016/B978-0-12-819810-0.00004-1`.

[105] Ming Zhang, Gao-Le Dai, Cai-Jun Zheng, Kai Wang, Yi-Zhong Shi, Xiao-Chun Fan, Hui Lin, Si-Lu Tao, and Xiao-Hong Zhang. Novel d-dâ€²-a structure thermally activated delayed fluorescence emitters realizing over 20% external quantum efficiencies in both evaporation- and solution-processed organic light-emitting diodes. *Organic Electronics*, 99:106312, December 2021. ISSN 1566-1199. doi:10.1016/j.orgel.2021.106312. URL `http://dx.doi.org/10.1016/j.orgel.2021.106312`.

[106] Jiajia Luo, Shaolong Gong, Yu Gu, Tianheng Chen, Yifan Li, Cheng Zhong, Guohua Xie, and Chuluo Yang. Multi-carbazole encapsulation as a simple strategy for the construction of solution-processed, non-doped thermally activated delayed fluorescence emitters. *Journal of Materials Chemistry C*, 4(13):2442–2446, 2016. ISSN 2050-7534. doi:10.1039/c6tc00418k. URL `http://dx.doi.org/10.1039/C6TC00418K`.

[107] Rama Dhali, D. K. Andrea Phan Huu, Francesco Bertocchi, Cristina Sissa, Francesca Terenziani, and Anna Painelli. Understanding tadf: a joint experimental and theoretical study of dmac-trz. *Physical Chemistry Chemical Physics*, 23(1):378–387, 2021. ISSN 1463-9084. doi:10.1039/d0cp05982j. URL `http://dx.doi.org/10.1039/D0CP05982J`.

[108] Runda Guo, Yaxiong Wang, Zhi Huang, Qing Zhang, Songpo Xiang, Shaofeng Ye, Wei Liu, and Lei Wang. Phenothiazine dioxide-containing derivatives as efficient hosts for blue, green and yellow thermally activated delayed fluorescence oleds. *Journal of Materials Chemistry C*, 8(11):3705–3714, 2020. ISSN 2050-7534. doi:10.1039/c9tc05917b. URL `http://dx.doi.org/10.1039/C9TC05917B`.

[109] Zhi Huang, Bo Wang, Qing Zhang, Songpo Xiang, Xialei Lv, Lixiang Ma, Bing Yang, Yu Gao, and Lei Wang. Highly twisted bipolar emitter for efficient nondoped deep-blue electroluminescence. *Dyes and Pigments*, 140:328–336, May 2017. ISSN 0143-7208. doi:10.1016/j.dyepig.2017.01.028. URL `http://dx.doi.org/10.1016/j.dyepig.2017.01.028`.

[110] Young Hoon Lee, Donggyun Lee, Taehwan Lee, Junseung Lee, Jaehoon Jung, Seunghyup Yoo, and Min Hyung Lee. Impact of boryl acceptors in para-acridine-appended triarylboron emitters on blue thermally activated delayed fluorescence oleds. *Dyes and Pigments*, 188:109224, April 2021. ISSN 0143-7208. doi:10.1016/j.dyepig.2021.109224. URL `http://dx.doi.org/10.1016/j.dyepig.2021.109224`.

[111] Zhang Di, Yang Tingting, Wang Zhengqin, Xu Huixia, Wang Hua, Yu Junsheng, and Xu Bingshe. Photoelectric properties of host materials based on diphenyl sulfone as acceptor and the performances in green phosphorescent oleds. *Optical Materials*, 109:110313, November 2020. ISSN 0925-3467. doi:10.1016/j.optmat.2020.110313. URL `http://dx.doi.org/10.1016/j.optmat.2020.110313`.

[112] Panpan Leng, Shuaiqiang Sun, Runda Guo, Qing Zhang, Wei Liu, Xialei Lv, Shaofeng Ye, and Lei Wang. Modifying the aie-tadf chromophore with host-substituents to achieve high efficiency and low roll-off non-doped oleds. *Organic Electronics*, 78:105602, March 2020. ISSN 1566-1199. doi:10.1016/j.orgel.2019.105602. URL `http://dx.doi.org/10.1016/j.orgel.2019.105602`.

[113] Jixiong Liang, Chenglong Li, Yuanyuan Cui, Zhiqiang Li, Jiaxuan Wang, and Yue Wang. Rational design of efficient orange-red to red thermally activated delayed fluorescence emitters for oleds with external quantum efficiency of up to 26.0% and reduced efficiency roll-off. *Journal of Materials Chemistry C*, 8(5):1614–1622, 2020. ISSN 2050-7534. doi:10.1039/c9tc05892c. URL `http://dx.doi.org/10.1039/C9TC05892C`.

[114] Chang-Jin Ou, Jin-Yi Lin, Jie Mao, Shuang-Quan Chu, Yu Zhao, Ling-Hai Xie, Hong-Tao Cao, Xin-Wen Zhang, Ying Wei, and Wei Huang. Friedel-crafts arylmethylation: A simple approach to synthesize bipolar host materials for efficient electroluminescence. *Organic Electronics*, 38:370–378, November 2016. ISSN 1566-1199. doi:10.1016/j.orgel.2016.08.018. URL `http://dx.doi.org/10.1016/j.orgel.2016.08.018`.

[115] Lei Xu, Mizhen Sun, Yannan Zhou, Jingli Lou, Mingliang Xie, Zipeng Li, Qikun Sun, Yuyu Pan, Shanfeng Xue, and Wenjun Yang. A new multifunctional fluorescent molecule for highly efficient non-doped deep-blue electro-fluorescence with high color-purity and efficient phosphorescent oleds. *Organic Chemistry Frontiers*, 10(2):490–498, 2023. ISSN 2052-4129. doi:10.1039/d2qo01807a. URL `http://dx.doi.org/10.1039/D2QO01807A`.

[116] Kaiyong Sun, Jie Wu, Lingling Zhu, Hongxiang Liu, Yu Zhou, Wenwen Tian, Zhaosheng Cai, Wei Jiang, and Yueming Sun. Highly efficient blue all-solution-processed organic light-emitting diodes based on the strategy of constructing a thermally cross-linkable tadf dendrimer. *Dyes and Pigments*, 198:109967, February 2022. ISSN 0143-7208. doi:10.1016/j.dyepig.2021.109967. URL `http://dx.doi.org/10.1016/j.dyepig.2021.109967`.

[117] Kaiyong Sun, Wenwen Tian, Haiyang Gao, Chenjie Bi, Jiamin Yao, Zhiguo Wang, Zhaosheng Cai, and Wei Jiang. Creation of a thermally cross-linkable encapsulated tadf molecule for highly efficient solution-processed hybrid white oleds. *Organic Electronics*, 102:106442, March 2022. ISSN 1566-1199. doi:10.1016/j.orgel.2022.106442. URL `http://dx.doi.org/10.1016/j.orgel.2022.106442`.

[118] Liang Cao, Lei Zhang, Qiang Wei, Jiasen Zhang, Dongjun Chen, Sheng Wang, Shi-jian Su, Tao Wang, and Ziyi Ge. Bipolar fluorophores based on intramolecular charge-transfer moieties of sulfone for nondoped deep blue solution-processed organic light-emitting diodes. *Dyes and Pigments*, 176:108242, May 2020. ISSN 0143-7208. doi:10.1016/j.dyepig.2020.108242. URL `http://dx.doi.org/10.1016/j.dyepig.2020.108242`.

[119] Yanying Chen, Nengquan Li, Zhongyan Huang, Guohua Xie, and Chuluo Yang. Molecular engineering by Ïf-linkers enables delayed fluorescence emitters for high-efficiency sky-blue solution-processed oleds. *Chemical Engineering Journal*, 430:133078, February 2022. ISSN 1385-8947. doi:10.1016/j.cej.2021.133078. URL `http://dx.doi.org/10.1016/j.cej.2021.133078`.

[120] Yang Liu, Baoyun Du, Xianchao Han, Xiaofu Wu, Hui Tong, and Lixiang Wang. Intramolecular-locked triazatruxene-based thermally activated delayed fluorescence emitter for efficient solution-processed deep-blue organic light emitting diodes. *Chemical Engineering Journal*, 446:137372, October 2022. ISSN 1385-8947. doi:10.1016/j.cej.2022.137372. URL `http://dx.doi.org/10.1016/j.cej.2022.137372`.

[121] Yinzhao Zhen, Fei Zhang, Hongli Liu, Yifei Yan, Xianggao Li, and Shirong Wang. Impact of peripheral groups on pyrimidine acceptor-based hlct materials for efficient deep blue oled devices. *Journal of Materials Chemistry C*, 10(27):9953–9960, 2022. ISSN 2050-7534. doi:10.1039/d2tc01766k. URL `http://dx.doi.org/10.1039/D2TC01766K`.

[122] Chae Yeong Kim, Jiwon Yoon, Suna Choi, Cheol Hun Jeong, Hyung Jong Kim, Ji-Eun Jeong, Seong Keun Kim, Hyuna Lee, Han Young Woo, Jang Hyuk Kwon, Min Ju Cho, and Dong Hoon Choi. Blue-emitting dendritic molecule with dual functionality as host and dopant for solution-processed white oleds with red-emitting material. *Synthetic Metals*, 258:116198, December 2019. ISSN 0379-6779. doi:10.1016/j.synthmet.2019.116198. URL `http://dx.doi.org/10.1016/j.synthmet.2019.116198`.

[123] Jaipal Devesing Girase, Aravind Babu Kajjam, Deepak Kumar Dubey, Kiran Kishore Kesavan, Jwo-Huei Jou, and Sivakumar Vaidyanathan. Unipolar 1-phenylimidazo[1,5-a]pyridine: a new class of ultra-bright sky-blue emitters for solution-processed organic light emitting diodes. *New Journal of Chemistry*, 46(35):16717–16729, 2022. ISSN 1369-9261. doi:10.1039/d2nj01938h. URL `http://dx.doi.org/10.1039/D2NJ01938H`.

[124] Gorakala Umasankar, Hidayath Ulla, Chakali Madhu, Gontu Ramanjaneya Reddy, Balaiah Shanigaram, Jagadeesh Babu Nanubolu, Bhanuprakash Kotamarthi, Galla V. Karunakar, M.N. Satyanarayan, and V. Jayathirtha Rao. Imidazole-pyrene hybrid luminescent materials for organic light-emitting diodes: Synthesis, characterization & electroluminescent properties. *Journal of Molecular Structure*, 1236:130306, July 2021. ISSN 0022-2860. doi:10.1016/j.molstruc.2021.130306. URL `http://dx.doi.org/10.1016/j.molstruc.2021.130306`.

[125] Lisi Zhan, Weimin Ning, Shaolong Gong, Guohua Xie, and Chuluo Yang. Difluoroboron locking tactic enhances photo- and electroluminescence of tadf emitter. *Dyes and Pigments*, 192:109392, August 2021. ISSN 0143-7208. doi:10.1016/j.dyepig.2021.109392. URL `http://dx.doi.org/10.1016/j.dyepig.2021.109392`.

[126] Simran Sharma and Amlan K. Pal. Recent advances of nir-tadf (λmaxpl/el > 700 nm) emitters and their applications in oleds. *Journal of Materials Chemistry C*, 10(42):15681–15707, 2022. ISSN 2050-7534. doi:10.1039/d2tc03316j. URL `http://dx.doi.org/10.1039/D2TC03316J`.

[127] Jiafang Li, Wen-Cheng Chen, He Liu, Zhanxiang Chen, Danyang Chai, Chun-Sing Lee, and Chuluo Yang. Double-twist pyridine-carbonitrile derivatives yielding excellent thermally activated delayed fluorescence emitters for high-performance oleds. *Journal of Materials Chemistry C*, 8(2):602–606, 2020. ISSN 2050-7534. doi:10.1039/c9tc05340a. URL `http://dx.doi.org/10.1039/C9TC05340A`.

[128] Xujun Zheng, Qiming Peng, Jie Lin, Yi Wang, Jie Zhou, Yan Jiao, Yuefeng Bai, Yan Huang, Feng Li, Xingyuan Liu, Xuemei Pu, and Zhiyun Lu. Simultaneous harvesting of triplet excitons in oleds by both guest and host materials with an intramolecular charge-transfer feature via triplet-triplet annihilation. *Journal of Materials Chemistry C*, 3(27):6970–6978, 2015. ISSN 2050-7534. doi:10.1039/c5tc00779h. URL `http://dx.doi.org/10.1039/C5TC00779H`.

[129] Shuo Chen, Pengju Zeng, Weigao Wang, Xuedong Wang, Yukun Wu, Pengju Lin, and Zhengchun Peng. Naphthalimide-arylamine derivatives with aggregation induced delayed fluorescence for realizing efficient green to red electroluminescence.

Journal of Materials Chemistry C, 7(10):2886–2897, 2019. ISSN 2050-7534. doi:10.1039/c8tc06163g. URL `http://dx.doi.org/10.1039/C8TC06163G`.

[130] Frédéric Dumur, Thanh-Tuân Bui, Sébastien Péralta, Marc Lepeltier, Guillaume Wantz, Gjergji Sini, Fabrice Goubard, and Didier Gigmes. Bis(diphenylamino)naphthalene host materials: careful selection of the substitution pattern for the design of fully solution-processed triple-layered electroluminescent devices. *RSC Advances*, 6(65):60565–60577, 2016. ISSN 2046-2069. doi:10.1039/c6ra13824a. URL `http://dx.doi.org/10.1039/C6RA13824A`.

[131] Cong Fan, Jingfang Pei, Juewen Zhao, Manli Huang, Wu Tang, Jiahui Hu, Bei Cao, Haochen Tan, Silu Tao, and Chuluo Yang. A yellow organic emitter with novel d-a3 architecture and hidden delayed fluorescence for highly efficient monochromatic oleds. *Organic Electronics*, 73:102–108, October 2019. ISSN 1566-1199. doi:10.1016/j.orgel.2019.06.002. URL `http://dx.doi.org/10.1016/j.orgel.2019.06.002`.

[132] Xinxin Ban, Feng Chen, Yan Liu, Jie Pan, Aiyun Zhu, Wei Jiang, and Yueming Sun. Design of efficient thermally activated delayed fluorescence blue host for high performance solution-processed hybrid white organic light emitting diodes. *Chemical Science*, 10(10):3054–3064, 2019. ISSN 2041-6539. doi:10.1039/c8sc05456h. URL `http://dx.doi.org/10.1039/C8SC05456H`.

[133] Tao Zhou, Kaizhi Zhang, Qingpeng Cao, Hui Xu, Xinxin Ban, Peng Zhu, Qile Li, Linxing Shi, Fengjie Ge, and Wei Jiang. Benzonitrile-based aie polymer host with a simple synthesis process for high-efficiency solution-processable green and blue tadf organic light emitting diodes. *Journal of Materials Chemistry C*, 10(6):2109–2120, 2022. ISSN 2050-7534. doi:10.1039/d1tc05010a. URL `http://dx.doi.org/10.1039/D1TC05010A`.

[134] Yuan Yu, Miao Cang, Wei Cui, Lei Xu, Runze Wang, Mizhen Sun, Huayi Zhou, Wenjun Yang, and Shanfeng Xue. Efficient red fluorescent oleds based on aggregation-induced emission combined with hybridized local and charge transfer state. *Dyes and Pigments*, 184:108770, January 2021. ISSN 0143-7208. doi:10.1016/j.dyepig.2020.108770. URL `http://dx.doi.org/10.1016/j.dyepig.2020.108770`.

[135] Praetip Khammultri, Pongsakorn Chasing, Chirawat Chitpakdee, Supawadee Namuangruk, Taweesak Sudyoadsuk, and Vinich Promarak. Red to orange thermally activated delayed fluorescence polymers based on 2-(4-(diphenylamino)-phenyl)-9h-thioxanthen-9-one-10,10-dioxide for efficient solution-processed oleds. *RSC Advances*, 11(40):24794–24806, 2021. ISSN 2046-2069. doi:10.1039/d1ra04599g. URL `http://dx.doi.org/10.1039/D1RA04599G`.

[136] Shaolong Gong, Jiajia Luo, Zian Wang, Yifan Li, Tianheng Chen, Guohua Xie, and Chuluo Yang. Tuning emissive characteristics and singlet-triplet energy splitting of fluorescent emitters by encapsulation group modification: Yellow tadf emitter for solution-processed oleds with high luminance and ultraslow efficiency roll-off. *Dyes and Pigments*, 139:593–600, April 2017. ISSN 0143-7208. doi:10.1016/j.dyepig.2016.12.058. URL `http://dx.doi.org/10.1016/j.dyepig.2016.12.058`.

[137] Futong Liu, Zhuang Cheng, Liang Wan, Lei Gao, Zhenyu Yan, Dehua Hu, Lei Ying, Ping Lu, and Yuguang Ma. Anthracene-based emitters for highly efficient deep blue organic light-emitting diodes with narrow emission spectrum. *Chemical Engineering Journal*, 426:131351, December 2021. ISSN 1385-8947. doi:10.1016/j.cej.2021.131351. URL `http://dx.doi.org/10.1016/j.cej.2021.131351`.

[138] Seokwoo Kang, Jin-Suk Huh, Jang-Joo Kim, and Jongwook Park. Highly efficient deep-blue fluorescence oleds with excellent charge balance based on phenanthro[9,10-d]oxazole-anthracene derivatives. *Journal of Materials Chemistry C*, 8(32):11168–11176, 2020. ISSN 2050-7534. doi:10.1039/d0tc01811b. URL `http://dx.doi.org/10.1039/D0TC01811B`.

[139] Sang Kyu Jeon, Hee-Jun Park, and Jun Yeob Lee. Blue-shifted emission color and high quantum efficiency in solution-processed blue thermally activated delayed fluorescence organic light-emitting diodes using an intermolecular interaction suppressing host decorated with blocking groups. *Journal of Materials Chemistry C*, 6(25):6778–6783, 2018. ISSN 2050-7534. doi:10.1039/c8tc02050g. URL `http://dx.doi.org/10.1039/C8TC02050G`.

[140] Mengyao Ma, Jiuyan Li, Di Liu, Deli Li, Ruizhi Dong, and Yongqiang Mei. Low efficiency roll-off thermally activated delayed fluorescence emitters for non-doped oleds: Substitution effect of thioether and sulfone groups. *Dyes and Pigments*, 194:109649, October 2021. ISSN 0143-7208. doi:10.1016/j.dyepig.2021.109649. URL `http://dx.doi.org/10.1016/j.dyepig.2021.109649`.

[141] Songpo Xiang, Runda Guo, Zhi Huang, Xialei Lv, Shuaiqiang Sun, Hongting Chen, Qing Zhang, and Lei Wang. Highly efficient yellow nondoped thermally activated delayed fluorescence oleds by utilizing energy transfer between dual conformations based on phenothiazine derivatives. *Dyes and Pigments*, 170:107636, November 2019. ISSN 0143-7208. doi:10.1016/j.dyepig.2019.107636. URL `http://dx.doi.org/10.1016/j.dyepig.2019.107636`.

[142] Cheng Qu, Guoqi Xia, Yincai Xu, Yunlong Zhu, Jixiong Liang, Hao Zhang, Jiaxuan Wang, Zuolun Zhang, and Yue Wang. Boron-containing d-a-a type tadf materials with tiny singlet-triplet energy splittings and high photoluminescence quantum yields for highly efficient oleds with low efficiency roll-offs. *Journal of Materials Chemistry C*, 8(11):3846–3854, 2020. ISSN 2050-7534. doi:10.1039/c9tc06497d. URL `http://dx.doi.org/10.1039/C9TC06497D`.

[143] Songpo Xiang, Zhi Huang, Shuaiqiang Sun, Xialei Lv, Lianwei Fan, Shaofeng Ye, Hongting Chen, Runda Guo, and Lei Wang. Highly efficient non-doped oleds using aggregation-induced delayed fluorescence materials based on 10-phenyl-10h-phenothiazine 5,5-dioxide derivatives. *Journal of Materials Chemistry C*, 6(42):11436–11443, 2018. ISSN 2050-7534. doi:10.1039/c8tc03648a. URL `http://dx.doi.org/10.1039/C8TC03648A`.

[144] Yi-Zhong Shi, Kai Wang, Xiao-Chun Fan, Hao Wu, Xue-Mei Ou, Jia Yu, Jian-Sheng Jie, and Xiao-Hong Zhang. Applying intermolecular hydrogen bonding to exploit tadf emitters for high-performance orange-red non-doped oleds. *Journal of Materials Chemistry C*, 10(12):4717–4722, 2022. ISSN 2050-7534. doi:10.1039/d1tc03803f. URL `http://dx.doi.org/10.1039/D1TC03803F`.

[145] Ning Zhang, Caijun Zheng, Zhipeng Chen, Juewen Zhao, Ming Zhang, Haoyu Yang, Zeyu He, Xiaoyang Du, and Silu Tao. Improving the efficiency of exciplex based oleds by controlling the different configurations of the donor. *Journal of Materials Chemistry C*, 9(2):600–608, 2021. ISSN 2050-7534. doi:10.1039/d0tc04315j. URL `http://dx.doi.org/10.1039/`

D0TC04315J.

[146] Xuan Zeng, Yu-Hsin Huang, Shaolong Gong, Pan Li, Wei-Kai Lee, Xiao Xiao, Yu Zhang, Cheng Zhong, Chung-Chih Wu, and Chuluo Yang. An unsymmetrical thermally activated delayed fluorescence emitter enables orange-red electroluminescence with 31.7% external quantum efficiency. *Materials Horizons*, 8(8):2286–2292, 2021. ISSN 2051-6355. doi:10.1039/d1mh00613d. URL http://dx.doi.org/10.1039/D1MH00613D.

[147] Xinxin Ban, Huange Xu, Guolong Yuan, Wei Jiang, Bin Huang, and Yueming Sun. Spirobifluorene/sulfone hybrid: Highly efficient solution-processable material for uv-violet electrofluorescence, blue and green phosphorescent oleds. *Organic Electronics*, 15(7):1678–1686, July 2014. ISSN 1566-1199. doi:10.1016/j.orgel.2014.03.035. URL http://dx.doi.org/10.1016/j.orgel.2014.03.035.

[148] Ruishan Huang, Hao Chen, Hao Liu, Zeyan Zhuang, Jianghui Wang, Maoxing Yu, Dezhi Yang, Dongge Ma, Zujin Zhao, and Ben Zhong Tang. Creating efficient delayed fluorescence luminogens with acridine-based spiro donors to improve horizontal dipole orientation for high-performance oleds. *Chemical Engineering Journal*, 435:134934, May 2022. ISSN 1385-8947. doi:10.1016/j.cej.2022.134934. URL http://dx.doi.org/10.1016/j.cej.2022.134934.

[149] Suna Choi, Mallesham Godumala, Ji Hyung Lee, Gyeong Heon Kim, Ji Su Moon, Jun Yun Kim, Dae-Wi Yoon, Joong Hwan Yang, Jinook Kim, Min Ju Cho, Jang Hyuk Kwon, and Dong Hoon Choi. Optimized structure of silane-core containing host materials for highly efficient blue tadf oleds. *Journal of Materials Chemistry C*, 5(26):6570–6577, 2017. ISSN 2050-7534. doi:10.1039/c7tc01357d. URL http://dx.doi.org/10.1039/C7TC01357D.

[150] Yonghong Chen, Shumeng Wang, Xiaofu Wu, Yuxiang Xu, Hua Li, Yang Liu, Hui Tong, and Lixiang Wang. Triazatruxene-based small molecules with thermally activated delayed fluorescence, aggregation-induced emission and mechanochromic luminescence properties for solution-processable nondoped oleds. *Journal of Materials Chemistry C*, 6(46):12503–12508, 2018. ISSN 2050-7534. doi:10.1039/c8tc04721a. URL http://dx.doi.org/10.1039/C8TC04721A.

[151] Guoyun Meng, Dongdong Zhang, Jinbei Wei, Yuewei Zhang, Tianyu Huang, Ziyang Liu, Chen Yin, Xiangchen Hong, Xiang Wang, Xuan Zeng, Dezhi Yang, Dongge Ma, Guomeng Li, and Lian Duan. Highly efficient and stable deep-blue oleds based on narrowband emitters featuring an orthogonal spiro-configured indolo[3,2,1-de]acridine structure. *Chemical Science*, 13 (19):5622–5630, 2022. ISSN 2041-6539. doi:10.1039/d2sc01543a. URL http://dx.doi.org/10.1039/D2SC01543A.

[152] Lingjuan Wei, Jie Li, Kai Xue, Shanghui Ye, and Hongji Jiang. Synthesis and structure-property correlation of blue fluorescence isomer emitters based on rigid pyrazine-bridged carbazole frameworks. *New Journal of Chemistry*, 43(42): 16629–16638, 2019. ISSN 1369-9261. doi:10.1039/c9nj04043a. URL http://dx.doi.org/10.1039/C9NJ04043A.

[153] Jessica C. Berrones-Reyes, C.C. Vidyasagar, Blanca M. Muñoz Flores, and Víctor M. Jiménez-Pérez. Luminescent molecules of main group elements: Recent advances on synthesis, properties and their application on fluorescent bioimaging (fbi). *Journal of Luminescence*, 195:290–313, March 2018. ISSN 0022-2313. doi:10.1016/j.jlumin.2017.11.042. URL http://dx.doi.org/10.1016/j.jlumin.2017.11.042.

[154] Chao Wu, Binyan Wang, Yafei Wang, Jianyong Hu, Jiaxing Jiang, Dongge Ma, and Qiang Wang. A universal host material with a simple structure for monochrome and white phosphorescent/tadf oleds. *Journal of Materials Chemistry C*, 7(3): 558–566, 2019. ISSN 2050-7534. doi:10.1039/c8tc05259j. URL http://dx.doi.org/10.1039/C8TC05259J.

[155] Wentong Gao, Wenlu Wu, Shihai Cao, Bing Han, and Nengquan Li. A simple bipolar host material based on triphenylamine and pyridine featuring Ïf-linkage for efficient solution-processed phosphorescent organic light-emitting diodes. *Optical Materials*, 133:112871, November 2022. ISSN 0925-3467. doi:10.1016/j.optmat.2022.112871. URL http://dx.doi.org/10.1016/j.optmat.2022.112871.

[156] Kaiyong Sun, Yibai Sun, Wei Jiang, Suli Huang, Wenwen Tian, and Yueming Sun. Highly efficient and color tunable thermally activated delayed fluorescent emitters and their applications for the solution-processed oleds. *Dyes and Pigments*, 139:326–333, April 2017. ISSN 0143-7208. doi:10.1016/j.dyepig.2016.12.037. URL http://dx.doi.org/10.1016/j.dyepig.2016.12.037.

[157] Chengwei Lin, Pengbo Han, Fenlan Qu, Shu Xiao, Yuanzhao Li, Dian Xie, Xianfeng Qiao, Dezhi Yang, Yanfeng Dai, Qian Sun, Anjun Qin, Ben Zhong Tang, and Dongge Ma. Suppressing singlet-triplet annihilation processes to achieve highly efficient deep-blue aie-based oleds. *Materials Horizons*, 9(9):2376–2383, 2022. ISSN 2051-6355. doi:10.1039/d2mh00627h. URL http://dx.doi.org/10.1039/D2MH00627H.

[158] Jinglai Zhang, Huijuan Yuan, Songyan Feng, Keke Wen, and Xugeng Guo. Theoretical studies on electroluminescent mechanism of a series of thermally activated delayed fluorescence emitters possessing asymmetric-triazine-cored triads. *Spectrochimica Acta Part A: Molecular and Biomolecular Spectroscopy*, 202:102–106, September 2018. ISSN 1386-1425. doi:10.1016/j.saa.2018.05.032. URL http://dx.doi.org/10.1016/j.saa.2018.05.032.

[159] Kaiyong Sun, Wenwen Tian, Chengyan Ge, Feng Gu, Yu Zhou, Wangxia Wang, Zhaosheng Cai, Wei Jiang, and Yueming Sun. Creation of efficient solution-processed oleds via a strategy of the host-guest system constructing with two small cross-linkable tadf molecules. *Organic Electronics*, 101:106417, February 2022. ISSN 1566-1199. doi:10.1016/j.orgel.2021.106417. URL http://dx.doi.org/10.1016/j.orgel.2021.106417.

[160] Yu Fu, Zecong Ye, Jingping Xiao, Liyun Liao, Lifen Chen, Yingxiao Mu, Shaomin Ji, Zujin Zhao, Hao-Li Zhang, and Yanping Huo. Large effects of tiny structural changes on the aie-tadf type xanthone derivatives in mechano-responsive luminescence and electroluminescence. *Dyes and Pigments*, 205:110550, September 2022. ISSN 0143-7208. doi:10.1016/j.dyepig.2022.110550. URL http://dx.doi.org/10.1016/j.dyepig.2022.110550.

[161] Zhao-Yi Wang, Lin-Xi Shi, Liang-Jin Xu, Li-Yi Zhang, Jin-Yun Wang, and Zhong-Ning Chen. Modulating the carrier transport of ptag2 heteronuclear complexes to attain highly efficient oleds with narrow-band emission. *Journal of Materials Chemistry C*, 9(16):5403–5410, 2021. ISSN 2050-7534. doi:10.1039/d1tc00678a. URL http://dx.doi.org/10.1039/D1TC00678A.

[162] Fangfang Wang, Jia Hu, Xudong Cao, Tao Yang, Youtian Tao, Ling Mei, Xinwen Zhang, and Wei Huang. A low-cost phenylbenzoimidazole containing electron transport material for efficient green phosphorescent and thermally activated delayed fluorescent oleds. *Journal of Materials Chemistry C*, 3(21):5533–5540, 2015. ISSN 2050-7534. doi: 10.1039/c5tc00350d. URL http://dx.doi.org/10.1039/C5TC00350D.

[163] Jaipal Devesing Girase, Shahnawaz, Jwo-Huei Jou, Sabita Patel, and Sivakumar Vaidyanathan. Solution-processed deep-blue fluorophores based on phenanthroimidazole integrated with benzimidazole with hlct character for efficient deep-blue organic light emitting devices. *Dyes and Pigments*, 206:110623, October 2022. ISSN 0143-7208. doi:10.1016/j.dyepig.2022.110623. URL http://dx.doi.org/10.1016/j.dyepig.2022.110623.

[164] Xiaorui Dong, Ronghua Li, Yanan Zheng, Jinnan Huo, Yinpeng Cao, and Heping Shi. Synthesis, photoluminescence and electroluminescence properties of a new blue emitter with aggregation-induced emission and thermally activated delayed fluorescence characteristics. *Spectrochimica Acta Part A: Molecular and Biomolecular Spectroscopy*, 291:122344, April 2023. ISSN 1386-1425. doi:10.1016/j.saa.2023.122344. URL http://dx.doi.org/10.1016/j.saa.2023.122344.

[165] Jia Hu, Xianping Zhang, Di Zhang, Xudong Cao, Tao Jiang, Xinwen Zhang, and Youtian Tao. Linkage modes on phthaloyl/triphenylamine hybrid compounds: Multi-functional aie luminogens, non-doped emitters and organic hosts for highly efficient solution-processed delayed fluorescence oleds. *Dyes and Pigments*, 137:480–489, February 2017. ISSN 0143-7208. doi:10.1016/j.dyepig.2016.10.029. URL http://dx.doi.org/10.1016/j.dyepig.2016.10.029.

[166] Paul Kautny, Chenyang Zhao, Dominik Schopf, Berthold Stöger, Ernst Horkel, Jiangshan Chen, Dongge Ma, Johannes Fröhlich, and Daniel Lumpi. Thieno[3,4-c]pyrrole-4,6-dione as novel building block for host materials for red pholeds. *Journal of Materials Chemistry C*, 5(8):1997–2004, 2017. ISSN 2050-7534. doi:10.1039/c6tc05248g. URL http://dx.doi.org/10.1039/C6TC05248G.

[167] Xing Wu, Jiajie Zeng, Xiaoluo Peng, Huijun Liu, Ben Zhong Tang, and Zujin Zhao. Robust sky-blue aggregation-induced delayed fluorescence materials for high-performance top-emitting oleds and single emissive layer white oleds. *Chemical Engineering Journal*, 451:138919, January 2023. ISSN 1385-8947. doi:10.1016/j.cej.2022.138919. URL http://dx.doi.org/10.1016/j.cej.2022.138919.

[168] Nengquan Li, Danyang Chai, Zhanxiang Chen, Changjiang Zhou, Fan Ni, Zhongyan Huang, Xiaosong Cao, Guohua Xie, Kai Li, and Chuluo Yang. Molecular engineering by Ïf-bond spacer enables solution-processable host materials for tadf emitter towards high-performance oleds. *Chemical Engineering Journal*, 396:125276, September 2020. ISSN 1385-8947. doi:10.1016/j.cej.2020.125276. URL http://dx.doi.org/10.1016/j.cej.2020.125276.

[169] Zilong Wu, Shaoxin Song, Xiangyu Zhu, Hao Chen, Jiajin Chi, Dongge Ma, Zujin Zhao, and Ben Zhong Tang. Highly efficient deep-blue fluorescent oleds based on anthracene derivatives with a triplet-triplet annihilation mechanism. *Materials Chemistry Frontiers*, 5(18):6978–6986, 2021. ISSN 2052-1537. doi:10.1039/d1qm00880c. URL http://dx.doi.org/10.1039/D1QM00880C.

[170] Ling Peng, Jichen Lv, Shu Xiao, Yumiao Huo, Yuchao Liu, Dongge Ma, Shian Ying, and Shouke Yan. High-performance non-doped near ultraviolet oleds with the eqe ∼ 6% and ciey ∼ 0.03 from high-lying reverse intersystem crossing. *Chemical Engineering Journal*, 450:138339, December 2022. ISSN 1385-8947. doi:10.1016/j.cej.2022.138339. URL http://dx.doi.org/10.1016/j.cej.2022.138339.

[171] Tae Hoon Ha, Jong-Kwan Bin, and Chil Won Lee. Phenylpyridine and carbazole based host materials for highly efficient blue tadf oleds. *Organic Electronics*, 102:106450, March 2022. ISSN 1566-1199. doi:10.1016/j.orgel.2022.106450. URL http://dx.doi.org/10.1016/j.orgel.2022.106450.

[172] Shaofeng Ye, Yaxiong Wang, Runda Guo, Qing Zhang, Xialei Lv, Yalei Duan, Panpan Leng, Shuaiqiang Sun, and Lei Wang. Asymmetric anthracene derivatives as multifunctional electronic materials for constructing simplified and efficient non-doped homogeneous deep blue fluorescent oleds. *Chemical Engineering Journal*, 393:124694, August 2020. ISSN 1385-8947. doi:10.1016/j.cej.2020.124694. URL http://dx.doi.org/10.1016/j.cej.2020.124694.

[173] Chen Zhang, Dongxin Ma, Ruihuan Liu, and Lian Duan. High-efficiency blue-green electroluminescence from sublimable cationic iridium(¡scp¿iii¡/scp¿) complexes with a pyrazole-type ligand. *Journal of Materials Chemistry C*, 7(12):3503–3511, 2019. ISSN 2050-7534. doi:10.1039/c9tc00465c. URL http://dx.doi.org/10.1039/C9TC00465C.

[174] Yang Liu, Yuliang Wu, Tong Wang, Qian Wang, Xianchao Han, Xiaofu Wu, Hui Tong, and Lixiang Wang. Bridged triazatruxene-based host materials for solution-processed thermally activated delayed fluorescence organic light emitting diodes with high power efficiency. *Organic Electronics*, 113:106720, February 2023. ISSN 1566-1199. doi:10.1016/j.orgel.2022.106720. URL http://dx.doi.org/10.1016/j.orgel.2022.106720.

[175] Bin Huang, Xinxin Ban, Kaiyong Sun, Zhongming Ma, Yanan Mei, Wei Jiang, Baoping Lin, and Yueming Sun. Thermally activated delayed fluorescence materials based on benzophenone derivative as emitter for efficient solution-processed non-doped green oled. *Dyes and Pigments*, 133:380–386, October 2016. ISSN 0143-7208. doi:10.1016/j.dyepig.2016.06.025. URL http://dx.doi.org/10.1016/j.dyepig.2016.06.025.

[176] Jee Hyun Maeng, Ramanaskanda Braveenth, Young Hun Jung, Soon Jae Hwang, Hyuna Lee, Hye Li Min, Jun Yun Kim, Chang Wook Han, and Jang Hyuk Kwon. Efficiency enhancement in orange red thermally activated delayed fluorescence oleds by using a rigid di-indolocarbazole donor moiety. *Dyes and Pigments*, 194:109580, October 2021. ISSN 0143-7208. doi:10.1016/j.dyepig.2021.109580. URL http://dx.doi.org/10.1016/j.dyepig.2021.109580.

[177] Shantaram Kothavale, Junseop Lim, and Jun Yeob Lee. Rational design of cn substituted dibenzo[a,c]phenazine acceptor for color tuning of thermally activated delayed fluorescent emitters. *Chemical Engineering Journal*, 431:134216, March 2022. ISSN 1385-8947. doi:10.1016/j.cej.2021.134216. URL http://dx.doi.org/10.1016/j.cej.2021.134216.

[178] Qing Zhang, Shuaiqiang Sun, Won Jae Chung, Sung Joon Yoon, Yaxiong Wang, Runda Guo, Shaofeng Ye, Jun Yeob Lee, and Lei Wang. Highly efficient tadf oleds with low efficiency roll-off based on novel acridine-carbazole hybrid

donor-substituted pyrimidine derivatives. *Journal of Materials Chemistry C*, 7(39):12248–12255, 2019. ISSN 2050-7534. doi:10.1039/c9tc04284a. URL http://dx.doi.org/10.1039/C9TC04284A.

[179] Dong Jin Shin, Soon Jae Hwang, Junseop Lim, Chae Yeon Jeon, Jun Yeob Lee, and Jang Hyuk Kwon. Reverse intersystem crossing accelerating assistant dopant for high efficiency and long lifetime in red hyperfluorescence organic light-emitting diodes. *Chemical Engineering Journal*, 446:137181, October 2022. ISSN 1385-8947. doi:10.1016/j.cej.2022.137181. URL http://dx.doi.org/10.1016/j.cej.2022.137181.

[180] Yifan Li, Tianheng Chen, Manli Huang, Yu Gu, Shaolong Gong, Guohua Xie, and Chuluo Yang. Tuning the twist angle of thermally activated delayed fluorescence molecules via a dendronization strategy: high-efficiency solution-processed non-doped oleds. *Journal of Materials Chemistry C*, 5(14):3480–3487, 2017. ISSN 2050-7534. doi:10.1039/c7tc00119c. URL http://dx.doi.org/10.1039/C7TC00119C.

[181] Zian Wang, Jingwen Yao, Lisi Zhan, Shaolong Gong, Dongge Ma, and Chuluo Yang. Purine-based thermally activated delayed fluorescence emitters for efficient organic light-emitting diodes. *Dyes and Pigments*, 180:108437, September 2020. ISSN 0143-7208. doi:10.1016/j.dyepig.2020.108437. URL http://dx.doi.org/10.1016/j.dyepig.2020.108437.

[182] Jayabalan Pandidurai, Jayachandran Jayakumar, Natarajan Senthilkumar, and Chien-Hong Cheng. Effects of intramolecular hydrogen bonding on the conformation and luminescence properties of dibenzoylpyridine-based thermally activated delayed fluorescence materials. *Journal of Materials Chemistry C*, 7(42):13104–13110, 2019. ISSN 2050-7534. doi:10.1039/c9tc04536h. URL http://dx.doi.org/10.1039/C9TC04536H.

[183] T. Huang, X. Song, M. Cai, D. Zhang, and L. Duan. Improving reverse intersystem crossing in exciplex-forming hosts by introducing heavy atom effect. *Materials Today Energy*, 21:100705, September 2021. ISSN 2468-6069. doi: 10.1016/j.mtener.2021.100705. URL http://dx.doi.org/10.1016/j.mtener.2021.100705.

[184] Juan Zhao, Zhan Yang, Xiaojie Chen, Zongliang Xie, Tiantian Liu, Zhihe Chi, Zhiyong Yang, Yi Zhang, Matthew P. Aldred, and Zhenguo Chi. Efficient triplet harvesting in fluorescence-tadf hybrid warm-white organic light-emitting diodes with a fully non-doped device configuration. *Journal of Materials Chemistry C*, 6(15):4257–4264, 2018. ISSN 2050-7534. doi:10.1039/c8tc01210e. URL http://dx.doi.org/10.1039/C8TC01210E.

[185] Gloria Hong, Changfeng Si, Abhishek Kumar Gupta, Claudia Bizzarri, Martin Nieger, Ifor D. W. Samuel, Eli Zysman-Colman, and Stefan Bräse. Fluorinated dibenzo[a,c]-phenazine-based green to red thermally activated delayed fluorescent oled emitters. *Journal of Materials Chemistry C*, 10(12):4757–4766, 2022. ISSN 2050-7534. doi:10.1039/d1tc04918f. URL http://dx.doi.org/10.1039/D1TC04918F.

[186] Pan Li, Yepeng Xiang, Shaolong Gong, Wei-Kai Lee, Yu-Hsin Huang, Chun-Yu Wang, Chuluo Yang, and Chung-Chih Wu. Quinazoline-based thermally activated delayed fluorescence emitters for high-performance organic light-emitting diodes with external quantum efficiencies about 28%. *Journal of Materials Chemistry C*, 9(37):12633–12641, 2021. ISSN 2050-7534. doi:10.1039/d1tc02633j. URL http://dx.doi.org/10.1039/D1TC02633J.

[187] Yasunori Matsui, Yudai Yokoyama, Takuya Ogaki, Kenta Ishiharaguchi, Akitsugu Niwa, Eisuke Ohta, Masaki Saigo, Kiyoshi Miyata, Ken Onda, Hiroyoshi Naito, and Hiroshi Ikeda. Aggregation-induced emission active thermally-activated delayed fluorescence materials possessing n-heterocycle and sulfonyl groups. *Journal of Materials Chemistry C*, 10(12): 4607–4613, 2022. ISSN 2050-7534. doi:10.1039/d1tc05196b. URL http://dx.doi.org/10.1039/D1TC05196B.

[188] Xiangchen Hong, Dongdong Zhang, Chen Yin, Qi Wang, Yuewei Zhang, Tianyu Huang, Jinbei Wei, Xuan Zeng, Guoyun Meng, Xiang Wang, Guomeng Li, Dezhi Yang, Dongge Ma, and Lian Duan. Tadf molecules with π-extended acceptors for simplified high-efficiency blue and white organic light-emitting diodes. *Chem*, 8(6):1705–1719, June 2022. ISSN 2451-9294. doi:10.1016/j.chempr.2022.02.017. URL http://dx.doi.org/10.1016/j.chempr.2022.02.017.

[189] Levani Skhirtladze, Karolis Leitonas, Audrius Bucinskas, Kai Lin Woon, Dmytro Volyniuk, Rasa KeruckienÄ—, Malek Mahmoudi, Mieczyslaw Lapkowski, Azhar Ariffin, and Juozas V. Grazulevicius. Turn on of room temperature phosphorescence of donor-acceptor-donor type compounds via transformation of excited states by rigid hosts for oxygen sensing. *Sensors and Actuators B: Chemical*, 380:133295, April 2023. ISSN 0925-4005. doi:10.1016/j.snb.2023.133295. URL http://dx.doi.org/10.1016/j.snb.2023.133295.

[190] Jiyoung Lee, Katsuyuki Shizu, Hiroyuki Tanaka, Hiroko Nomura, Takuma Yasuda, and Chihaya Adachi. Oxadiazole- and triazole-based highly-efficient thermally activated delayed fluorescence emitters for organic light-emitting diodes. *Journal of Materials Chemistry C*, 1(30):4599, 2013. ISSN 2050-7534. doi:10.1039/c3tc30699b. URL http://dx.doi.org/10.1039/C3TC30699B.

[191] Xiangan Song, Zhangshan Liu, Mengyao Lu, Shengnan Zou, Fengyun Guo, Shiyong Gao, Zujin Zhao, Ben Zhong Tang, and Yong Zhang. Efficient thermally activated delayed fluorescent emitter based on a spiro-type benzo[b]acridine donor and a benzophenone acceptor. *Journal of Materials Chemistry C*, 10(46):17550–17556, 2022. ISSN 2050-7534. doi:10.1039/d2tc03421b. URL http://dx.doi.org/10.1039/D2TC03421B.

[192] Sunyoung Sohn, Bong Hyun Koh, Jae Yeul Baek, Hyun Chan Byun, Jae Hyun Lee, Dong-Seon Shin, Hyungju Ahn, Han-Koo Lee, Jaeyoung Hwang, Sungjune Jung, and Yun-Hi Kim. Synthesis and characterization of diphenylamine derivative containing malononitrile for thermally activated delayed fluorescent emitter. *Dyes and Pigments*, 140:14–21, May 2017. ISSN 0143-7208. doi:10.1016/j.dyepig.2017.01.010. URL http://dx.doi.org/10.1016/j.dyepig.2017.01.010.

[193] Qian Li, Jingyi Xu, Shuer Tan, Yu Dai, Jie Xue, and Juan Qiao. Approaching 800Â nm near-infrared thermally activated delay fluorescence materials via simple malononitrile condensation strategy. *Organic Electronics*, 110:106645, November 2022. ISSN 1566-1199. doi:10.1016/j.orgel.2022.106645. URL http://dx.doi.org/10.1016/j.orgel.2022.106645.

[194] Xialei Lv, Shuaiqiang Sun, Qing Zhang, Shaofeng Ye, Wei Liu, Yaxiong Wang, Runda Guo, and Lei Wang. A strategy to construct multifunctional tadf materials for deep blue and high efficiency yellow fluorescent devices. *Journal of Materials Chemistry C*, 8(14):4818–4826, 2020. ISSN 2050-7534. doi:10.1039/d0tc00039f. URL http://dx.doi.org/10.1039/

D0TC00039F.

[195] Fei-Xiang Huang, Hao-Ze Li, Feng-Ming Xie, Xin-Yi Zeng, Yan-Qing Li, Ying-Yuan Hu, Jian-Xin Tang, and Xin Zhao. Efficient orange-red thermally activated delayed fluorescence material containing a cyano group. *Dyes and Pigments*, 195:109731, November 2021. ISSN 0143-7208. doi:10.1016/j.dyepig.2021.109731. URL `http://dx.doi.org/10.1016/j.dyepig.2021.109731`.

[196] Masatsugu Taneda, Katsuyuki Shizu, Hiroyuki Tanaka, and Chihaya Adachi. High efficiency thermally activated delayed fluorescence based on 1,3,5-tris(4-(diphenylamino)phenyl)-2,4,6-tricyanobenzene. *Chemical Communications*, 51(24): 5028–5031, 2015. ISSN 1364-548X. doi:10.1039/c5cc00511f. URL `http://dx.doi.org/10.1039/C5CC00511F`.

[197] He Liu, Jiafang Li, Wen-Cheng Chen, Zhanxiang Chen, Zhiwen Liu, Qun Zhan, Xiaosong Cao, Chun-Sing Lee, and Chuluo Yang. Modulating the acceptor structure of dicyanopyridine based tadf emitters: Nearly 30% external quantum efficiency and suppression on efficiency roll-off in oled. *Chemical Engineering Journal*, 401:126107, December 2020. ISSN 1385-8947. doi:10.1016/j.cej.2020.126107. URL `http://dx.doi.org/10.1016/j.cej.2020.126107`.

[198] Hannes Puntscher, Paul Kautny, Berthold Stöger, Antoine Tissot, Christian Hametner, Hans R. Hagemann, Johannes Fröhlich, Thomas Baumgartner, and Daniel Lumpi. Structure-property studies of p-triarylamine-substituted dithieno[3,2-b:2',3'-d]phospholes. *RSC Advances*, 5(114):93797–93807, 2015. ISSN 2046-2069. doi:10.1039/c5ra13651b. URL `http://dx.doi.org/10.1039/C5RA13651B`.

[199] R. Keruckiene, M. Guzauskas, E. Narbutaitis, U. Tsiko, D. Volyniuk, Pei-Hsi Lee, Chia-Hsun Chen, Tien-Lung Chiu, Chi-Feng Lin, Jiun-Haw Lee, and J.V. Grazulevicius. Exciplex-forming derivatives of 2,7-di-tert-butyl-9,9-dimethylacridan and benzotrifluoride for efficient oleds. *Organic Electronics*, 78:105576, March 2020. ISSN 1566-1199. doi:10.1016/j.orgel.2019.105576. URL `http://dx.doi.org/10.1016/j.orgel.2019.105576`.

[200] Xiang-Dong Zhu, Qi-Sheng Tian, Qi Zheng, Ya-Kun Wang, Yi Yuan, Yun Li, Zuo-Quan Jiang, and Liang-Sheng Liao. Deep-blue thermally activated delayed fluorescence materials with high glass transition temperature. *Journal of Luminescence*, 206:146–153, February 2019. ISSN 0022-2313. doi:10.1016/j.jlumin.2018.10.017. URL `http://dx.doi.org/10.1016/j.jlumin.2018.10.017`.

[201] Jianfeng Zhang, Xinjun Xu, Chuang Yao, Jinghong Peng, Manping Jia, and Lidong Li. A novel ternary organic microwire radial heterojunction with high photoconductivity. *Journal of Materials Chemistry C*, 4(20):4505–4511, 2016. ISSN 2050-7534. doi:10.1039/c6tc00214e. URL `http://dx.doi.org/10.1039/C6TC00214E`.

[202] Guimin Zhao, Renyin Zhou, Guanghao Zhang, Haowen Chen, Daiyu Ma, Wenwen Tian, Wei Jiang, and Yueming Sun. A periphery hindered strategy with a dopant and sensitizer for solution-processed red tsf-oleds with high color purity. *Journal of Materials Chemistry C*, 10(13):5230–5239, 2022. ISSN 2050-7534. doi:10.1039/d2tc00238h. URL `http://dx.doi.org/10.1039/D2TC00238H`.

[203] Kenkera Rayappa Naveen, Hyuna Lee, Ramanaskanda Braveenth, Ki Joon Yang, Soon Jae Hwang, and Jang Hyuk Kwon. Deep blue diboron embedded multi-resonance thermally activated delayed fluorescence emitters for narrowband organic light emitting diodes. *Chemical Engineering Journal*, 432:134381, March 2022. ISSN 1385-8947. doi:10.1016/j.cej.2021.134381. URL `http://dx.doi.org/10.1016/j.cej.2021.134381`.

[204] Yepeng Xiang, Ze-Lin Zhu, Dongjun Xie, Shaolong Gong, Kailong Wu, Guohua Xie, Chun-Sing Lee, and Chuluo Yang. Revealing the new potential of an indandione unit for constructing efficient yellow thermally activated delayed fluorescence emitters with short emissive lifetimes. *Journal of Materials Chemistry C*, 6(26):7111–7118, 2018. ISSN 2050-7534. doi:10.1039/c8tc01656a. URL `http://dx.doi.org/10.1039/C8TC01656A`.

[205] Zhengqi Xiao, Nengquan Li, Wei Yang, Zhongyan Huang, Xiaosong Cao, Taian Huang, Zhanxiang Chen, and Chuluo Yang. Saccharin-derived multifunctional emitters featuring concurrently room temperature phosphorescence, thermally activated delayed fluorescence and aggregation-induced enhanced emission. *Chemical Engineering Journal*, 419:129628, September 2021. ISSN 1385-8947. doi:10.1016/j.cej.2021.129628. URL `http://dx.doi.org/10.1016/j.cej.2021.129628`.

[206] Shantaram Kothavale, Won Jae Chung, and Jun Yeob Lee. High efficiency and long lifetime orange-red thermally activated delayed fluorescent organic light emitting diodes by donor and acceptor engineering. *Journal of Materials Chemistry C*, 9 (2):528–536, 2021. ISSN 2050-7534. doi:10.1039/d0tc04465b. URL `http://dx.doi.org/10.1039/D0TC04465B`.

[207] Ju Hui Yun and Jun Yeob Lee. Benzoisoquinoline-1,3-dione acceptor based red thermally activated delayed fluorescent emitters. *Dyes and Pigments*, 144:212–217, September 2017. ISSN 0143-7208. doi:10.1016/j.dyepig.2017.05.036. URL `http://dx.doi.org/10.1016/j.dyepig.2017.05.036`.

[208] Zhen Zhang, Dongxue Ding, Ying Wei, Jing Zhang, Chunmiao Han, and Hui Xu. Excited-state engineering of universal ambipolar hosts for highly efficient blue phosphorescence and thermally activated delayed fluorescence organic light-emitting diodes. *Chemical Engineering Journal*, 382:122485, February 2020. ISSN 1385-8947. doi:10.1016/j.cej.2019.122485. URL `http://dx.doi.org/10.1016/j.cej.2019.122485`.

[209] Jia-Xiong Chen, Wen-Wen Tao, Ya-Fang Xiao, Shuang Tian, Wen-Cheng Chen, Kai Wang, Jia Yu, Feng-Xia Geng, Xiao-Hong Zhang, and Chun-Sing Lee. Isomeric thermally activated delayed fluorescence emitters based on indolo[2,3-b]acridine electron-donor: a compromising optimization for efficient orange-red organic light-emitting diodes. *Journal of Materials Chemistry C*, 7(10):2898–2904, 2019. ISSN 2050-7534. doi:10.1039/c8tc06081a. URL `http://dx.doi.org/10.1039/c8tc06081a`.

[210] Xiang-Dong Zhu, Chen-Chen Peng, Fan-Cheng Kong, Sheng-Yi Yang, Hong-Cheng Li, Sarvendra Kumar, Tong-Tong Wang, Zuo-Quan Jiang, and Liang-Sheng Liao. Acceptor modulation for improving a spiro-type thermally activated delayed fluorescence emitter. *Journal of Materials Chemistry C*, 8(25):8579–8584, 2020. ISSN 2050-7534. doi:10.1039/d0tc00743a. URL `http://dx.doi.org/10.1039/D0TC00743A`.

[211] Keiro Nasu, Tetsuya Nakagawa, Hiroko Nomura, Chi-Jen Lin, Chien-Hong Cheng, Mei-Rurng Tseng, Takuma Yasuda, and Chihaya Adachi. A highly luminescent spiro-anthracenone-based organic light-emitting diode exhibiting thermally activated

delayed fluorescence. *Chemical Communications*, 49(88):10385–10387, 2013. ISSN 1364-548X. doi:10.1039/c3cc44179b. URL `http://dx.doi.org/10.1039/C3CC44179B`.

[212] Xun Liu, Yin-Feng Wang, Meng Li, Yongheng Zhu, and Chuan-Feng Chen. Aromatic-imide-based tadf material as emitter for efficient yellow and white organic light-emitting diodes. *Organic Electronics*, 88:106017, January 2021. ISSN 1566-1199. doi:10.1016/j.orgel.2020.106017. URL `http://dx.doi.org/10.1016/j.orgel.2020.106017`.

[213] Xu Gong, Chen-Han Lu, Wei-Kai Lee, Pan Li, Yu-Hsin Huang, Zhanxiang Chen, Lisi Zhan, Chung-Chih Wu, Shaolong Gong, and Chuluo Yang. High-efficiency red thermally activated delayed fluorescence emitters based on benzothiophene-fused spiro-acridine donor. *Chemical Engineering Journal*, 405:126663, February 2021. ISSN 1385-8947. doi:10.1016/j.cej.2020.126663. URL `http://dx.doi.org/10.1016/j.cej.2020.126663`.

[214] Yin Chen, Yun-Xin Wang, Chin-Wei Lu, and Hai-Ching Su. Deep-red light-emitting electrochemical cells based on phosphor-sensitized thermally activated delayed fluorescence. *Journal of Materials Chemistry C*, 10(31):11211–11219, 2022. ISSN 2050-7534. doi:10.1039/d2tc01727j. URL `http://dx.doi.org/10.1039/D2TC01727J`.

[215] Wei Yang, Weiming Ning, Shaolong Gong, and Chuluo Yang. Deep-red thermally activated delayed fluorescence emitters based on a phenanthroline-containing planar acceptor. *Dyes and Pigments*, 192:109474, August 2021. ISSN 0143-7208. doi:10.1016/j.dyepig.2021.109474. URL `http://dx.doi.org/10.1016/j.dyepig.2021.109474`.

[216] Shantaram Kothavale, Won Jae Chung, and Jun Yeob Lee. Color tuning of dibenzo[a,c]phenazine-2,7-dicarbonitrile-derived thermally activated delayed fluorescence emitters from yellow to deep-red. *Journal of Materials Chemistry C*, 8(21): 7059–7066, 2020. ISSN 2050-7534. doi:10.1039/d0tc00960a. URL `http://dx.doi.org/10.1039/D0TC00960A`.

[217] Shin Hyung Choi, Chan Hee Lee, Chihaya Adachi, and Sae Youn Lee. Highly effective nicotinonitrile-derivatives-based thermally activated delayed fluorescence emitter with asymmetric molecular architecture for high-performance organic light-emitting diodes. *Dyes and Pigments*, 172:107849, January 2020. ISSN 0143-7208. doi:10.1016/j.dyepig.2019.107849. URL `http://dx.doi.org/10.1016/j.dyepig.2019.107849`.

[218] Jinho Park, Junyoung Moon, Junseop Lim, Jeongkyu Woo, Seung Soo Yoon, and Jun Yeob Lee. Fine-tuned asymmetric blue multiple resonance thermally activated delayed fluorescence emitters with high efficiency and narrow emission band. *Journal of Materials Chemistry C*, 10(34):12300–12306, 2022. ISSN 2050-7534. doi:10.1039/d2tc02283d. URL `http://dx.doi.org/10.1039/D2TC02283D`.

[219] Jinnan Huo, Shu Xiao, Yuanyuan Wu, Mengxing Li, Hongbo Tong, Heping Shi, Dongge Ma, and Ben Zhong Tang. Molecular engineering of blue diphenylsulfone-based emitter with aggregation-enhanced emission and thermally activated delayed fluorescence characteristics: impairing intermolecular electron-exchange interactions using steric hindrance. *Chemical Engineering Journal*, 452:138957, January 2023. ISSN 1385-8947. doi:10.1016/j.cej.2022.138957. URL `http://dx.doi.org/10.1016/j.cej.2022.138957`.

[220] Jin Won Sun, Jang Yeol Baek, Kwon-Hyeon Kim, Jin-Suk Huh, Soon-Ki Kwon, Yun-Hi Kim, and Jang-Joo Kim. Azasiline-based thermally activated delayed fluorescence emitters for blue organic light emitting diodes. *Journal of Materials Chemistry C*, 5(5):1027–1032, 2017. ISSN 2050-7534. doi:10.1039/c6tc04653c. URL `http://dx.doi.org/10.1039/C6TC04653C`.

[221] D. H. Kim, K. Inada, L. Zhao, T. Komino, N. Matsumoto, J. C. Ribierre, and C. Adachi. Organic light emitting diodes with horizontally oriented thermally activated delayed fluorescence emitters. *Journal of Materials Chemistry C*, 5(5): 1216–1223, 2017. ISSN 2050-7534. doi:10.1039/c6tc04786f. URL `http://dx.doi.org/10.1039/C6TC04786F`.

[222] Minghan Cai, Morgan Auffray, Dongdong Zhang, Yuewei Zhang, Ryo Nagata, Zesen Lin, Xun Tang, Chin-Yiu Chan, Yi-Ting Lee, Tianyu Huang, Xiaozeng Song, Youichi Tsuchiya, Chihaya Adachi, and Lian Duan. Enhancing spin-orbital coupling in deep-blue/blue tadf emitters by minimizing the distance from the heteroatoms in donors to acceptors. *Chemical Engineering Journal*, 420:127591, September 2021. ISSN 1385-8947. doi:10.1016/j.cej.2020.127591. URL `http://dx.doi.org/10.1016/j.cej.2020.127591`.

[223] Yuan-Lan Zhang, Quan Ran, Qiang Wang, Qi-Sheng Tian, Fan-Cheng Kong, Jian Fan, and Liang-Sheng Liao. High-performance sky-blue phosphorescent organic light-emitting diodes employing wide-bandgap bipolar host materials with thermally activated delayed fluorescence characteristics. *Organic Electronics*, 81:105660, June 2020. ISSN 1566-1199. doi:10.1016/j.orgel.2020.105660. URL `http://dx.doi.org/10.1016/j.orgel.2020.105660`.

[224] Hyung Jong Kim, Seong Keun Kim, Mallesham Godumala, Jiwon Yoon, Chae Yeong Kim, Ji-Eun Jeong, Han Young Woo, Jang Hyuk Kwon, Min Ju Cho, and Dong Hoon Choi. Novel molecular triad exhibiting aggregation-induced emission and thermally activated fluorescence for efficient non-doped organic light-emitting diodes. *Chemical Communications*, 55(64): 9475–9478, 2019. ISSN 1364-548X. doi:10.1039/c9cc05391c. URL `http://dx.doi.org/10.1039/C9CC05391C`.

[225] Jia-Xiong Chen, Hui Wang, Lu Zhou, Kai Wang, Jia Yu, and Xiao-Hong Zhang. Structure-property investigation of two red tadf isomers with different d-a conjugation for superior exciton utilization. *Dyes and Pigments*, 208:110801, January 2023. ISSN 0143-7208. doi:10.1016/j.dyepig.2022.110801. URL `http://dx.doi.org/10.1016/j.dyepig.2022.110801`.

[226] You-Ping Ma, Guoliang Wang, Min Zhao, Zi-Fa Shi, Yanqin Miao, Xiao-Ping Cao, and Hao-Li Zhang. A red thermally activated delayed fluorescence emitter based on benzo[c][1,2,5]thiadiazole. *Dyes and Pigments*, 212:111084, April 2023. ISSN 0143-7208. doi:10.1016/j.dyepig.2023.111084. URL `http://dx.doi.org/10.1016/j.dyepig.2023.111084`.

[227] Rajendra Kumar Konidena, Kyung Hyung Lee, and Jun Yeob Lee. 6h-benzo[4,5]thieno[2,3-b]indole as a novel donor for efficient thermally activated delayed fluorescence emitters with eqes over 20%. *Journal of Materials Chemistry C*, 7(44): 13912–13919, 2019. ISSN 2050-7534. doi:10.1039/c9tc04679h. URL `http://dx.doi.org/10.1039/C9TC04679H`.

[228] Ha Lim Lee, Won Jae Chung, and Jun Yeob Lee. Selective efficiency boosting in thermally activated delayed fluorescence emitters by a secondary donor. *Chemical Engineering Journal*, 408:127293, March 2021. ISSN 1385-8947. doi:10.1016/j.cej.2020.127293. URL `http://dx.doi.org/10.1016/j.cej.2020.127293`.

[229] Zetong Ma, Zhiqiang Yang, Lan Mu, Lisong Deng, Liangjian Chen, Bohan Wang, Xianfeng Qiao, Dehua Hu, Bing Yang, Dongge Ma, Junbiao Peng, and Yuguang Ma. Converting molecular luminescence to ultralong room-temperature phosphorescence via the excited state modulation of sulfone-containing heteroaromatics. *Chemical Science*, 12(44): 14808–14814, 2021. ISSN 2041-6539. doi:10.1039/d1sc04118e. URL http://dx.doi.org/10.1039/D1SC04118E.

[230] Fan Ni, Zhongbin Wu, Zece Zhu, Tianheng Chen, Kailong Wu, Cheng Zhong, Kebin An, Danqing Wei, Dongge Ma, and Chuluo Yang. Teaching an old acceptor new tricks: rationally employing 2,1,3-benzothiadiazole as input to design a highly efficient red thermally activated delayed fluorescence emitter. *Journal of Materials Chemistry C*, 5(6):1363–1368, 2017. ISSN 2050-7534. doi:10.1039/c7tc00025a. URL http://dx.doi.org/10.1039/C7TC00025A.

[231] Peng Wang, Junsheng Yu, Shanyong Chen, Hong Yu, Xingwu Yan, Youwei Guan, Jinlei Chen, and Lu Li. 3-benzoyl-4h-chromen-4-one: A novel twisted acceptor for highly efficient thermally activated delayed fluorescence emitters. *Dyes and Pigments*, 183:108744, December 2020. ISSN 0143-7208. doi:10.1016/j.dyepig.2020.108744. URL http://dx.doi.org/10.1016/j.dyepig.2020.108744.

[232] Kihoon Shin, Euihoo Lee, Taehwan Lee, Young Hoon Lee, Doo Hong Kim, Chaerin Kim, Jaehoon Jung, Byung Jun Jung, and Min Hyung Lee. Efficient tadf from carbon-carbon bonded donor-acceptor molecules based on boron-carbonyl hybrid acceptor. *Dyes and Pigments*, 209:110937, February 2023. ISSN 0143-7208. doi:10.1016/j.dyepig.2022.110937. URL http://dx.doi.org/10.1016/j.dyepig.2022.110937.

[233] Manish Mannulal Raikwar, Seung Chan Kim, and Jun Yeob Lee. Highly efficient thermally activated delayed fluorescence emitter based on the 5h-benzo[d]benzo[4,5]imidazo[1,2-a]imidazole donor. *Materials Chemistry Frontiers*, 6(22):3382–3390, 2022. ISSN 2052-1537. doi:10.1039/d2qm00806h. URL http://dx.doi.org/10.1039/D2QM00806H.

[234] Haobin Zhao, Zhiheng Wang, Xinyi Cai, Kunkun Liu, Zuozheng He, Xin Liu, Yong Cao, and Shi-Jian Su. Highly efficient thermally activated delayed fluorescence materials with reduced efficiency roll-off and low on-set voltages. *Materials Chemistry Frontiers*, 1(10):2039–2046, 2017. ISSN 2052-1537. doi:10.1039/c7qm00195a. URL http://dx.doi.org/10.1039/C7QM00195A.

[235] Huiqin Wang, Bingjie Zhao, Chao Qu, Chunbo Duan, Zhe Li, Peng Ma, Peng Chang, Chunmiao Han, and Hui Xu. 2,3-dicyanopyrazino phenanthroline enhanced charge transfer for efficient near-infrared thermally activated delayed fluorescent diodes. *Chemical Engineering Journal*, 436:135080, May 2022. ISSN 1385-8947. doi:10.1016/j.cej.2022.135080. URL http://dx.doi.org/10.1016/j.cej.2022.135080.

[236] Quan Ran, Yuan-Lan Zhang, Xiaochen Hua, Man-Keung Fung, Liang-Sheng Liao, and Jian Fan. Modulation of p-type units in tripodal bipolar hosts towards highly efficient red phosphorescent oleds. *Dyes and Pigments*, 162:632–639, March 2019. ISSN 0143-7208. doi:10.1016/j.dyepig.2018.10.076. URL http://dx.doi.org/10.1016/j.dyepig.2018.10.076.

[237] Sarvendra Kumar, Yu-Yang Ma, Aziz Khan, Yi Yuan, Sheng-Yi Yang, Zuo-Quan Jiang, Man-Keung Fung, and Liang-Sheng Liao. Structurally controlled singlet-triplet splitting for blue star-shaped thermally activated delayed fluorescence emitters incorporating the tricarbazoles-triazine motifs. *Organic Electronics*, 84:105783, September 2020. ISSN 1566-1199. doi:10.1016/j.orgel.2020.105783. URL http://dx.doi.org/10.1016/j.orgel.2020.105783.

[238] Gyeong Heon Kim, Raju Lampande, Joon Beom Im, Jung Min Lee, Ju Young Lee, and Jang Hyuk Kwon. Controlling the exciton lifetime of blue thermally activated delayed fluorescence emitters using a heteroatom-containing pyridoindole donor moiety. *Materials Horizons*, 4(4):619–624, 2017. ISSN 2051-6355. doi:10.1039/c6mh00579a. URL http://dx.doi.org/10.1039/C6MH00579A.

[239] Karolis Leitonas, Matas Guzauskas, Uliana Tsiko, Jurate Simokaitiene, Dmytro Volyniuk, and Juozas Vidas Grazulevicius. White vertical organic permeable-base light-emitting transistors obtained by mixing of blue exciton and orange interface exciplex emissions. *Journal of Materials Chemistry C*, 10(26):9786–9793, 2022. ISSN 2050-7534. doi:10.1039/d2tc01326f. URL http://dx.doi.org/10.1039/D2TC01326F.

[240] Yi-Kuan Chen, Jayachandran Jayakumar, Chang-Lun Ko, Wen-Yi Hung, Tien-Lin Wu, and Chien-Hong Cheng. Increase the molecular length and donor strength to boost horizontal dipole orientation for high-efficiency oleds. *Journal of Materials Chemistry C*, 10(24):9241–9248, 2022. ISSN 2050-7534. doi:10.1039/d2tc01435a. URL http://dx.doi.org/10.1039/D2TC01435A.

[241] Ajay Kumar, Jihun Oh, Juhee Kim, Jaehoon Jung, and Min Hyung Lee. Facile color tuning of thermally activated delayed fluorescence by substituted ortho-carbazole-appended triarylboron emitters. *Dyes and Pigments*, 168:273–280, September 2019. ISSN 0143-7208. doi:10.1016/j.dyepig.2019.05.002. URL http://dx.doi.org/10.1016/j.dyepig.2019.05.002.

[242] Eigirdas Skuodis, Oleksandr Bezvikonnyi, Ausra Tomkeviciene, Dmytro Volyniuk, Viktorija Mimaite, Algirdas Lazauskas, Audrius Bucinskas, Rasa Keruckiene, Gjergji Sini, and Juozas Vidas Grazulevicius. Aggregation, thermal annealing, and hosting effects on performances of an acridan-based tadf emitter. *Organic Electronics*, 63:29–40, December 2018. ISSN 1566-1199. doi:10.1016/j.orgel.2018.09.002. URL http://dx.doi.org/10.1016/j.orgel.2018.09.002.

[243] Jia-Xiong Chen, Hui Wang, Xiang Zhang, Ya-Fang Xiao, Kai Wang, Lu Zhou, Yi-Zhong Shi, Jia Yu, Chun-Sing Lee, and Xiao-Hong Zhang. Using fullerene fragments as acceptors to construct thermally activated delayed fluorescence emitters for high-efficiency organic light-emitting diodes. *Chemical Engineering Journal*, 435:134731, May 2022. ISSN 1385-8947. doi:10.1016/j.cej.2022.134731. URL http://dx.doi.org/10.1016/j.cej.2022.134731.

[244] Dongjun Chen, Xinyi Cai, Xiang-Long Li, Zuozheng He, Chengsong Cai, Dongcheng Chen, and Shi-Jian Su. Efficient solution-processed red all-fluorescent organic light-emitting diodes employing thermally activated delayed fluorescence materials as assistant hosts: molecular design strategy and exciton dynamic analysis. *Journal of Materials Chemistry C*, 5 (21):5223–5231, 2017. ISSN 2050-7534. doi:10.1039/c7tc01164d. URL http://dx.doi.org/10.1039/C7TC01164D.

[245] Yaodong Zhao, Weigao Wang, Chen Gui, Li Fang, Xinlei Zhang, Shujuan Wang, Shuming Chen, Heping Shi, and Ben Zhong Tang. Thermally activated delayed fluorescence material with aggregation-induced emission properties for highly efficient organic light-emitting diodes. *Journal of Materials Chemistry C*, 6(11):2873–2881, 2018. ISSN 2050-7534.

doi:10.1039/c7tc04934j. URL http://dx.doi.org/10.1039/C7TC04934J.

[246] Yaxing Zhang, Jinyan Zhang, Changsheng Shi, Ning Sun, and Qiang Wang. Dipyrido[3,2-a:2',3'-c]phenazine acceptor based thermally activated delayed fluorescence emitters. *Dyes and Pigments*, 206:110634, October 2022. ISSN 0143-7208. doi:10.1016/j.dyepig.2022.110634. URL http://dx.doi.org/10.1016/j.dyepig.2022.110634.

[247] Jonathan S. Ward, Andrew Danos, Patrycja Stachelek, Mark A. Fox, Andrei S. Batsanov, Andrew P. Monkman, and Martin R. Bryce. Exploiting trifluoromethyl substituents for tuning orbital character of singlet and triplet states to increase the rate of thermally activated delayed fluorescence. *Materials Chemistry Frontiers*, 4(12):3602–3615, 2020. ISSN 2052-1537. doi:10.1039/d0qm00429d. URL http://dx.doi.org/10.1039/D0QM00429D.

[248] Ling Yu, Zhongbin Wu, Guohua Xie, Cheng Zhong, Zece Zhu, Dongge Ma, and Chuluo Yang. An efficient exciton harvest route for high-performance oleds based on aggregation-induced delayed fluorescence. *Chemical Communications*, 54(11): 1379–1382, 2018. ISSN 1364-548X. doi:10.1039/c7cc09925h. URL http://dx.doi.org/10.1039/C7CC09925H.

[249] Jiyoung Lee, Katsuyuki Shizu, Hiroyuki Tanaka, Hajime Nakanotani, Takuma Yasuda, Hironori Kaji, and Chihaya Adachi. Controlled emission colors and singlet-triplet energy gaps of dihydrophenazine-based thermally activated delayed fluorescence emitters. *Journal of Materials Chemistry C*, 3(10):2175–2181, 2015. ISSN 2050-7534. doi:10.1039/c4tc02530j. URL http://dx.doi.org/10.1039/C4TC02530J.

[250] Bin Huang, Wei Jiang, Li Yang, Xingyu Zhang, Yan Li, Wen-Cheng Chen, and Ning Gu. The effect of electron donor and acceptor conformations on thermally activated delayed fluorescence. *Organic Electronics*, 111:106657, December 2022. ISSN 1566-1199. doi:10.1016/j.orgel.2022.106657. URL http://dx.doi.org/10.1016/j.orgel.2022.106657.

[251] Usman Shakeel and Jai Singh. Study of processes of reverse intersystem crossing (risc) and thermally activated delayed fluorescence (tadf) in organic light emitting diodes (oleds). *Organic Electronics*, 59:121–124, August 2018. ISSN 1566-1199. doi:10.1016/j.orgel.2018.04.035. URL http://dx.doi.org/10.1016/j.orgel.2018.04.035.

[252] You-Jun Yu, Xun Tang, Hui-Ting Ge, Yi Yuan, Zuo-Quan Jiang, and Liang-Sheng Liao. Fluorenone-based thermally activated delayed fluorescence materials for orange-red emission. *Organic Electronics*, 73:240–246, October 2019. ISSN 1566-1199. doi:10.1016/j.orgel.2019.06.008. URL http://dx.doi.org/10.1016/j.orgel.2019.06.008.

[253] Ramanaskanda Braveenth, Kanthasamy Raagulan, Yu-Jin Kim, and Bo-Mi Kim. Recent advances in green thermally activated delayed fluorescence emitters towards high colour purity and good electroluminescence performance. *Materials Advances*, 4(2):374–388, 2023. ISSN 2633-5409. doi:10.1039/d2ma00967f. URL http://dx.doi.org/10.1039/D2MA00967F.

[254] Hui Wang, Xiaopeng Lv, Lingqiang Meng, Xiaofang Wei, Ying Wang, and Pengfei Wang. Novel thioxanthone host material with thermally activated delayed fluorescence for reduced efficiency roll-off of phosphorescent oleds. *Chinese Chemical Letters*, 29(3):471–474, March 2018. ISSN 1001-8417. doi:10.1016/j.cclet.2017.07.025. URL http://dx.doi.org/10.1016/j.cclet.2017.07.025.

[255] Keming Chen, Fujun Zhang, Asu Li, Ru Zhang, Ren Sheng, Yu Duan, Yi Zhao, and Ping Chen. High efficiency, ultra-low roll-offs in orange phosphorescent organic light-emitting devices using a novel exciplex system. *Organic Electronics*, 106:106536, July 2022. ISSN 1566-1199. doi:10.1016/j.orgel.2022.106536. URL http://dx.doi.org/10.1016/j.orgel.2022.106536.

[256] Zuozheng He, Xinyi Cai, Zhiheng Wang, Yunchuan Li, Zhida Xu, Kunkun Liu, Dongcheng Chen, and Shi-Jian Su. Sky-blue thermally activated delayed fluorescence material employing a diphenylethyne acceptor for organic light-emitting diodes. *Journal of Materials Chemistry C*, 6(1):36–42, 2018. ISSN 2050-7534. doi:10.1039/c7tc02763j. URL http://dx.doi.org/10.1039/C7TC02763J.

[257] Hui Wang, Lu Zhou, Yi-Zhong Shi, Xiao-Chun Fan, Jia-Xiong Chen, Kai Wang, Jia Yu, and Xiao-Hong Zhang. A facile strategy for enhancing reverse intersystem crossing of red thermally activated delayed fluorescence emitters. *Chemical Engineering Journal*, 433:134423, April 2022. ISSN 1385-8947. doi:10.1016/j.cej.2021.134423. URL http://dx.doi.org/10.1016/j.cej.2021.134423.

[258] Chunlong Shi, Di Liu, Jiuyan Li, Zhaolong He, Kai Song, Botao Liu, Qi Wu, and Min Xu. tert-butyltriazine-diphenylaminocarbazole based tadf materials: Ï€-bridge modification for enhanced krisc and efficiency stability. *Dyes and Pigments*, 204:110430, August 2022. ISSN 0143-7208. doi:10.1016/j.dyepig.2022.110430. URL http://dx.doi.org/10.1016/j.dyepig.2022.110430.

[259] Xiuqing Dong, Shujuan Wang, Chen Gui, Heping Shi, Fangqin Cheng, and Ben Zhong Tang. Synthesis, aggregation-induced emission and thermally activated delayed fluorescence properties of two new compounds based on phenylethene, carbazole and 9,9',10,10'-tetraoxidethianthrene. *Tetrahedron*, 74(4):497–505, January 2018. ISSN 0040-4020. doi:10.1016/j.tet.2017.12.022. URL http://dx.doi.org/10.1016/j.tet.2017.12.022.

[260] Yingyu Zhu, Zhanxiang Chen, Ao Ying, Shaolong Gong, Tao Wang, and Chuluo Yang. Nematic liquid crystals induce and amplify the circularly polarized luminescence of chiral tadf emitters. *Journal of Materials Chemistry C*, 10(13):5065–5069, 2022. ISSN 2050-7534. doi:10.1039/d2tc00344a. URL http://dx.doi.org/10.1039/D2TC00344A.

[261] Tengxiao Liu and Guohua Xie. Exploiting new feasibility of a phenylquinoline unit for establishing efficient green thermally activated delayed fluorescent emitter with short delayed fluorescent lifetime. *Organic Electronics*, 106:106518, July 2022. ISSN 1566-1199. doi:10.1016/j.orgel.2022.106518. URL http://dx.doi.org/10.1016/j.orgel.2022.106518.

[262] Jian Song, Fujun Zhang, Liping Yang, Keming Chen, Asu Li, Ren Sheng, Yu Duan, and Ping Chen. Highly efficient, ultralow turn-on voltage red and white organic light-emitting devices based on a novel exciplex host. *Materials Advances*, 2(11):3677–3684, 2021. ISSN 2633-5409. doi:10.1039/d0ma01005g. URL http://dx.doi.org/10.1039/D0MA01005G.

[263] Liang Zhang, Yin-Feng Wang, Meng Li, Qing-Yu Gao, and Chuan-Feng Chen. Quinoline-based aggregation-induced delayed fluorescence materials for highly efficient non-doped organic light-emitting diodes. *Chinese Chemical Letters*, 32(2):740–744, February 2021. ISSN 1001-8417. doi:10.1016/j.cclet.2020.07.041. URL http://dx.doi.org/10.1016/j.cclet.2020.07.041.

[264] Ho Jung Lee, Ha Lim Lee, Si Hyun Han, and Jun Yeob Lee. Novel secondary acceptor based molecular design for superb lifetime in thermally activated delayed fluorescent organic light-emitting diodes through high bond energy and fast up-conversion. *Chemical Engineering Journal*, 427:130988, January 2022. ISSN 1385-8947. doi:10.1016/j.cej.2021.130988. URL http://dx.doi.org/10.1016/j.cej.2021.130988.

[265] Jia-Xiong Chen, Wen-Wen Tao, Kai Wang, Cai-Jun Zheng, Wei Liu, Xing Li, Xue-Mei Ou, and Xiao-Hong Zhang. Highly efficient thermally activated delayed fluorescence emitters based on novel indolo[2,3-b]acridine electron-donor. *Organic Electronics*, 57:327–334, June 2018. ISSN 1566-1199. doi:10.1016/j.orgel.2018.03.024. URL http://dx.doi.org/10.1016/j.orgel.2018.03.024.

[266] Vilas Venunath Patil, Kyung Hyung Lee, and Jun Yeob Lee. 11,11-dimethyl-11h-indeno[1,2-b]indolo[1,2,3-jk]carbazole: A rigid chromophore with novel amalgamation strategy for long lifetime blue fluorescent organic light-emitting diodes. *Chemical Engineering Journal*, 395:125125, September 2020. ISSN 1385-8947. doi:10.1016/j.cej.2020.125125. URL http://dx.doi.org/10.1016/j.cej.2020.125125.

[267] Xinyu Zhang, Dan Wang, Yunxiang Lei, Miaochang Liu, Zhengxu Cai, Huayue Wu, Guoming Shen, Xiaobo Huang, and Yuping Dong. Selenium atoms induce organic doped systems to produce pure phosphorescence emission. *Chemical Communications*, 58(8):1179–1182, 2022. ISSN 1364-548X. doi:10.1039/d1cc06380d. URL http://dx.doi.org/10.1039/D1CC06380D.

[268] Minyu Chen, Jiali Yang, Zhonghua Ye, Shuanglong Wang, Zhenyu Tang, Guo Chen, Yanqiong Zheng, Ying Shi, Bin Wei, and Wai-Yeung Wong. Extremely low-efficiency roll-off of phosphorescent organic light-emitting diodes at high brightness based on acridine heterocyclic derivatives. *Journal of Materials Chemistry C*, 6(36):9713–9722, 2018. ISSN 2050-7534. doi:10.1039/c8tc02739k. URL http://dx.doi.org/10.1039/C8TC02739K.

[269] He Liu, Jiafang Li, Ganggang Li, Bing Zhang, Qun Zhan, Zhiwen Liu, Changjiang Zhou, Kai Li, Zhiming Wang, and Chuluo Yang. A simple strategy to achieve efficient thermally activated delayed fluorescent emitters via enhancing electron donating ability of donors. *Dyes and Pigments*, 180:108521, September 2020. ISSN 0143-7208. doi:10.1016/j.dyepig.2020.108521. URL http://dx.doi.org/10.1016/j.dyepig.2020.108521.

[270] Uliana Tsiko, Oleksandr Bezvikonnyi, Galyna Sych, Rasa Keruckiene, Dmytro Volyniuk, Jurate Simokaitiene, Iryna Danyliv, Yan Danyliv, Audrius Bucinskas, Xiaofeng Tan, and Juozas Vidas Grazulevicius. Multifunctional derivatives of pyrimidine-5-carbonitrile and differently substituted carbazoles for doping-free sky-blue oleds and luminescent sensors of oxygen. *Journal of Advanced Research*, 33:41–51, November 2021. ISSN 2090-1232. doi:10.1016/j.jare.2021.01.014. URL http://dx.doi.org/10.1016/j.jare.2021.01.014.

[271] Vilas Venunath Patil, Kyung Hyung Lee, and Jun Yeob Lee. Isomeric fused benzocarbazole as a chromophore for blue fluorescent organic light-emitting diodes. *Journal of Materials Chemistry C*, 8(24):8320–8327, 2020. ISSN 2050-7534. doi:10.1039/d0tc01268h. URL http://dx.doi.org/10.1039/D0TC01268H.

[272] Zhongyan Huang, Chih-Wei Huang, Yu-Kun Tang, Zhengqi Xiao, Nengquan Li, Tao Hua, Xiaosong Cao, Changjiang Zhou, Chung-Chih Wu, and Chuluo Yang. Chiral thermally activated delayed fluorescence emitters for circularly polarized luminescence and efficient deep blue oleds. *Dyes and Pigments*, 197:109860, January 2022. ISSN 0143-7208. doi:10.1016/j.dyepig.2021.109860. URL http://dx.doi.org/10.1016/j.dyepig.2021.109860.

[273] Youngnam Lee, Seung-Je Woo, Jang-Joo Kim, and Jong-In Hong. Linear-shaped thermally activated delayed fluorescence emitter using 1,5-naphthyridine as an electron acceptor for efficient light extraction. *Organic Electronics*, 78:105600, March 2020. ISSN 1566-1199. doi:10.1016/j.orgel.2019.105600. URL http://dx.doi.org/10.1016/j.orgel.2019.105600.

[274] Youngnam Lee and Jong-In Hong. High-efficiency thermally activated delayed fluorescence emitters via a high horizontal dipole ratio and controlled dual emission. *Journal of Materials Chemistry C*, 8(24):8012–8017, 2020. ISSN 2050-7534. doi:10.1039/d0tc01644f. URL http://dx.doi.org/10.1039/D0TC01644F.

[275] Iryna Hladka, Dmytro Volyniuk, Oleksandr Bezvikonnyi, Vasyl Kinzhybalo, Tamara J. Bednarchuk, Yan Danyliv, Roman Lytvyn, Algirdas Lazauskas, and Juozas V. Grazulevicius. Polymorphism of derivatives of tert-butyl substituted acridan and perfluorobiphenyl as sky-blue oled emitters exhibiting aggregation induced thermally activated delayed fluorescence. *Journal of Materials Chemistry C*, 6(48):13179–13189, 2018. ISSN 2050-7534. doi:10.1039/c8tc04867c. URL http://dx.doi.org/10.1039/C8TC04867C.

[276] Jing-Xing Liang, Ze-Hui Pan, Kai Zhang, Dezhi Yang, Jing-Wen Tai, Chuan-Kui Wang, Man-Keung Fung, Dongge Ma, and Jian Fan. A facile method to achieve red thermally activated delayed fluorescence emitters with eqe over 30% via molecular aspect ratio engineering. *Chemical Engineering Journal*, 457:141074, February 2023. ISSN 1385-8947. doi:10.1016/j.cej.2022.141074. URL http://dx.doi.org/10.1016/j.cej.2022.141074.

[277] Xiaofang Wei, Taiping Hu, Zhiyi Li, Yanwei Liu, Xiaoxiao Hu, Honglei Gao, Guanhao Liu, Pengfei Wang, Yuanping Yi, and Ying Wang. Rational strategy of exciplex-type thermally activated delayed fluorescent (tadf) emitters: Stacking of donor and acceptor units of the intramolecular tadf molecule. *Chemical Engineering Journal*, 433:133546, April 2022. ISSN 1385-8947. doi:10.1016/j.cej.2021.133546. URL http://dx.doi.org/10.1016/j.cej.2021.133546.

[278] Zhi Huang, Songpo Xiang, Qing Zhang, Xialei Lv, Shaofeng Ye, Runda Guo, and Lei Wang. Highly efficient green organic light emitting diodes with phenanthroimidazole-based thermally activated delayed fluorescence emitters. *Journal of Materials Chemistry C*, 6(9):2379–2386, 2018. ISSN 2050-7534. doi:10.1039/c7tc05576e. URL http://dx.doi.org/10.1039/C7TC05576E.

[279] Ping Wu, Feng-ming Xie, Huai-xin Wei, Yan-Qing Li, Guo-liang Dai, Yan Wang, Jian-Xin Tang, and Xin Zhao. Thermally activated delayed fluorescent emitters based on 3-(phenylsulfonyl)pyridine. *Chemical Physics Letters*, 771:138474, May 2021. ISSN 0009-2614. doi:10.1016/j.cplett.2021.138474. URL http://dx.doi.org/10.1016/j.cplett.2021.138474.

[280] Shian Ying, Jichen Lv, Yuanzhao Li, Yumiao Huo, Yuchao Liu, Dongge Ma, Ling Peng, and Shouke Yan. A large-scale deep-blue tetraphenylbenzene-bridged hybridized local and charge transfer fluorophore exhibiting small efficiency roll-off

and low amplified spontaneous emission threshold. *Materials Chemistry Frontiers*, 6(15):2085–2094, 2022. ISSN 2052-1537. doi:10.1039/d2qm00506a. URL http://dx.doi.org/10.1039/D2QM00506A.

[281] Binyan Wang, Xianfeng Qiao, Zhou Yang, Yafei Wang, Shengzhong Liu, Dongge Ma, and Qiang Wang. Realizing efficient red thermally activated delayed fluorescence organic light-emitting diodes using phenoxazine/phenothiazine-phenanthrene hybrids. *Organic Electronics*, 59:32–38, August 2018. ISSN 1566-1199. doi:10.1016/j.orgel.2018.04.045. URL http://dx.doi.org/10.1016/j.orgel.2018.04.045.

[282] Jia-Xiong Chen, Ya-Fang Xiao, Kai Wang, Xiao-Chun Fan, Chen Cao, Wen-Cheng Chen, Xiang Zhang, Yi-Zhong Shi, Jia Yu, Feng-Xia Geng, Xiao-Hong Zhang, and Chun-Sing Lee. Origin of thermally activated delayed fluorescence in a donor-acceptor type emitter with an optimized nearly planar geometry. *Journal of Materials Chemistry C*, 8(38): 13263–13269, 2020. ISSN 2050-7534. doi:10.1039/d0tc03747h. URL http://dx.doi.org/10.1039/D0TC03747H.

[283] Yi-Fan Shen, Meng Li, Wen-Long Zhao, Yin-Feng Wang, Hai-Yan Lu, and Chuan-Feng Chen. Quinoline-based tadf emitters exhibiting aggregation-induced emission for efficient non-doped organic light-emitting diodes. *Materials Chemistry Frontiers*, 5(2):834–842, 2021. ISSN 2052-1537. doi:10.1039/d0qm00628a. URL http://dx.doi.org/10.1039/D0QM00628A.

[284] Xiang-Yang Liu, Feng Liang, Yi Yuan, Lin-Song Cui, Zuo-Quan Jiang, and Liang-Sheng Liao. An effective host material with thermally activated delayed fluorescence formed by confined conjugation for red phosphorescent organic light-emitting diodes. *Chemical Communications*, 52(52):8149–8151, 2016. ISSN 1364-548X. doi:10.1039/c6cc02856j. URL http://dx.doi.org/10.1039/C6CC02856J.

[285] Chan Hee Lee, Shin Hyung Choi, Sung Joon Oh, Jun Hyeon Lee, Jae Won Shim, Chihaya Adachi, and Sae Youn Lee. Highly effective organic light-emitting diodes containing thermally activated delayed fluorescence emitters with horizontal molecular orientation. *RSC Advances*, 10(70):42897–42902, 2020. ISSN 2046-2069. doi:10.1039/d0ra07865d. URL http://dx.doi.org/10.1039/D0RA07865D.

[286] Jing-Wen Tai, Yukun Tang, Kai Zhang, Chen-Zong Yang, Ze-Hui Pan, Yu-Ching Lin, Yu-Wei Shih, Chia-Hsun Chen, Tien-Lung Chiu, Jiun-Haw Lee, Chuan-Kui Wang, Chung-Chih Wu, and Jian Fan. 13.2% eqe near-infrared tadf oled with emission peak at 761Å nm. *Chemical Engineering Journal*, 452:139534, January 2023. ISSN 1385-8947. doi:10.1016/j.cej.2022.139534. URL http://dx.doi.org/10.1016/j.cej.2022.139534.

[287] Heng-Yuan Zhang, Hao-Yu Yang, Ming Zhang, Hui Lin, Si-Lu Tao, Cai-Jun Zheng, and Xiao-Hong Zhang. A novel orange-red thermally activated delayed fluorescence emitter with high molecular rigidity and planarity realizing 32.5% external quantum efficiency in organic light-emitting diodes. *Materials Horizons*, 9(9):2425–2432, 2022. ISSN 2051-6355. doi:10.1039/d2mh00639a. URL http://dx.doi.org/10.1039/D2MH00639A.

[288] P. Justin Jesuraj, Sivaraman Somasundaram, Eswaran Kamaraj, Hassan Hafeez, Changmin Lee, Donghyun Kim, Sang Hee Won, Sung Tae Shin, Myungkwan Song, Chang-Su Kim, Sanghyuk Park, and Seung Yoon Ryu. Intramolecular charge transfer-based spirobifluorene-coupled heteroaromatic moieties as efficient hole transport layer and host in phosphorescent organic light-emitting diodes. *Organic Electronics*, 85:105825, October 2020. ISSN 1566-1199. doi:10.1016/j.orgel.2020.105825. URL http://dx.doi.org/10.1016/j.orgel.2020.105825.

[289] Seung Ji Cha, Noh Soo Han, Jae Kyu Song, So-Ra Park, Young Min Jeon, and Min Chul Suh. Efficient deep blue fluorescent emitter showing high external quantum efficiency. *Dyes and Pigments*, 120:200–207, September 2015. ISSN 0143-7208. doi:10.1016/j.dyepig.2015.04.020. URL http://dx.doi.org/10.1016/j.dyepig.2015.04.020.

[290] Ranran Pei, Jingli Lou, Ganggang Li, He Liu, Xiaojun Yin, Changjiang Zhou, Zhiming Wang, and Chuluo Yang. Modulating lumo extension of spiro-junction tadf emitters for efficient oleds with relieved efficiency roll-off. *Chemical Engineering Journal*, 437:135222, June 2022. ISSN 1385-8947. doi:10.1016/j.cej.2022.135222. URL http://dx.doi.org/10.1016/j.cej.2022.135222.

[291] Xiao-Chun Fan, Kai Wang, Cai-Jun Zheng, Gao-Le Dai, Yi-Zhong Shi, Yan-Qing Li, Jia Yu, Xue-Mei Ou, and Xiao-Hong Zhang. Thermally activated delayed fluorescence emitters with low concentration sensitivity for highly efficient organic light emitting devices. *Journal of Materials Chemistry C*, 7(29):8923–8928, 2019. ISSN 2050-7534. doi:10.1039/c9tc02032b. URL http://dx.doi.org/10.1039/C9TC02032B.

[292] Ju Hui Yun, Jae-Min Kim, Won Jae Chung, Junseop Lim, Jun Yeob Lee, Yoonkyoo Lee, and Changwoong Choo. A novel electroplex host with dual triplet exciton up-converting channels suppressing triplet exciton induced degradation mechanisms in blue organic light-emitting diodes. *Journal of Materials Chemistry C*, 9(42):15242–15250, 2021. ISSN 2050-7534. doi:10.1039/d1tc03225a. URL http://dx.doi.org/10.1039/D1TC03225A.

[293] Tetsuya Nakagawa, Sung-Yu Ku, Ken-Tsung Wong, and Chihaya Adachi. Electroluminescence based on thermally activated delayed fluorescence generated by a spirobifluorene donor–acceptor structure. *Chemical Communications*, 48(77):9580, 2012. ISSN 1364-548X. doi:10.1039/c2cc31468a. URL http://dx.doi.org/10.1039/C2CC31468A.

[294] Chunbo Duan, Ying Xin, Zicheng Wang, Jing Zhang, Chunmiao Han, and Hui Xu. High-efficiency hyperfluorescent white light-emitting diodes based on high-concentration-doped tadf sensitizer matrices via spatial and energy gap effects. *Chemical Science*, 13(1):159–169, 2022. ISSN 2041-6539. doi:10.1039/d1sc05753g. URL http://dx.doi.org/10.1039/D1SC05753G.

[295] Dongdong Zhang, Lian Duan, Deqiang Zhang, Juan Qiao, Guifang Dong, Liduo Wang, and Yong Qiu. Extremely low driving voltage electrophosphorescent green organic light-emitting diodes based on a host material with small singlet-triplet exchange energy without p- or n-doping layer. *Organic Electronics*, 14(1):260–266, January 2013. ISSN 1566-1199. doi:10.1016/j.orgel.2012.11.003. URL http://dx.doi.org/10.1016/j.orgel.2012.11.003.

[296] Oleksandr Bezvikonnyi, Dalius Gudeika, Dmytro Volyniuk, Viktorija Mimaite, Bernard Ronit Sebastine, and Juozas V. Grazulevicius. Effect of donor substituents on thermally activated delayed fluorescence of diphenylsulfone derivatives. *Journal of Luminescence*, 206:250–259, February 2019. ISSN 0022-2313. doi:10.1016/j.jlumin.2018.10.018. URL http://dx.doi.org/10.1016/j.jlumin.2018.10.018.

[297] Danyang Chai, Xuan Zeng, Xiaoxuan Su, Changjiang Zhou, Yang Zou, Cheng Zhong, Shaolong Gong, and Chuluo Yang. A simple and effective strategy to lock the quasi-equatorial conformation of acridine by h-h repulsion for highly efficient thermally activated delayed fluorescence emitters. *Chemical Communications*, 56(15):2308–2311, 2020. ISSN 1364-548X. doi:10.1039/c9cc09769d. URL `http://dx.doi.org/10.1039/C9CC09769D`.

[298] Yanyan Liu, Jiaji Yang, Zhu Mao, Yuyuan Wang, Juan Zhao, Shi-Jian Su, and Zhenguo Chi. Isomeric thermally activated delayed fluorescence emitters for highly efficient organic light-emitting diodes. *Chemical Science*, 14(6):1551–1556, 2023. ISSN 2041-6539. doi:10.1039/d2sc06335b. URL `http://dx.doi.org/10.1039/D2SC06335B`.

[299] Y. Zhao, C. Fu, L. Fu, Y. Liu, Z. Lu, and X. Pu. Data-driven machine learning models for quick prediction of thermal stability properties of oled materials. *Materials Today Chemistry*, 22:100625, December 2021. ISSN 2468-5194. doi:10.1016/j.mtchem.2021.100625. URL `http://dx.doi.org/10.1016/j.mtchem.2021.100625`.

[300] U. Tsiko, D. Volyniuk, V. Andruleviciene, K. Leitonas, G. Sych, O. Bezvikonnyi, V. Jasinskas, V. Gulbinas, P. Stakhira, and J.V. Grazulevicius. Triphenylamino or 9-phenyl carbazolyl-substituted pyrimidine-5-carbonitriles as bipolar emitters and hosts with triplet harvesting abilities. *Materials Today Chemistry*, 25:100955, September 2022. ISSN 2468-5194. doi:10.1016/j.mtchem.2022.100955. URL `http://dx.doi.org/10.1016/j.mtchem.2022.100955`.

[301] Kenkera Rayappa Naveen, Hyuna Lee, Lee Hyun Seung, Young Hun Jung, C.P. Keshavananda Prabhu, Subramanian Muruganantham, and Jang Hyuk Kwon. Modular design for constructing narrowband deep-blue multiresonant thermally activated delayed fluorescent emitters for efficient organic light emitting diodes. *Chemical Engineering Journal*, 451:138498, January 2023. ISSN 1385-8947. doi:10.1016/j.cej.2022.138498. URL `http://dx.doi.org/10.1016/j.cej.2022.138498`.

[302] Gábor Méhes, Kenichi Goushi, William J. Potscavage, and Chihaya Adachi. Influence of host matrix on thermally-activated delayed fluorescence: Effects on emission lifetime, photoluminescence quantum yield, and device performance. *Organic Electronics*, 15(9):2027–2037, September 2014. ISSN 1566-1199. doi:10.1016/j.orgel.2014.05.027. URL `http://dx.doi.org/10.1016/j.orgel.2014.05.027`.

[303] Yepeng Xiang, Shaolong Gong, Yongbiao Zhao, Xiaojun Yin, Jiajia Luo, Kailong Wu, Zheng-Hong Lu, and Chuluo Yang. Asymmetric-triazine-cored triads as thermally activated delayed fluorescence emitters for high-efficiency yellow oleds with slow efficiency roll-off. *Journal of Materials Chemistry C*, 4(42):9998–10004, 2016. ISSN 2050-7534. doi:10.1039/c6tc02702d. URL `http://dx.doi.org/10.1039/C6TC02702D`.

[304] Jee Hyun Maeng, Dae Hyun Ahn, Hyuna Lee, Young Hun Jung, Durai Karthik, Ju Young Lee, and Jang Hyuk Kwon. Rigid indolocarbazole donor moiety for highly efficient thermally activated delayed fluorescent device. *Dyes and Pigments*, 180:108485, September 2020. ISSN 0143-7208. doi:10.1016/j.dyepig.2020.108485. URL `http://dx.doi.org/10.1016/j.dyepig.2020.108485`.

[305] Shuai Wang, Haiyang Shu, Xianchao Han, Xiaofu Wu, Hui Tong, and Lixiang Wang. A highly efficient purely organic room-temperature phosphorescence film based on a selenium-containing emitter for sensitive oxygen detection. *Journal of Materials Chemistry C*, 9(31):9907–9913, 2021. ISSN 2050-7534. doi:10.1039/d1tc02324a. URL `http://dx.doi.org/10.1039/D1TC02324A`.

[306] Zhanxiang Chen, Zhongbin Wu, Fan Ni, Cheng Zhong, Weixuan Zeng, Danqing Wei, Kebin An, Dongge Ma, and Chuluo Yang. Emitters with a pyridine-3,5-dicarbonitrile core and short delayed fluorescence lifetimes of about 1.5 μs: orange-red tadf-based oleds with very slow efficiency roll-offs at high luminance. *Journal of Materials Chemistry C*, 6(24):6543–6548, 2018. ISSN 2050-7534. doi:10.1039/c8tc01698d. URL `http://dx.doi.org/10.1039/C8TC01698D`.

[307] Jae-Ryung Cha, Chil Won Lee, and Myoung-Seon Gong. Effect of increasing electron donor units for high-efficiency blue thermally activated delayed fluorescence. *Dyes and Pigments*, 140:399–406, May 2017. ISSN 0143-7208. doi:10.1016/j.dyepig.2017.01.053. URL `http://dx.doi.org/10.1016/j.dyepig.2017.01.053`.

[308] Ruige Su, Yuling Zhao, Shiqiang Liu, Peiying Li, Jiaying Ma, Di Zhang, Minghu Han, and Tianzhi Yu. Synthesis and luminescence properties of functionalized v-shaped bis-coumarin derivatives. *New Journal of Chemistry*, 46(14):6793–6803, 2022. ISSN 1369-9261. doi:10.1039/d1nj05960b. URL `http://dx.doi.org/10.1039/D1NJ05960B`.

[309] Xinxin Ban, Suyu Qiu, Qingpeng Cao, Kaizhi Zhang, Tao Zhou, Hui Xu, Ming Pei, Fengjie Ge, Zhiwei Tong, and Wei Jiang. Exciplex polymer with strong aie for constructing fully-solution-processed organic light-emitting diodes with 100-fold efficiency improvement compared to physically blended exciplex. *Polymer Chemistry*, 13(47):6500–6511, 2022. ISSN 1759-9962. doi:10.1039/d2py01306a. URL `http://dx.doi.org/10.1039/D2PY01306A`.

[310] Xu-Lin Chen, Chen-Sheng Lin, Xiao-Yuan Wu, Rongming Yu, Teng Teng, Qi-Kai Zhang, Qing Zhang, Wen-Bing Yang, and Can-Zhong Lu. Highly efficient cuprous complexes with thermally activated delayed fluorescence and simplified solution process oleds using the ligand as host. *Journal of Materials Chemistry C*, 3(6):1187–1195, 2015. ISSN 2050-7534. doi:10.1039/c4tc02255f. URL `http://dx.doi.org/10.1039/C4TC02255F`.

[311] Ken Albrecht, Kenichi Matsuoka, Daisuke Yokoyama, Yoshiya Sakai, Akira Nakayama, Katsuhiko Fujita, and Kimihisa Yamamoto. Thermally activated delayed fluorescence oleds with fully solution processed organic layers exhibiting nearly 10% external quantum efficiency. *Chemical Communications*, 53(16):2439–2442, 2017. ISSN 1364-548X. doi:10.1039/c6cc09275f. URL `http://dx.doi.org/10.1039/C6CC09275F`.

[312] Dong Ryun Lee, Si Hyun Han, Chil Won Lee, and Jun Yeob Lee. Bis(diphenyltriazine) as a new acceptor of efficient thermally activated delayed fluorescent emitters. *Dyes and Pigments*, 151:75–80, April 2018. ISSN 0143-7208. doi:10.1016/j.dyepig.2017.12.048. URL `http://dx.doi.org/10.1016/j.dyepig.2017.12.048`.

[313] De-Qi Wang, Ming Zhang, Kai Wang, Cai-Jun Zheng, Yi-Zhong Shi, Jia-Xiong Chen, Hui Lin, Si-Lu Tao, and Xiao-Hong Zhang. Fine-tuning the emissions of highly efficient thermally activated delayed fluorescence emitters with different linking positions of electron-deficient substituent groups. *Dyes and Pigments*, 143:62–70, August 2017. ISSN 0143-7208. doi:10.1016/j.dyepig.2017.04.024. URL `http://dx.doi.org/10.1016/j.dyepig.2017.04.024`.

[314] Haichao Liu, Qing Bai, Liang Yao, Haiyan Zhang, Hai Xu, Shitong Zhang, Weijun Li, Yu Gao, Jinyu Li, Ping Lu, Hongyan Wang, Bing Yang, and Yuguang Ma. Highly efficient near ultraviolet organic light-emitting diode based on a meta-linked donor-acceptor molecule. *Chemical Science*, 6(7):3797–3804, 2015. ISSN 2041-6539. doi:10.1039/c5sc01131k. URL `http://dx.doi.org/10.1039/C5SC01131K`.

[315] Lu Zhou, Hui Wang, Yi-Zhong Shi, Xiao-Chun Fan, Jia-Xiong Chen, Kai Wang, Jia Yu, and Xiao-Hong Zhang. Controlling the conjugation extension inside acceptors for enhancing reverse intersystem crossing of red thermally activated delayed fluorescence emitters. *Chemical Engineering Journal*, 440:135775, July 2022. ISSN 1385-8947. doi:10.1016/j.cej.2022.135775. URL `http://dx.doi.org/10.1016/j.cej.2022.135775`.

[316] Pachaiyappan Rajamalli, Dongyang Chen, Wenbo Li, Ifor D. W. Samuel, David B. Cordes, Alexandra M. Z. Slawin, and Eli Zysman-Colman. Enhanced thermally activated delayed fluorescence through bridge modification in sulfone-based emitters employed in deep blue organic light-emitting diodes. *Journal of Materials Chemistry C*, 7(22):6664–6671, 2019. ISSN 2050-7534. doi:10.1039/c9tc01498e. URL `http://dx.doi.org/10.1039/C9TC01498E`.

[317] Xue Zhou, Yepeng Xiang, Shaolong Gong, Zhanxiang Chen, Fan Ni, Guohua Xie, and Chuluo Yang. Simple construction of deep-red hexaazatrinaphthylene-based thermally activated delayed fluorescence emitters for efficient solution-processed oleds with a peak at 692 nm. *Chemical Communications*, 55(94):14190–14193, 2019. ISSN 1364-548X. doi:10.1039/c9cc06804j. URL `http://dx.doi.org/10.1039/C9CC06804J`.

[318] J.H. Kim, W.J. Chung, J. Kim, and J.Y. Lee. Concentration quenching-resistant multiresonance thermally activated delayed fluorescence emitters. *Materials Today Energy*, 21:100792, September 2021. ISSN 2468-6069. doi:10.1016/j.mtener.2021.100792. URL `http://dx.doi.org/10.1016/j.mtener.2021.100792`.

[319] Tomas Serevičius, Rokas Skaisgiris, Irina Fiodorova, Vytautas Steckis, Jelena Dodonova, Dovydas Banevičius, Karolis Kazlauskas, Saulius Juršėnas, and Sigitas Tumkevičius. Achieving efficient deep-blue tadf in carbazole-pyrimidine compounds. *Organic Electronics*, 82:105723, July 2020. ISSN 1566-1199. doi:10.1016/j.orgel.2020.105723. URL `http://dx.doi.org/10.1016/j.orgel.2020.105723`.